ADSORPTION ON KAOLINITE

AND

A WATER covered SURFACE

by

DAVID MALCOLM REES, B.Sc.

A thesis submitted for the degree
of DOCTOR OF PHILOSOPHY in the
University of London

Physical Chemistry Laboratories,
Imperial College of Science and Technology,
London, S.W.7.

September, 1959.

ABSTRACT

The differential heats of adsorption of argon and nitrogen at 77°K. and of water at 25°C, have been measured on a sample of sodium kaolinite by means of a non-adiabatic calorimeter. Heats of adsorption of argon and nitrogen on an ice surface, formed by freezing two molecular layers of water on to the same sample of sodium kaolinite, have also been measured at 77°K. in the same calorimeter. Isotherm data corresponding to all the above systems were also obtained, and the evaluation of the differential entropies of sorbed argon at 77°K. and sorbed water at 25°C. thereby carried out.

The sorbent was prepared by electrodialysis of a sample of natural kaolinite of particle size 2-5 microns, followed by titration with sodium hydroxide. Gas increments were measured volumetrically, and the apparatus which was designed for the gravimetric measurement of small increments of water is also described.

The B.E.T. theory was applied to the data obtained from all three sorbate molecules. The area occupied by a sorbed water molecule (11.0-11.5 $Å^2$) could therefore be calculated, and theories of the nature of water layers sorbed on clay minerals were discussed in the light of this molecular area and the heats of sorption data.

High heats of sorption on sodium kaolinite were

observed at low surface coverage. This has been attributed to the presence of active sites at the kaolinite surface, identifiable with the electrostatic field rather than with dispersion forces. In fact, these high heats of sorption are probably due to the presence of Na^+ ions.

The electrostatic field has been calculated over two positions on the ice-covered sodium kaolinite surface. An attempt to account for the difference between the heats of sorption of argon on the ice surface and the heat of sublimation of argon by means of the expression $u = -\frac{1}{2}\alpha F^2$ resulted, however, in an unreasonably small value for the distance between the sorbed argon atoms and the ice surface. In a similar manner, an attempt was made to explain the difference between the initial heats of sorption of nitrogen and of argon on the ice surface by calculation of the interaction of the nitrogen quadrupole with the field gradients occurring at the ice surface. In this case, a more reasonable value for the distance between the nitrogen molecules and the ice surface was obtained. It has been shown that the contribution to the heats of sorption of nitrogen from the interaction of the nitrogen quadrupole with the field gradients at the surface is significant both on the sodium kaolinite surface and on the ice surface, which is electrostatically more uniform.

No maximum was observed at high surface coverage

in the differential heat curve of argon on the ice surface. The absence of a maximum could not be explained by the induced dipole-induced dipole repulsion, since the value of this repulsion at any reasonable argon-argon distance was too small to nullify the van der Waals attraction. A theory was therefore advanced in terms of close packing of argon atoms on the ice surface, the interatomic distance having such a value that the van der Waals forces would be negligible.

The differential entropies, and hence the thermal entropies, of adsorbed argon and adsorbed water were calculated from the experimental data. From the entropy data the mean vibrational and rotational frequencies of adsorbed water molecule were calculated. The value of the rotational frequency indicated that free rotation was not permissible, but that the water molecules experience a librational motion with a mean frequency of c.a. 400 cm^{-1}.

ACKNOWLEDGEMENTS

The author wishes to express his sincere thanks to Dr. G. L. Kington, who suggested this topic for research, and whose constant advice and encouragement made its completion possible.

Thanks are also due to the British Ceramics Research Association for the award of a bursary enabling this work to be undertaken, and to English Clays Lovering Pochin and Co., Ltd., who supplied the kaolinite.

CONTENTS

CHAPTER I

INTRODUCTION

Marshall (1949) remarked that 'no measurements are available on the differential heats of adsorption on pure clay minerals'. Although there have been a few attempts at determining heats of adsorption on kaolinite in recent years (see, for example, Goates and Bennett, 1957), there have been no calorimetric measurements prior to the presentwork.

In order to understand the surface properties of kaolinite, a knowledge of the crystal structure is required. The problem of the crystal structure of kaolinite was discussed in many publications from the late 19th century onwards, but was not solved until Pauling(1930) suggested the true nature of the kaolinite structure, which was subsequently proved by Gruner (1932) and refined by Brindley and Robinson (1946a).

The structure of kaolinite is now well established, although the composition may vary somewhat from the ideal. The structural formula is $(OH)_8Si_4Al_4O_{10}$, and the structure is composed of a single silica tetrahedral sheet and a single alumina octahedral sheet, combined in a unit so that the tips of the silica tetrahedrons and one of the layers of the octahedral sheet form a common layer (Fig. 1). All the tips of the silica tetrahedrons point

in the same direction, towards the centre of the unit. The dimensions of the sheets of the tetrahedral units and of the octahedral units are closely similar in their a and b dimensions, and consequently composite layers are readily formed, and hydrogen bonding occurs between the oxygen and hydroxyl planes in adjacent units. Consequently, the layers are fairly tightly bound and cleavage is not so pronounced in kaolinite as in other clay minerals. There appears to be no room for penetration of ions or small molecules between the sheets.

The minerals of the kaolinite group, kaolinite, nacrite and dickite, consist of sheet units of the type just described continuous in the a and b directions and stacked one above the other in the c direction. The variation between members in this group is in the way the unit layers are stacked above each other, and possibly in the position of the aluminium atoms in the three positions open to them in the octahedral layer.

In the case of kaolinite itself, Brindley (1951) has investigated the stacking of the unit layers (Fig. 2). Successive unit layers are so arranged that oxygen atoms and hydroxyl groups of adjacent layers approach one another in pairs. This disposition can be obtained in a variety of ways, with the c axis perpendicular to the a b plane or by displacement of one layer relative to its neighbour

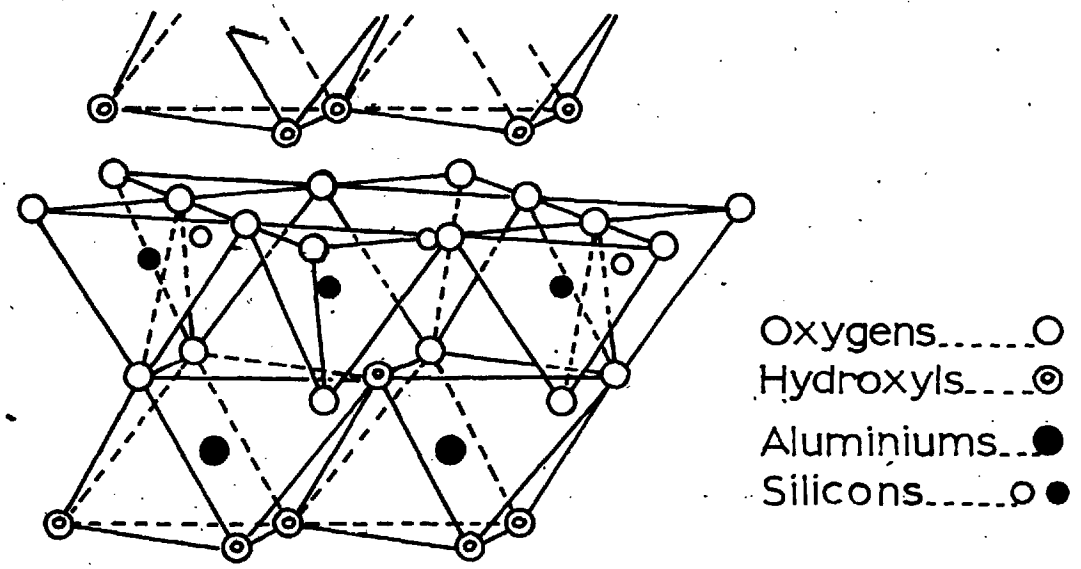

Fig.1. Diagrammatic sketch of the structure of kaolinite, after Gruner (1932).

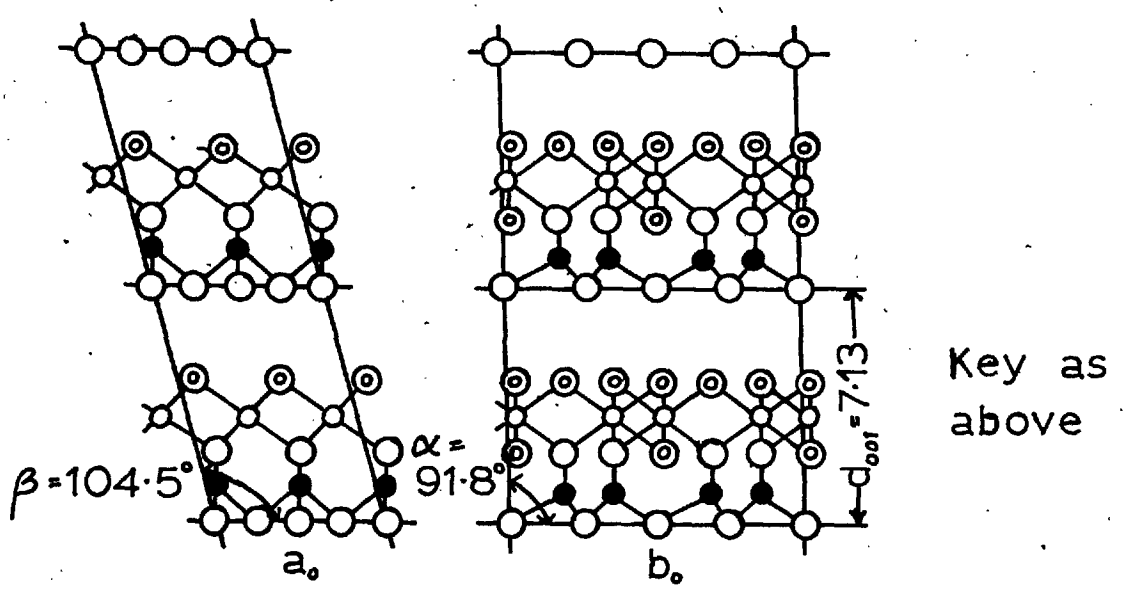

Fig.2. The stacking of unit layers of kaolinite along the a and b axes, after Brindley (1951).

so that the displacement is $na_0/6$ or $mb_0/6$, where n and m are integral and a_0 and b_0 are cell dimensions. This displacement for kaolinite is m = 0 and n = 2.

Brindley and Robinson (1946b), Grimshaw, Heaton and Roberts (1945), and Grim (1947) have all reported a kaolinite mineral of lower crystallinity than that described above. Brindley and Robinson have investigated in detail some examples of rather poorly crystallized kaolinite and state that the structure is highly disordered along the b-axis, with the unit layers randomly displaced by multiples of $b_0/3$. There is also some randomness in the distribution of aluminium atoms among octahedral positions.

The surface of kaolinite therefore consists of a layer of oxygen ions at one basal surface and a layer of hydroxyl groups at the other. The broken bonds which must be formed at the edges probably take up water to form hydroxyl groups. Exchangeable cations are also present but their position is unknown.

In recent years several authors have published isotherms, mainly of water, on natural and various ionic forms of kaolinite. Keenan, Mooney and Wood (1951) prepared ionic forms of kaolinite by electrodialysis of a natural gradation and a fraction of particle size < 0.5 microns, followed by titration to pH 8 with the appropriate

hydroxide. Surface areas were determined by low temperature nitrogen adsorption, and the effect of various cations on water adsorption was investigated. The sodium kaolinite prepared fro. the fraci.onated sample had a surface area of 27.8 metres^2/gm., a water monolayer of 6.10 mgm./gm., and an ion exchange capacity of 4.18 m.equivs./100 gm. All these values are higher than those obtained for the sodium kaolinite used in the experiments described in this thesis, presumably because of the smaller particle size of the fraction used by Keenan et al.

Keenan, Mooney and Wood observed that the adsorption of water per unit surface on lithium kaolinite was independent of the number of Li^+ ions present. This result, however, was based on a comparison of water sorption on lithium kaolinite prepared from (a) the fraction of < 0.5 microns and (b) the natural gradation. The assumption was made that the water sorbed per unit surface area was unaffected by a change in particle size and depended solely on the cations present. Keenan et al concluded that the Li^+ ion is of such a size that it fits into a position in the lattice where its hydration is prevented by steric factors. Therefore, by subtracting the weight of water sorbed on the lithium kaolinite from that sorbed on any other ionic form, they obtained the number of water molecules associated with each exchangeable

ion. This seems to be an oversimplification of the problem, but the value obtained for sodium kaolinite was 1.8 molecules of water per Na^+ ion, which is in reasonable agreement with the estimate of one molecule per Na^+ ion arrived at from the heat data obtained in these experiments (see p. 118).

Orchiston (1954) measured isotherms of water on natural kaolinite, and Goates and Bennett (1957) did the same on a sodium clay of particle size 0.15 to 0.35 microns, prepared by leaching with excess NaCl solution. The latter also calculated the heats of adsorption from the equation

$$\left(\frac{\partial \ln p}{\partial \frac{1}{T}} \right)_w = -\frac{\Delta \bar{H}}{R}$$

The heats of adsorption as $\theta = 0.5 \rightarrow 1.0$ fell from 14.5 to 13.0 k.cal./mole, compared to 13.5 to 12.5 k.cal./mole measured for the same surface coverage in this work. The water monolayer calculated by Goates and Bennett contains 30 per cent less weight of water and, at the completion of the monolayer, the pressure is 20 per cent greater than the corresponding figures of the sodium kaolinite used here.

The nature of water physically adsorbed on kaolinite has been the subject of considerable speculation in the literature. Evidence has been advanced that the

water is in a physical state different to that of liquid water (see, for example, Grim and Cuthbert, 1945), and several theories have been postulated regarding the actual configuration of the water layers.

Hendricks and Jefferson (1938) proposed that the water layer is composed of an extended network of water molecules arranged in a hexagonal configuration. Each side of a hexagon corresponds to a hydrogen bond between two water molecules, leaving one hydrogen atom every two water molecules which is not involved in bonding within the net. The net is therefore tied to the surface of the clay mineral by hydrogen bonding of these hydrogen atoms to the surface oxygen layer. In the case of kaolinite, the surface hydroxyl groups are also available for hydrogen bonding to oxygen atoms in the water layer. A separation of 3.0 $\mathring{A}$ between the oxygen atoms of the water layer is required in order to acheive a geometrical fit to the clay mineral lattice.

Macey (1942) has postulated that the initially adsorbed water has the structure of ice. His theory again depends on a geometrical fit between the water layer and the clay lattice, but in this case the oxygen atoms of the water molecules are 4.52 $\mathring{A}$ apart, and this looser packing would result in a ratio of three water molecules per unit cell area. Hydrogen bonding to the

oxygen and hydroxyl surfaces of kaolinite occurs as before.

Barshad (1949) has suggested another concept based on careful dehydration measurements with montmorillonite, the surface of which is composed of two basal planes of oxygen ions exactly similar to the oxygen surface of kaolinite. He proposes that at low states of hydration the water molecules form tetrahedrons with three oxygen ions of the silica tetrahedrons. The hexagon thus formed is reduced in radius at higher states of hydration and the water molecules adopt a position directly above an oxygen ion. Finally, at still higher states of hydration the water molecules fill the centres of the hexagonal water rings, and the centres of the hexagonal oxygen rings of the silica tetrahedrons not occupied by exchangeable cations.

On the basis of the cross-sectional area occupied by each adsorbed water molecule, which has been calculated from the present work by the application of the B.E.T. theory, Macey's ice concept is unacceptable (see p. 115). All three theories neglect the influence of the exchangeable cations, and since it has been shown that the initial high heats of sorption of water are attributable to the presence of cations (p. 118) this must be considered as a serious omission. The heat data indicate that in the water monolayer, one water molecule in five is associated with a cation. It is difficult to reconcile this conclusion

with the above theories of a regular hexagonal network of water molecules.

Water sorbed onclay minerals has been considered denser and more viscous than ordinary liquid water. The specific characteristics of this water which distinguish it from ordinary water are probably restricted to relatively short distances from the clay-particle surfaces, generally of the order of three to ten molecular layers of water. Terzaghi (1928) has attempted to explain the nature of the initially adsorbed water on the basis of the dipole character of the water molecule. He considers the water layers to be highly oriented, but the degree of orientation decreases with increasing distance from the surface because of the thermal energy of the water molecules. No evidence for the existence of this so-called non liquid water has been found during the present study however.

Williamson (1951) has suggested that the high density of sorbed water which has been reported may be due to a 'tightening' of the water structure in the vicinity of the cations. He also states that it is probable that while some water hydrates the cations, other water is held directly on the basal plane of the clay mineral. This theory is substantiated by the heat data obtained during these experiments (see p. 119).

In the theory of intermolecular forces there are

four types of forces normally considered:

(i) dispersion forces,

(ii) repulsive forces,

(iii) polarisation forces,

(iv) electrostatic interaction between permanent electric moments.

These forces are also operative in the physical sorption of a molecule on a surface but the part played by each is normally complicated and often obscured, by the heterogeneity of the surface. Thus, for example, the effect of the van der Waals attraction between sorbed molecules which must occur if the molecular separation is close to the equilibrium separation is seldom observed as a maximum in a plot of the differential heat as a function of concentration. It is usually assumed that the lateral interaction between the adsorbed molecules is 'smeared out' by the heterogeneity of the surface (see, for example, Beebe, Millard and Cynarski, 1953).

Attempts to explain the heterogeneity of any solid involve one or other of three possibilities.

(1) The decrease in the heat of sorption is due to active sites existing a priori in the sorbent surface. These sites have been identified with, for example, edges and corners, lattice defects and grain boundaries.

(2) The heterogeneity is due to electrostatic rather

than dispersion forces, i.e. the interaction of the molecular charge distribution with the surface electric field varies with concentration because the magnitude of the interacting field depends on the position of the sorbed molecule above the lattice. The electrostatic forces arise from field-induced moment (polarisation), field-dipole and field quadrupole effects.

(3) A decrease in the heat of sorption may be produced by repulsive forces between sorbed molecules. Usually, however, repulsive interactions can only account for a fall in the heat curve at high values of θ.

Thus, the factors which contribute to the fall in the heat of sorption with coverage have received precise expression but the problem as applied to real cases is still largely unsolved. In this study, however, it has been shown that the sites of high energy on the sodium kaolinite lattice are associated with electrostatic rather than dispersion forces, and are probably due to the presence of exchangeable cations (see p. 118). The high initial heats of sorption of argon and nitrogen observed on the sodium kaolinite surface disappear completely when this surface is covered with two molecular layers of water, because the ice surface forms a much more homogeneous sorbent and the active sites of the kaolinite lattice are covered.

When a polar molecule is physically sorbed on to the surface of an ionic solid all four types of the forces listed above are involved. The total interaction can be experimentally determined as the heat of sorption but an absolute calculation of any single interaction is impracticable for even the simplest system.

In these experiments two surfaces were involved, (a) sodium kaolinite and (b) the ice surface, produced by freezing two molecular layers of water on to the sodium kaolinite. The calculation of the electrostatic field above the ice surface followed the method used by Orr (1939) to calculate the field above ionic crystals such as potassium chloride. It involved a summation of some 70 molecules followed by an integration to infinity (see Appendices I and II), and the knowledge of the field made it possible to interpret the heat data more fully in terms of the interaction of sorbed molecules with the field.

Three sorbate molecules were used, (a) argon, which is non-polar, (b) nitrogen, which has a permanent quadrupole moment and (c) water, which has a permanent dipole moment. By combining the heat data obtained from the physical sorption of these molecules on both surfaces it has been possible, in some cases, to attribute a part of the total heat of sorption to a particular interaction. In this way, the distance of approach of the sorbed argon

and nitrogen molecules to the ice layer was calculated. An attempt to explain the heat data for argon on the ice surface showed that the induced dipole-induced dipole repulsion was too small to account for the fall in the heat curve, and a theory in terms of close packing of argon was postulated. The importance of the contribution of the nitrogen quadrupole moment to the heats of sorption of nitrogen on both surfaces was also shown.

CHAPTER II.

EXPERIMENTAL.

2.1. Materials.

2.1a. The Sorbent.

The sorbent used in these investigations was supplied by English Clays Lovering Pochin and Co., Ltd., from kaolinite mined in Cornwall. The purest kaolinite possible was obtained by sedimentation of the naturally occurring mineral, from which the fraction of particle size 0.5 to 2.5 microns was taken. In order to obtain a precisely defined surface, particularly with regard to exchangeable ions, the kaolinite was electrodialysed and the so-called hydrogen clay then titrated to pH 8 with NaOH solution.

The electrodialysis cell (Fig. 3) consisted of a polythene beaker A and two Soxhlet extraction thimbles, one 90 x 123 mms. and the other 30 x 100 mms. The smaller thimble C became the anode compartment, the suspension was placed in the larger thimble B, and the polythene beaker became the cathode compartment. Support was provided where necessary by pieces of polythene so that the introduction of extraneous ions was kept to a minimum. The cathode D consisted of a spiral of nickel wire wound round the outside of the large thimble. The anode E was constructed from two pieces of platinum foil, each 1 sq. inch, bent into a

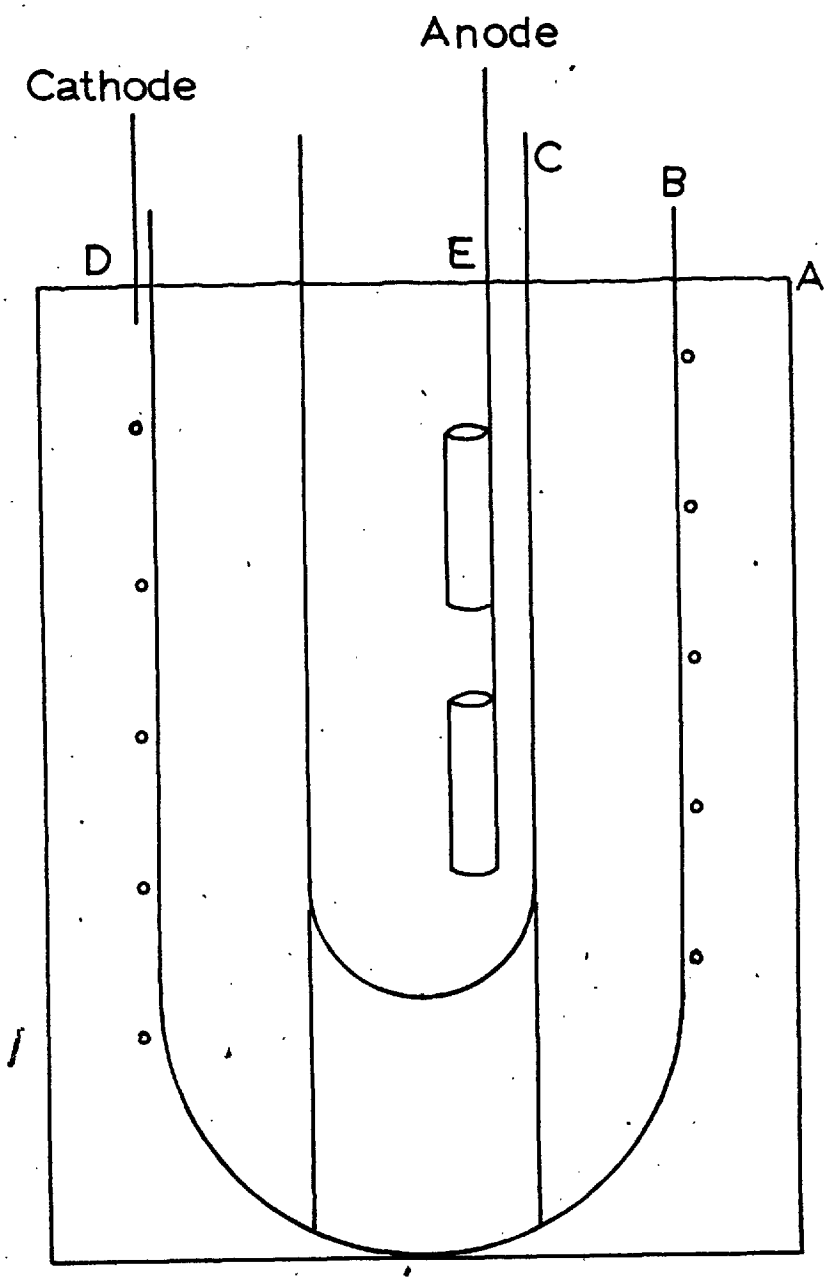

Fig. 3.

cylinder and spot welded on to platinum wire. A continuous flow of distilled water (about one drop per second) was passed through the cathode from a 5 litre aspirator and overflowed from the polythene beaker.

A voltage of 220 volts d.c. was used and prior to the electrodialysis of a kaolinite suspension this voltage was applied overnight with distilled water only in the cell in order to remove any ionisable impurity. A mirimum value of about 20 milliamps was observed when electrodialysing a sample of kaolinite and as well as the current, the pH of the supernatant liquid above the suspension and the sodium ion content of the cathode compartment (measured by flame photometer) were plotted against time. The suspension tended to settle at the bottom of the large thimble but it was thought that the only affect of stirring would be to shorten the total electrodialysis time required to reach the end point.

1 Kgm. of the natural kaolinite was first rolled in a drum mill for $2\frac{1}{2}$ hours in order to obtain a homogeneous mixture from which all samples used for these experiments were taken. The kaolinite was stored in a large stoppered porcelain jar.

Following the method of Johnson and Norton (1941) a preliminary sample of 60 gms of kaolinite in about 600 mls of distilled water was electrodialysed in order to gain

experience for the preparation of the sample to be used in the calorimeter. The hydrogen kaolinite thus obtained was washed out of the cell with distilled water and the resultant suspension divided into two parts.

The first part was used to obtain a complete titration curve with NaOH solution (Fig 4). The shape of this curve agreed remarkably well with that obtained by Johnson and Norton in spite of the difference in conditions, the latter allowing the mixture to stand for two days before measuring the pH. A sharp rise in pH from 7.5 to 9.0 indicated pH 8 as a suitable end-point for the titration when preparing the sodium kaolinite.

The second part of the hydrogen kaolinite suspension was titrated to pH 8 and kept in a desiccator over NaOH pellets to prevent reaction with atmospheric CO_2. Overnight the pH fell to 6.8 and the titration was repeated until pH 8 was maintained overnight. The suspension was then centrifuged, the supernatant liquid decanted and the sodium kaolinite dried at 70°C.

It was evident from the above observations that some slow reaction occurred between the hydrogen clay and the sodium hydroxide. Gregg, Parker and Stephens (1953) have suggested that this slow rate of reaction during titration may be due to the presence of a film of presumably amorphous material on the surface of the electrodialysed clay.

Fig. 4.

Titration of Electrodialysed Kaolinite with NaOH.

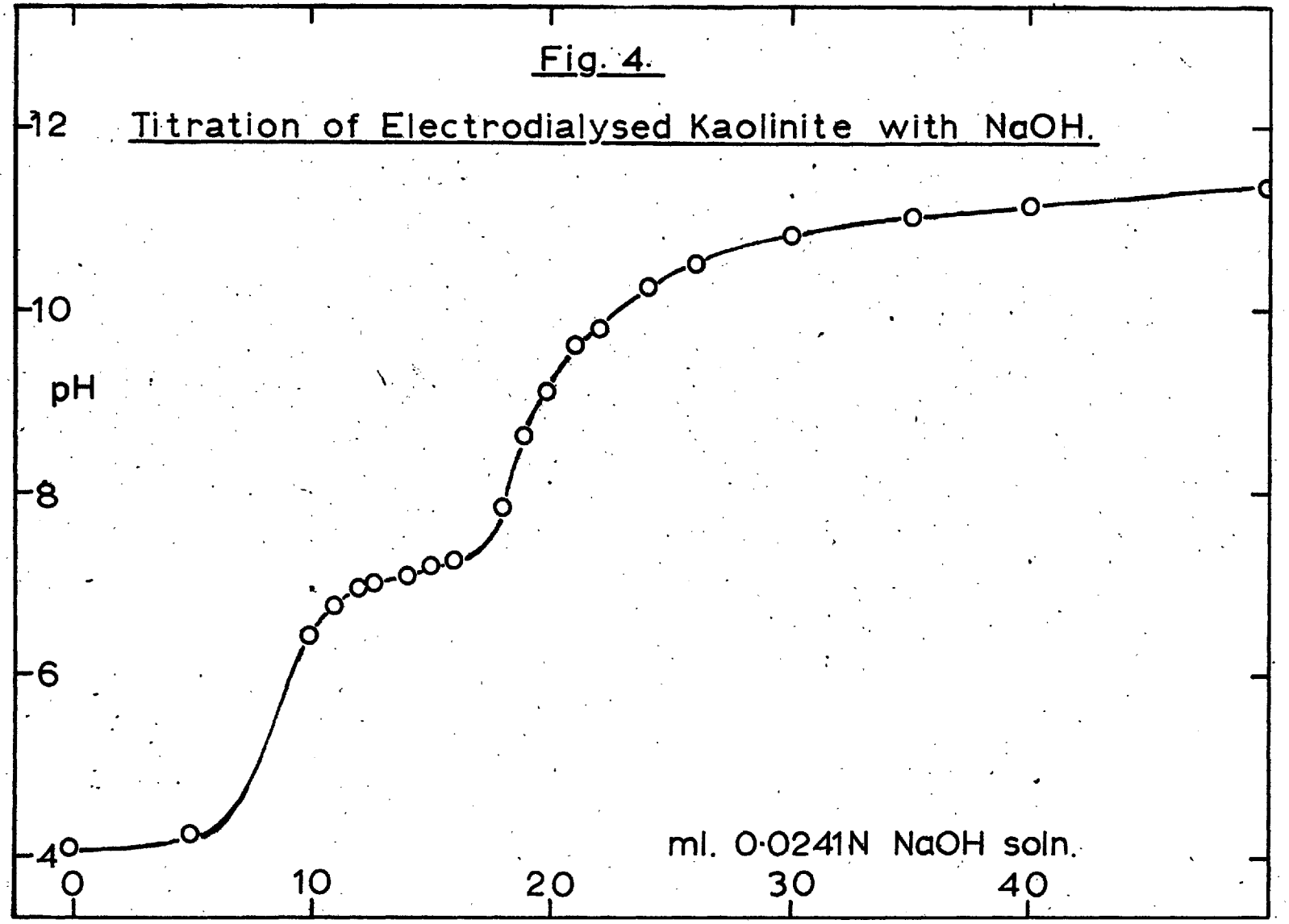

18

A second sample of 60 gms. of natural kaolinite in 600 mls. of distilled water was electrodialysed exactly as before. 220 volts d.c. was used and the current, pH and sodium ion concentration were observed as above. Distilled water was passed through the cathode compartment. Considerable fluctuations were observed in current readings and it was not found possible to obtain consistent values of pH. This may have been due to the method used which consisted of pipetting 50 mls. of the supernatant liquid from above the suspension. Consequently liquid flowed into the central compartment from the anode and cathode and the value of the pH was affected especially since the anode contained a considerable concentration of anions. The best indication that the end point had been reached seemed to come from the concentration of sodium ions in the cathode compartment which fell to a minimum of 0.1 parts per million.

The electrodialysis was allowed to proceed for 235 hours. The flow of distilled water was then stopped, and the current fell from 40 milliamps to 20 milliamps in a further 5 hours. The hydrogen kaolinite was washed out of the cell with distilled water and the suspension titrated to pH 8 with NaOH solution and stood overnight in a desiccator containing NaOH pellets. The titration to pH 8 was repeated as before until the value was maintained overnight. This took 11 days and the final pH was 8.34. The suspension was then centrifuged for 4 hours decanted and

dried to constant weight at 70°C. From the total weight of sodium kaolinite obtained the exchange capacity was calculated to be 3.00 milliequivs per 100 gms kaolinite. After its removal from the centrifuge bottles the sodium kaolinite was lightly crushed and powdered with a nickel spatula. The total weight of sorbent packed into the calorimeter was 15.86 gms.

X-ray diffraction patterns of the natural and of the sodium kaolinite, prepared as above, were obtained on the Guinier camera in this department. No difference could be detected between the two samples indicating that the process of electrodialysis had not affected the kaolinite structure.

2.1b. The Sorbates.

Argon, nitrogen, hydrogen and water have been used. The gases were supplied by British Oxygen Company in sealed pyrex glass bulbs. The argon was stated to be spectrally pure as was the helium used to give thermal conductivity in the calorimeter. An approximate analysis of the gases used, given by B.O.C., was as follows:

a) Nitrogen.

Nitrogen	99.9%
Oxygen	0.05%
Carbon dioxide	5 v.p.m.
Hydrogen	1 "
Rare gases	7 "

b) Argon.

Argon	99.95%
Nitrogen	0.05%
Oxygen	5 v.p.m.
Carbon monoxide	5 "
Hydrogen	0.5 "

c) Hydrogen.

Hydrogen	99.9%
Oxygen	0.05%
Nitrogen	0.05%
CO_2, CO etc.	40 v.p.m.

In the case of the water the main problem was to remove dissolved air and carbon dioxide since these would markedly affect the low pressure region of the isotherm. A 100 mls. round bottomed flask containing about 30 mls. of distilled water was sealed on to the main line via a liquid air trap. The latter prevented diffusion of mercury vapour into the water supply. The water was frozen in liquid oxygen and the air remaining above the ice pumped out. A good vacuum was obtained after about five minutes pumping. The ice was then allowed to melt and the air which had been trapped passed into the gas phase. The freezing, pumping and melting procedure was repeated twice more with liquid oxygen and twice with solid carbon dioxide as the refrigerant. Complete removal of air was proved by checking the vapour pressure of the water with a mercury manometer. With the

water supply at 21.5°C the value observed was within 1% of the accepted value for this temperature.

2.1c. The Mercury.

Most of the mercury used was supplied by F. W. Berk and Co. Ltd. and stated to be 'redistilled A.R.' Mercury from any other source was purified by (1) filtration (2) bubbling with 5% nitric acid, (3) washing until acid-free and drying at 110°C. (4) distilling in an electrically heated vacuum still in which the mercury to be distilled formed part of the circuit.

2.2 Apparatus (Fig 5).

'Pyrex' glass was used throughout and whenever possible wide bore tubing and taps were used to give high pumping speeds.

2.2a. The Pumping System and Main Line.

The pumping system consisted of an Edwards' Speedivac two stage rotary oil pump backing a single stage divergent nozzle type mercury diffusion pump. The latter was heated by a 250 watt strip heater and lagged with two layers of $\frac{1}{4}$" asbestos rope. The oil trap A prevented oil sucking back through the apparatus in the event of a power failure. The liquid air trap B, which could be emptied when necessary by breaking its narrow tip, protected the oil and mercury of the pumping system from contamination by condensable impurities. A simple mercury cut-off C

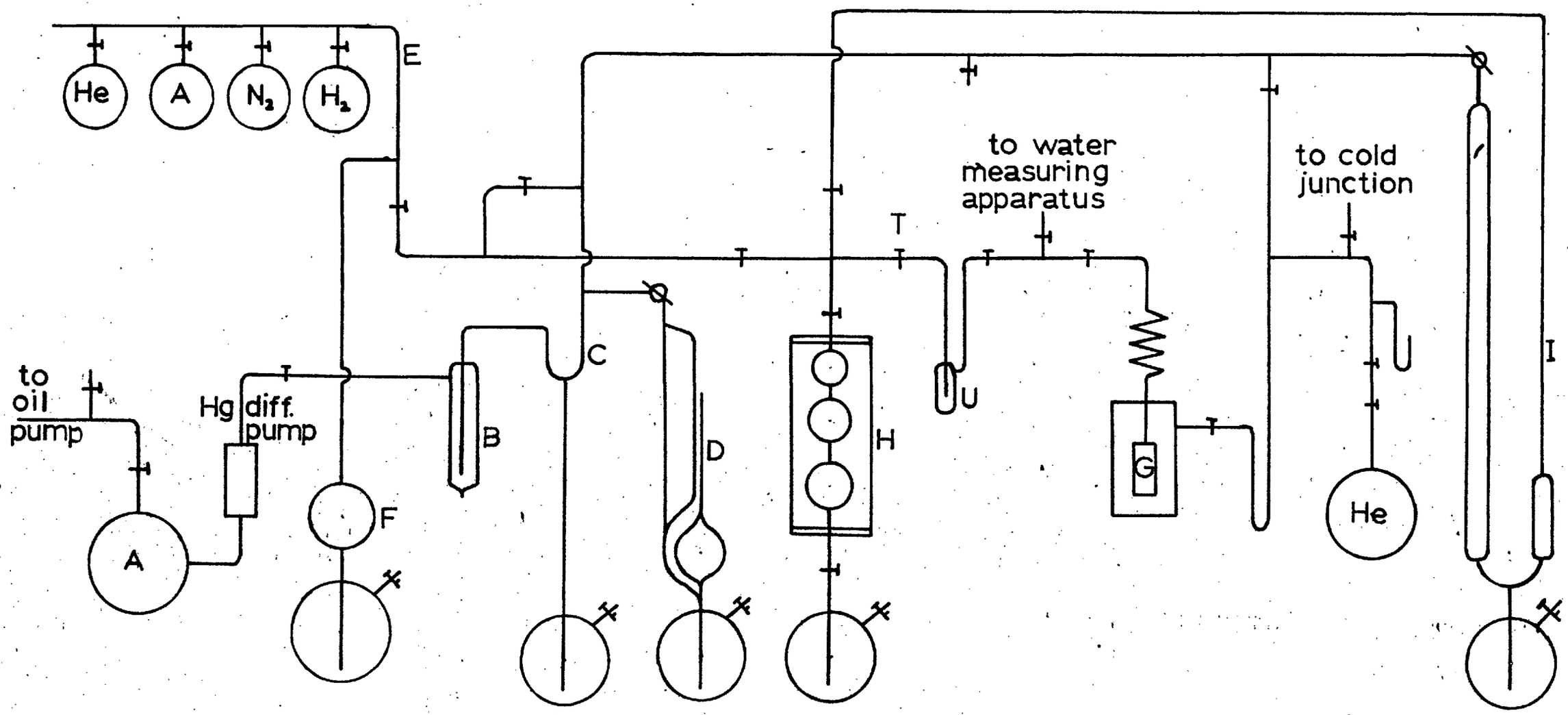
He
A
N₂
H₂
E
to water measuring apparatus
to cold junction
T
to oil pump
Hg diff. pump
B
C
D
H
U
G
I
F
A
He

Fig. 5.

enabled isolation of the rest of the apparatus from the pumping system in order to determine 'leak-rates'. It was also valuable in the detection of leaks in metal parts during construction of the apparatus.

The Macleod gauge D had two pumping arms, one of roughly 12 mm bore and the other of capillary tubing with a mean diameter of 0.608 mms determined by the mercury slug method. The closed capillary consisted of 22 cms of the same capillary tubing. The bulb volume was determined by mercury weighing as 255 mls. The gauge was not intended as an accurate measuring instrument but gave an indication of the vacuum in the system at any time and was used to determine leak rates. A scale covering the range 1×10^{-2} mm Hg to 1×10^{-6} mm Hg was made from graph paper on stiff board. This was permanently in position so that readings could be rapidly observed. The ultimate vacuum determined with this gauge was 1×10^{-6} mm Hg and the 'leak-rate', i.e. the rate of build-up of pressure in the closed system, about 1×10^{-5} mm Hg per hour.

There was an Edwards' Speedivac single stage rotary oil pump used as a source of 'low' vacuum to lower the mercury from gauges etc.

2.2b. The Gas Storage.

Gases were supplied from the gas manifold E into which the B.O.C. cylinders were sealed via a tap. The compressor F enabled maximum use of the cylinder gases and

was particularly useful when higher pressures were required towards the end of a sorption run. It was also used as a storage bulb when helium was present in the calorimeter G to avoid contamination of the cylinder gases.

2.2c. The Gas measuring System.

To determine the volume of gas sorbed in an increment it was necessary to have an exact knowledge of the volume the temperature and the pressure in all parts of the gas phase, before and after exposure to the sorbent.

The fundamental calibrated volume in the gas measuring system was the gas burette H and from this the volume of any other part of the system could be determined (see p. 57).

Most of the gas line was at room temperature and fine mercury-in-glass thermometers were used to measure the temperature in various parts of the apparatus. These were all 0-50°C in range and were checked against the departmental N.P.L. thermometer between 15° and 30°C the expected variation in room temperature.

The gas burette was surrounded by an air jacket to reduce temperature fluctuations in this relatively large volume. A 0-50°C thermometer was suspended centrally within the jacket. Two other 0-50°C thermometers were distributed around the gas lines which in order to keep dead-space volumes to a minimum were entirely of 2 mm. capillary connected by 3 mm. taps. During later runs the

temperature of the liquid nitrogen bath surrounding the calorimeter was measured by an oxygen vapour pressure thermometer but for earlier, less-accurate runs this temperature was assumed to be 77.5°K.

Pressure measurements were made on a precision manometer I carefully mounted to reduce vibrations. The manometer was constructed from 16 mm. 'Veridia' tubing. On the gas side this wide bore tubing was connected to 2 mm. capillary tubing to reduce the dead-space. When taking a pressure reading the mercury level was adjusted so that the meniscus on the gas side was within the 6 cms. of 'Veridia' tubing at the bottom of the gas side arm. The manometer tubes, which had been carefully cleaned in hot chromic acid solution and washed thoroughly in distilled water, were mounted in split brass bearing blocks on a heavy $\frac{1}{4}$" steel plate. This was fixed to a $2\frac{3}{8}$" diameter steel pipe rigidly clamped between the roof and floor of the laboratory. The steel plate also formed the back of a box structure surrounding the manometer to reduce temperature fluctuations. The sides of this box were of wood lined with aluminium which reduced the vertical temperature gradient in the box to about 0.2°C. The front of the box was of plate glass. Hinges at one side of the steel plate allowed the box to be swung aside giving access to the manometers. The mercury reservoirs were supported on a shelf of $\frac{1}{4}$" steel welded to the pipe. A reference mark was fixed to the outside of the gas side of the

manometer and gas phase volumes calculated with respect to this. After setting the mercury levels to the required position, well-formed menisci, necessary to allow for capillary depression, were obtained by exerting a small additional pressure on the mercury surface of the reservoir by closing a screw clip on a closed rubber tube attached to the reservoir bulb. With the rigid support for the manometer described above a steady, vibration-free surface was obtained. General illumination in the box was afforded by a shaded 40 watt tubular lamp. The backgrounds of individual menisci were illuminated with a galvanometer spotlight using a 12 volt, 24 watt bulb. The mercury levels were read with a cathetometer, made by the Precision Tool and Instrument Co., Ltd., mounted on a triangular steel base about 1 metre from the manometer. Before taking readings the cathetometer bar was made vertical using the spirit level on the telescope. In fact the bar was not quite straight and the telescope therefore not horizontal at all levels. The spirit level was therefore calibrated and by observation of the bubble position a correction was applied to each reading of the mercury level.

2.2d. The Water-measuring System (Fig. 6).

Measurement of small quantities of water by the volumetric method used for gases presents problems because of the adsorption of water by the walls of the glass vessel at room temperature. Gas phase imperfection for water at 25°C

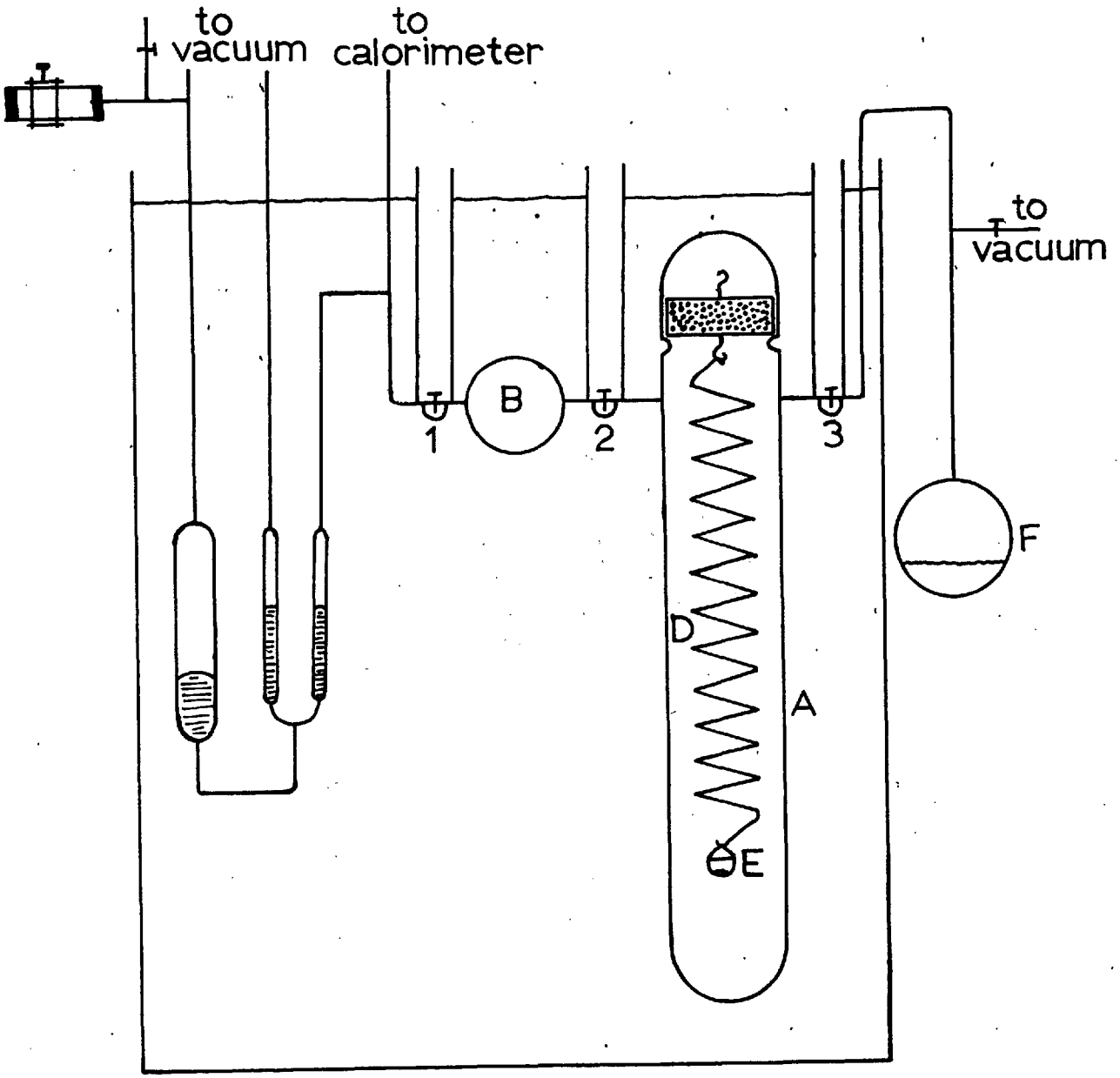
to
vacuum
to
calorimeter
to
vacuum
B
1
2
3
F
D
A
E

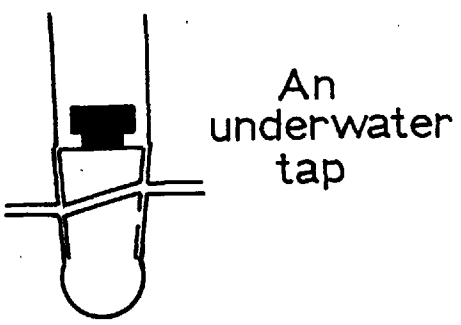
An
underwater
tap

Fig. 6.

was negligible. In order to minimise the uncertainty in the measurement of increments of water a gravimetric method was devised which entailed only a small correction, calculated volumetrically, for the water vapour in the line to the calorimeter (see p. 60)

The apparatus was designed to measure the extension of the spring before and after admitting the increment so that the weight lost from the saturated solution could be calculated. The presence of the saturated KBr solution ensured that, the temperature being constant, the vapour pressure between taps 1 and 3 was the same during both measurements and the effect of the vessel walls was therefore eliminated. The weight sorbed in the increment was then equal to the weight lost from E minus the increased weight in the vapour phase (calculated volumetrically).

The apparatus consisted of a balance case A, 3 cms. in diameter and about 65 cms. long. The balance case was connected to a 100 mls. bulb B via one of the three under-water taps used. This volume was calculated to give a measurable deflection on the galvanometer when the water vapour it contained was exposed to the sorbent.

The vapour pressure of the water above the sorbent was measured by the mercury manometer C, in which both arms were constructed from the same piece of 10 mm tubing. A fixed mark, made from fine-gauge wire, was attached to the gas side arm and all volumes determined with

respect to it. Well-defined menisci were obtained, as with the precision manometer, by exerting a small additional pressure on the mercury reservoir by means of a screw clip attached to sealed rubber tubing. The mercury levels were read by the same cathetometer as was used with the precision manometer.

The balance case was first tested for optical distortion by fixing a pointer inside it and observing the cathetometer reading for various positions of the glass tubing. The maximum deviation from the mean value was 0.003 cms, indicating that the optical distortion was negligible.

The weight of water in an increment was measured by observation of the change in length of a fine silica spring D suspended within the balance case. This was supplied by Thermal Syndicate Ltd. who quoted the following properties:

Maximum load	100 mgms.
Sensitivity(approx)	460 cms/gm.
Extension	57 cms.

The spring had been stored in a light oil. It was cleaned by washing it three times in benzene and then allowing this to evaporate in the air. This was followed by dipping the spring into hot dichromate/sulphuric acid cleaning mixture and washing it thoroughly, several times, in distilled water. Finally it was hung in the air to dry.

The spring, when in situ, was suspended from a glass hook which was itself attached to a sealed glass container filled with lead shot to ensure stability. The latter rested on an annular constriction near the top of the balance case. As a check on vibration the spring was placed in situ with a 65 mgm. weight suspended from it. No vibration was observed.

The spring was calibrated with nine small riders made from 24 gauge copper wire and covering the range 47.2 to 98.15 mgms. The calibrations were done at 23.2°C. 25.0°C, 28.2°C, and a recheck with 3 or 4 of the weights at 25.0°C showed that no hysteresis had occurred during the calibration. The effect of change of temperature on the extension was only about 0.05% for 3°C. A plot of extension against weight for the 25°C calibration produced a smooth curve not deviating greatly from a straight line. An arbitrary straight line $y = mx + c$ was therefore drawn through the calibration points at 63.65 mgms. and 98.15 mgms. and the slope and intercept calculated, $m = 0.4569$ cm./mgm. and $c = 11.446$ cm. Therefore, for any value of the extension y, the uncorrected weight x could be calculated. A graph showing the deviation of the calibration points from this straight line (Fig. 7) gave a smooth curve with a maximum of 0.20 mgms. The correction corresponding to any extension was read off from this graph and subtracted from x to give the actual weight equivalent to the given extension.

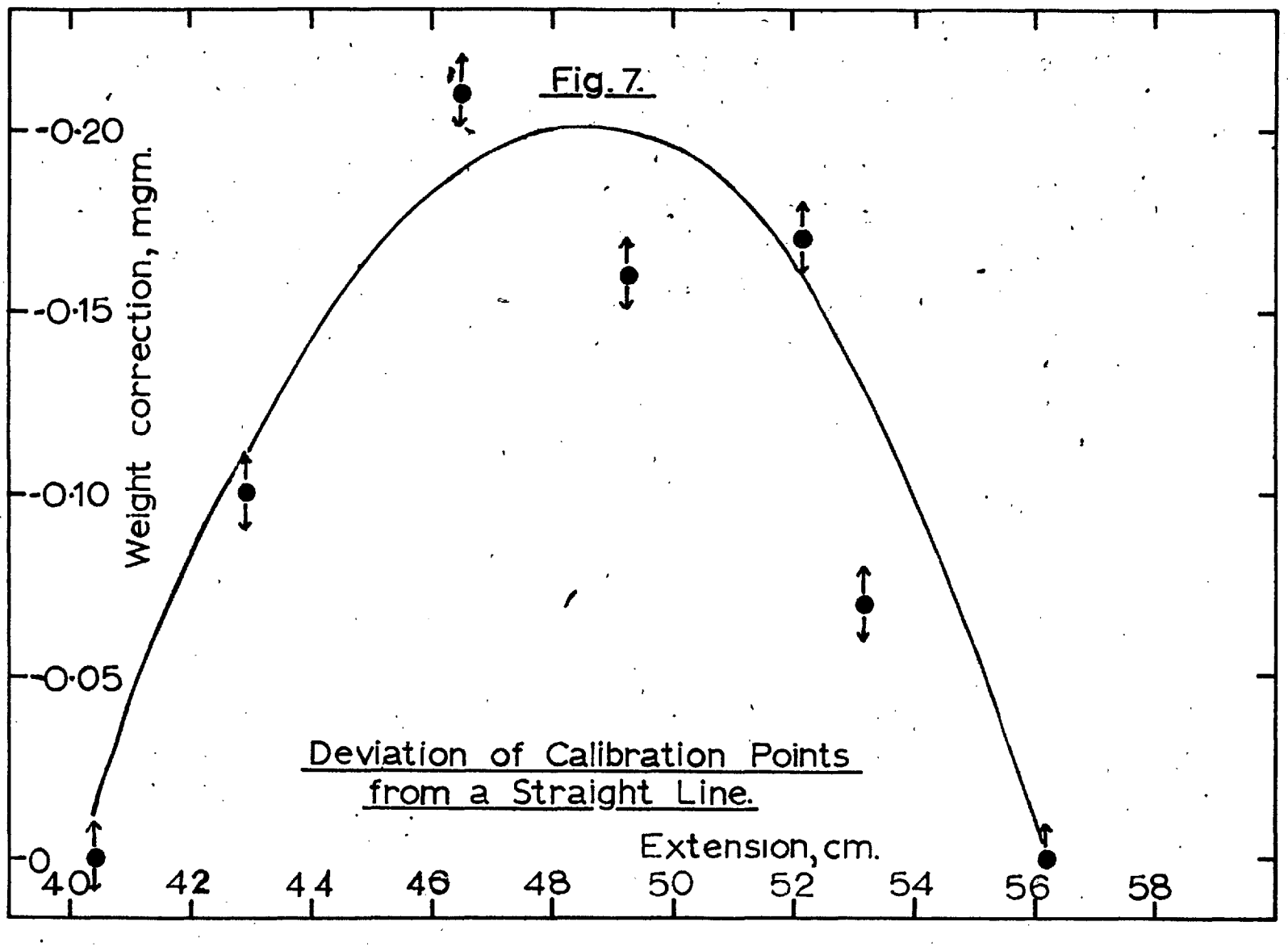
Fig. 7.
-0·20
-0·15
-0·10
-0·05
0
Weight correction, mgm.
Deviation of Calibration Points
from a Straight Line.
Extension, cm.
40
42
44
46
48
50
52
54
56
58

The spring was now sealed into its case with a tiny glass bucket E, weighing 62.2 mgms. and containing about 13 mgms. of AR. potassium bromide crystals (dry weight), hung from the bottom. A saturated solution of potassium bromide contains about 40 gms. KBr in 100 gms of saturated solution. Therefore up to 19 mgms of water could be added to the bucket without the solution becoming unsaturated. This amounted to a total weight of 94 mgms.

The purpose of the saturated solution was to obtain a constant vapour pressure in the balance case and 100 mls. bulb. Potassium bromide was chosen because its saturated solution had a suitable vapour pressure (84% of that of water) and because it formed a saturated solution after only a few hours exposure to the water supply.

The whole of the measuring apparatus, including the manometer, was immersed in a water thermostat constructed from $\frac{3}{8}$" perspex in the workshops of this department. The water bath contained a stirrer about 26" long with three 3" paddle wheels distributed about its length. This was driven by a $\frac{1}{25}$ H.P. Sun Electric Motor, 230-250 volts, 3500 R.P.M. controlled by a variac. Temperature control was effected by a benzene / mercury thermoregulator which controlled a 60 watt bulb covered with aluminium foil. The thermostat bath contained a 0-50°C mercury-in-glass thermometer. The bath having been set at 25°C no variation in temperature was observed. A variation of 0.05°C could have been seen on the

thermometer and it was concluded that thermostatting was effective at least within this limit and probably better. The bath also contained a booster heater of about 1 kilowatt used to bring the bath to 25°C after filling. To reduce corrosion of rods and clamps a few grams of sodium chromate were added to the water and proved very effective.

The water supply to the balance case came from a 100 mls. round bottomed flask F containing about 30 mls of water. This was suspended outside the thermostat tank and the water was degassed as described on p.21.

A secondary water measuring system was built for the determination of more rapid isotherms by the adsorption of larger increments than were possible by the use of the silica spring. This consisted simply of a piece of precision bore capillary tubing 0.5 mm. in diameter into which an unbroken column of water was condensed from a round bottomed flask. Dissolved air had previously been removed from the water as described in 2.1b. The water in the capillary tubing was kept below room temperature to prevent condensation in the line.

The principle of the method was to note the upper level of the column of water, expose it to the sorbent for a few minutes, shut the tap and allow it to equilibrate at the same temperature so that the vapour pressure remained the same. The level was again observed and the weight sorbed was then equal to the weight lost from the column of water

(calculated from a knowledge of the volume change, $\pi r^2 h$, and the density) minus the increased weight in the vapour phase (calculated from the dead-space volume and the pressure).

Using 0.5 mm. diameter tubing, a column of water 12 cms. long was equivalent to a weight of about 0.1 gms. or about two molecular layers on the sorbent in the calorimeter. Therefore an increment which produced a change in length of 2 - 3 cms. could be measured with an accuracy of 3 - 4% using a glass backed scale, and considerably more accurately using a cathetometer.

This secondary system was successfully used to measure the total weight of water sorbed (95.2 mgm.) prior to runs 15 and 16 (at liquid oxygen temperature). A later attempt to use this method however, was unsuccessful because of the extreme difficulty in obtaining an unbroken column of water which filled the lower end of the capillary. At every attempt a bubble, presumably of water vapour, formed at the bottom of the capillary and attempts to remove it invariably failed. It has been found that the difficulty can be overcome by the use of wider tubing, with a resultant loss of accuracy, of course. The author also feels that the problem could be overcome by fitting a connection to vacuum via a vacuum tap at the lower end of the capillary tube. It was found comparatively easy to obtain a continuous column of water in the upper parts

of the tube, and this column could then be pulled down into position at the bottom of the tube.

2.2e. The Calorimeter. (Fig. 8)

The calorimeter contained the sample of sodium kaolinite on which all calorimetric heats of sorption and accurate sorption isotherms were determined. During sorption runs (except water sorption) it was immersed in a large Dewar of liquid nitrogen. The Dewar was 8" in diameter and 23" deep. It had a fairly high evaporation rate (poor vacuum) and steady boiling of the liquid nitrogen took place. Although this increased the amount of liquid nitrogen used it had the advantage of greatly reducing the temperature drift of the bath due to superheating.

During water sorption the calorimeter was immersed in an oil bath thermostat 8" in diameter and 27" deep. The oil used was Shell Risella Oil 17, which was of low viscosity and effectively overcame the problem of corrosion which would have arisen if a water bath had been used. The oil bath contained a stirrer 26" long with three 3" paddle wheels distributed about its length. This was driven by a Siemens 110 volt. d.c. motor, $\frac{1}{6}$ h.p. Temperature control was effected by a benzene/mercury thermoregulator which controlled a 40 watt bulb dipping into the oil.

The oil bath contained a 0-50°C mercury-in-glass thermometer on which no change was detectable when the bath

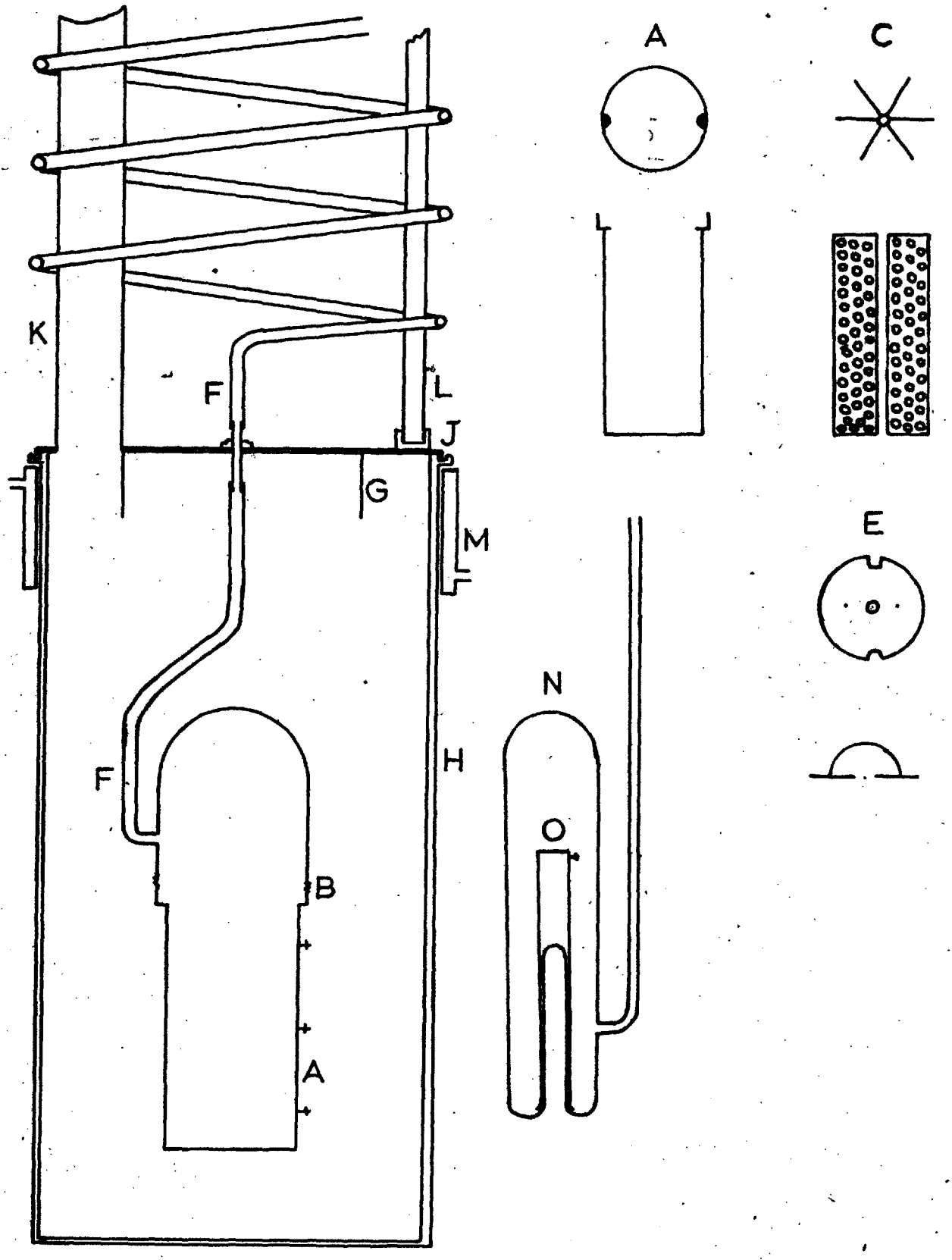

Fig.8.

was controlling at 25.0°C. The calorimeter thermocouple was used to check the effectiveness of the thermostatting by pumping the helium from the calorimeter outer jacket (isolating the calorimeter from temperature fluctuations) while helium remained in the cold junction. A trace was then recorded so that any bath temperature fluctuations would be seen as a change in temperature of the cold junction relative to the calorimeter junction. Fluctuations on this trace were < 1 mm., which was equivalent to a temperature control of $\pm$ 0.005°C.

The calorimeter was protected both inside and outside against mercury amalgamation by liquid nitrogen traps. It consisted of a copper pot A which in order to keep the heat capacity of the metal parts to a minimum, was constructed from .010" copper. The base and thermocouple screws were made as light as possible and were silver soldered in position, since the calorimeter had to withstand a baking-out temperature of 200°C. At the top the copper pot was silver soldered to a ring of 'Kovar' B which carried a graded seal through to 'Pyrex' glass.

At the centre of the calorimeter was a narrow copper tube C about $\frac{1}{8}$" in diameter intended to house the electric heater. The tube was fitted with six peripheral copper vanes, punched with holes to reduce their heat capacity, which distributed the heat throughout the calorimeter. The tube was also drilled with very small

holes to enable the free flow of gas during gas sorption. A small copper cap E fitted over the top of the vanes to prevent sorbent being scattered on evacuation of the calorimeter.

The sorbent was packed between the vanes and the calorimeter finally held 15.86 gms. of sodium kaolinite. The heater was wound non-inductively on a piece of brass wire and consisted of about 14' of 2.951 ohms per foot glass insulated constantan wire. Since oil is used in spinning on the glass insulation the heater was washed several times in A.R. benzene. This was finally allowed to evaporate and the heater baked at 300 - 350°C in vacuo. The heater leads were spot welded to nickel through beaded tungsten to nickel again. Two side arms each containing a beaded tungsten seal, came out from the glass dome of the calorimeter on either side of the gas inlet tube F. In this way the wires were brought from the interior of the calorimeter while still enabling a vacuum to be maintained. On the outside of the calorimeter the nickel wire was silver soldered to .004" copper wire covered with silicone varnished double silk insulation. This in turn was soft soldered at the bottom of the cooling cylinder G to .010" copper wire with double silk insulation painted with impregnating varnish not intended to withstand high temperatures.

The outer jacket H of the calorimeter was made from a length of stainless steel tubing 2" in diameter 14½"

long and about $\frac{1}{8}$" thick. The base was also of stainless steel and was welded in position. The outer jacket lid J was made of brass and, for ease of access to the calorimeter, was held in position by Woods metal. The calorimeter gas inlet tube was taken through the centre of the lid by means of a glass-Kovar-glass seal. To one side of the lid was a $\frac{1}{2}$" diameter, thin walled copper nickel tube K, through which the outer jacket was evacuated. This and a Tufnol rod L on the other side of the lid supported the whole assembly which was hung from a special brass clamp. The connection between the copper-nickel tube and the pumping system was made by means of a piece of glass tubing which was a sliding fit over the metal tube. The join was sealed with picein wax. When equilibration of the calorimeter with the liquid nitrogen bath was required a small pressure of helium was let into the outer jacket. A small u-tube or 'click' manometer served to indicate the helium pressure in the jacket.

Under the outer jacket lid was attached a copper cylinder G 1" deep. The heater and thermocouple leads, which were brought into the outer jacket via the copper-nickel tube, each had three complete turns wound round this cylinder and were varnished securely to it. In this way the heat leak to the calorimeter down the leads was minimised.

Between sorption runs it was intended that the

sorbent should be baked out at temperatures up to 200°C. It was therefore necessary to have some form of cooling for the upper part of the outer jacket so that during this baking out the Woods metal seals would be preserved. The cooling jacket M was made of copper as a separate unit from the stainless steel outer jacket. It was a sliding fit over the outer jacket and was held by three screws to a flange at the top, extending two inches below this flange. With a furnace at 230°C one inch below the cooling jacket, which had a steady flow of cold water running through it the outer jacket lid was kept below room temperature. It was found necessary to turn off the flow of water whenever cooling was not actually required. If this was not done condensation onto the Woods metal caused rapid corrosion and made it impossible to maintain a vacuum in the outer jacket.

The electrical leads to the calorimeter consisted of 8 of .010" double silk covered H.C. copper, supplied by The London Electric Wire Co., and Smiths, Ltd., and 2 of .010" double glass covered constantan 2.951 ohms per foot, supplied by Driver-Harris Co., Harrison N. J. The wires were first varnished individually in eight foot lengths with impregnating varnish (supplied by I.C.I., L.D. - 10476, thinner L.D. - 10477). Since the glass insulation is very fragile, two coats were applied to the constantan wires. The wires were then pulled through the copper-nickel tube and

at one end were wound round the cooling cylinder and varnished to it as described above. At the other end an exit from the vacuum system was acheived by taking the leads through a glass u-tube which was afterwards sealed with picein wax. The method proved to be completely effective. The ten wires were 4 heater leads, 2 spares, 2 copper and 2 constantan thermocouple leads. The heater leads have been described above. It was thought unlikely that the insulation of the .010" copper wire would stand up to the temperature necessary in baking out the sorbent. Therefore, as these wires left the cooling cylinder they were soft soldered on to .004" copper wire which was insulated with double silk painted with silicone varnish. The reduction in diameter of the wires reduced the heat leak down them to the calorimeter.

The thermocouple consisted of a double junction. The double junction at the calorimeter was mounted on the central terminal screw. Being external it was easily accessible but was still in good thermal contact with the calorimeter.

The cold junction N was a separate assembly positioned alongside the calorimeter outer jacket. It consisted of a glass tube leading into a wider glass vessel, made from 25 mm. tubing, which contained the double junction. The latter was mounted on a piece of 18 gauge copper tubing 0.6" long, which fitted loosely over a re-entrant in

the glass container. The thermocouple wires were wound round and varnished on to this copper tube, and the heat leak when the whole was immersed in liquid nitrogen thereby minimised. The large mass of copper also minimised the effect of small temperature fluctuations in the liquid nitrogen bath.

The double junction at the calorimeter had to withstand temperatures of about 200°C. The copper and constantan wires were silver soldered and electrical insulation of each junction was acheived by sandwiching it between thin strips of mica before squeezing it into the small copper tag which was attached to the calorimeter. In this way thermal contact was fully preserved. In the cold junction, which at no time had to withstand high temperatures the same effect was accomplished by the use of cigarette paper painted with impregnating varnish.

At all stages of the assembly of the calorimeter and cold junction the insulation of wires, between one another and between each wire and the metal parts of the calorimeter, was frequently checked with the 'Avometer' and the 'Insulation Tester'. The resistance in all cases was $\geqslant$ 20 megohms.

The incoming gas line F was of 2 mm. capillary and, in order to ensure that the entering gas was brought to the temperature of the bath before reaching the calorimeter, it was wound into a spiral of five turns 3" in diameter.

The entering gas therefore passed through about 4' of capillary tubing immersed in liquid nitrogen before reaching the calorimeter. The efficiency of this spiral was tested by admitting a volume of helium to the calorimeter and recording the energy change on a photographic trace (p. 62). A very small deflection (c.a. 1 mm) was observed, indicating a small temperature rise in the calorimeter. On withdrawing the helium from the calorimeter a similar deflection was detected in the opposite direction. The three possible effects involved are (1) sorption of helium, (2) compression effects in the gas phase and (3) inefficient cooling of the gas. The above test showed that (3) was not contributing since the energy change was reversible, which applies only to (1) and (2).

2.2f. The Oxygen Vapour Pressure Thermometer (Fig. 9)

The temperature of the liquid nitrogen bath was measured in later runs by an oxygen vapour pressure thermometer. This consisted of a small bulb A connected via 2 mm. capillary tubing to a mercury manometer B, the two arms of which were made from the same piece of 12 mm. tubing to eliminate meniscus effects. The capillary tubing leading from bulb A was wrapped in aluminium foil to distribute heat along its length and so eliminate the 'cold spot' effect of boiling which took place at the liquid nitrogen surface.

Oxygen was supplied to the thermometer from the cyclinder of pure oxygen C (British Oxygen Company Ltd.).

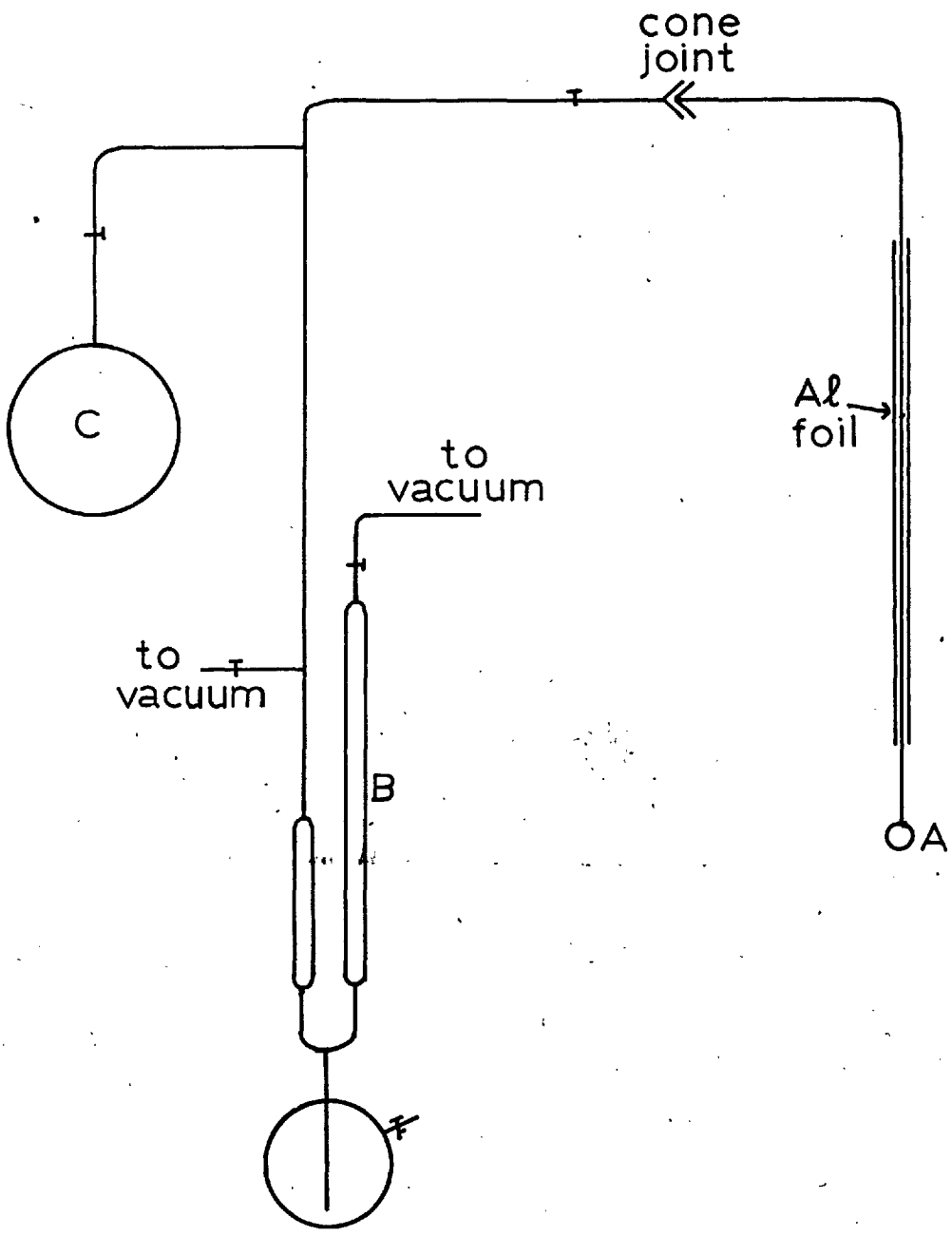

Fig. 9.

The tap from this cylinder was opened when bulb A was immersed in liquid nitrogen and oxygen condensed into it. At the end of a sorption run the majority of the oxygen could be re-collected in the cylinder. The oxygen vapour pressure was read off to the nearest 0.4 mms. Hg on a mirror-backed scale fixed in position behind the manometer arms. The temperature was therefore known to $\pm$0.2°C.

2.3 Electrical Equipment

2.3a. The Calorimeter Thermocouple Circuit (Fig 10a)

When energy was liberated in the calorimeter either electrically or by sorption of gas an electromotive force was generated in the thermocouple A. This e.m.f. was fed through shielded copper leads and a galvanometer selector switch B into a mirror galvanometer C. This galvanometer made by H. Tinsley and Co., Ltd., was type 4500 A, internal resistance 4.6 ohms, critical damping resistance 90 ohms, periodic time 2 seconds, sensitivity 94.5 mms. per microamp at 1 metre.

The galvanometer system was housed in a light-proof tunnel, $4\frac{3}{4}$ metres long, constructed from Dexion and hard-board. The tunnel was bolted on to a shelf which ran along one of the walls of the laboratory to which it was rigidly fixed on heavy angle iron supports imbedded in the wall. Vibration difficulties were overcome by mounting the galvanometer on three layers of foam rubber under a heavy

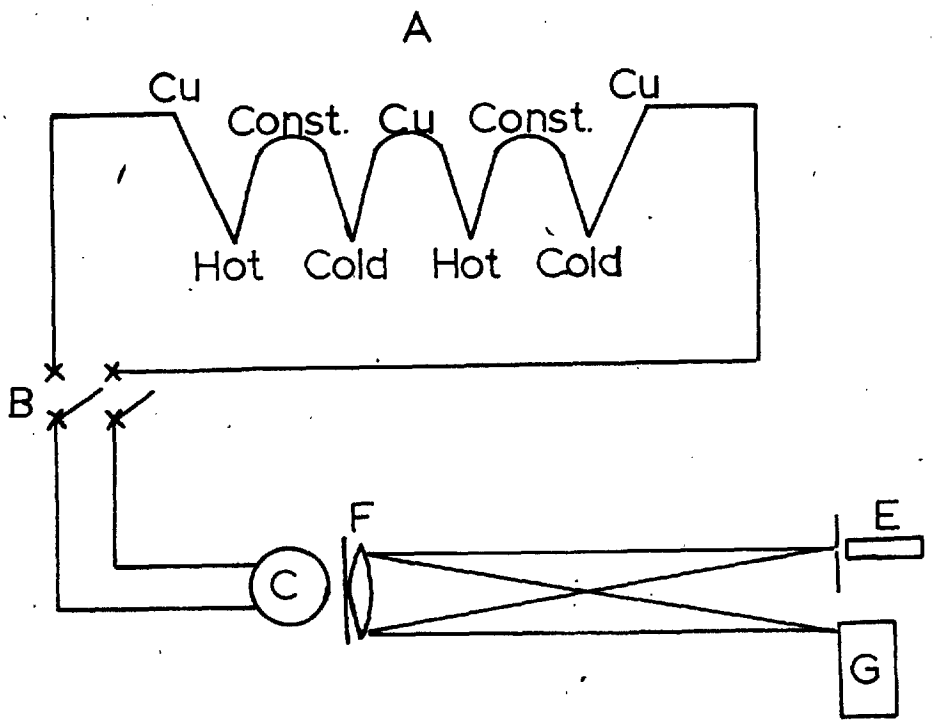

Fig. 10a.

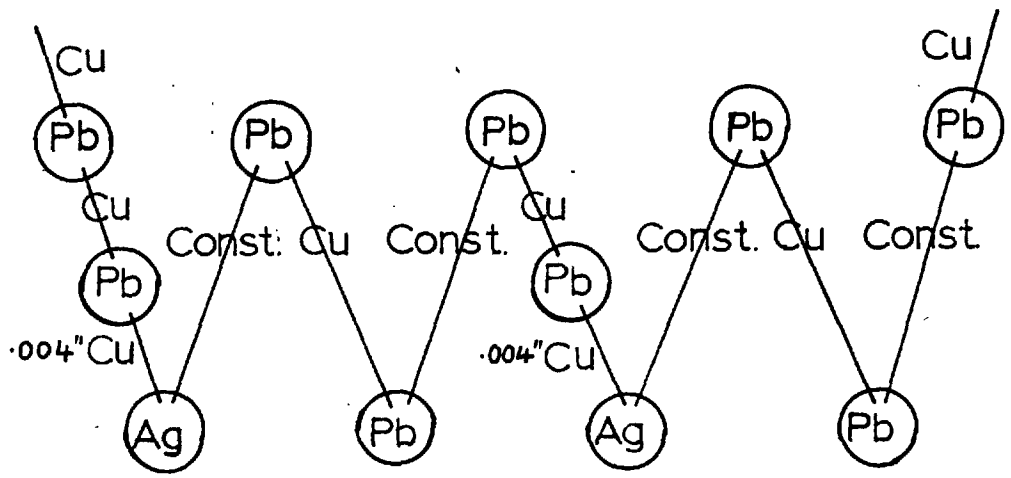

Fig. 10b.

lead block. A 4 metre light beam was used so that the resultant sensitivity of the galvanometer system was 4.4 mms. per microvolt.

The external circuit was of copper except for the knives of the switch which were of beryllium copper, stated to have a low contact potential against copper. The switch and the galvanometer were shielded with earthed copper boxes and the shielded cable was also earthed.

The light source for the optical lever was a galvanometer spotlight E mounted behind an adjustable slit the focal length of lens F distant from C. Light reflected by the galvanometer mirror was directed at the cylindrical lens of a rotating drum camera G, also the focal length of F distant. The drum camera, made by Kipp and Zonen of Delft, recorded photographically the movement of the light beam as a function of distance. It was driven by a synchronous motor at about one revolution per hour. The photographic paper used was Kodak recording paper RP30, developed with Kodak ID33 and fixed with acid hypo fixer IF2. The traces were dried between sheets of blotting paper and did not suffer any detectable distortion.

The double junction thermocouple is shown, together with the solders used, in Fig. 10b. It can be seen that there were several 'potential' thermal e.m.fs. due to the solders, but providing their pairs of junctions were at the same temperature the only e.m.f. in the circuit would

be the copper-constantan one. The lead soldered joins external to the calorimeter outer jacket and the cold junction were mounted on a wooden distribution board in the laboratory. At first, stray e.m.fs. producing a deflection of up to 1 cm. (about 2 microvolts) were observed on the traces, but as soon as the distribution board was covered with a thick wad of cotton wool this heavy 'background' disappeared completely. It had evidently been due to the thermal effects of draughts on the soldered joins.

No accurate temperature scale existed for the calorimeter thermocouple. By means of the electrical calibration of the system the deflection was related directly to energy and this relationship was used for the calculation of heats of sorption. The thermocouple was also used, however, to measure the temperature of the calorimeter during baking out. It was roughly calibrated by preparing a single junction thermocouple exactly similar to one half of the calorimeter thermocouple. This single junction was itself calibrated against a 0 360°C mercury-in-glass thermometer. The e.m.f. was measured on a portable potentiometer (Cambridge Instrument Co., Ltd. No. L340396) and the assumption made that at the same temperature difference the calorimeter thermocouple would produce twice the e.m.f. of the single junction thermocouple.

2.3b. The Calorimeter Calibration Circuit (Fig. 11)

When a gas increment was sorbed in the calorimeter

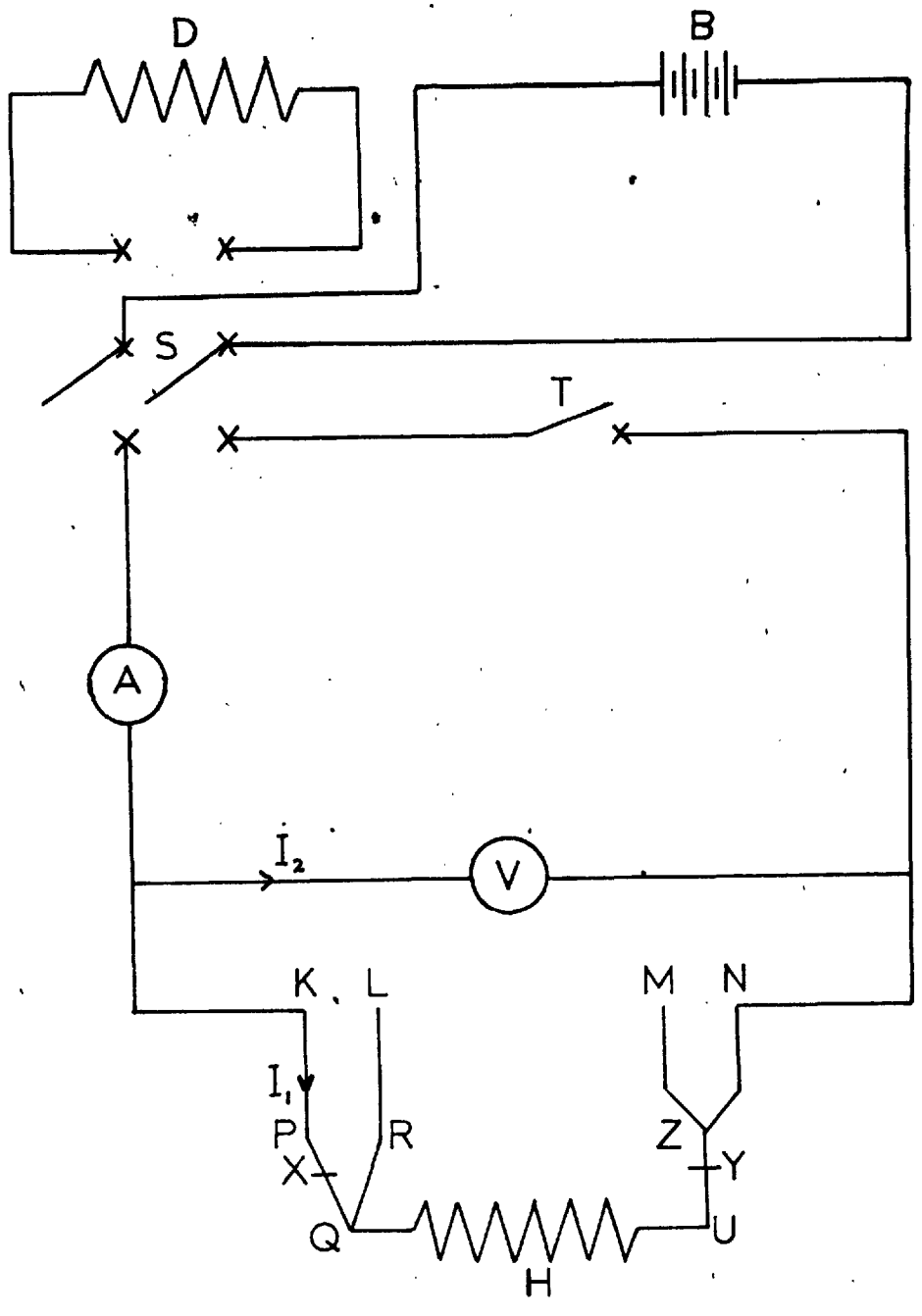

Fig. 11.

energy was liberated, measured as a temperature difference between the calorimeter and its surroundings by the thermocouple circuit. In order to evaluate this energy change it was necessary to calibrate the system in terms of a measured electrical energy input.

Current from the dry batteries B (1.5 or 4.5 volts) was stabilised by passing it through a dummy heater D of about 130 ohms resistance. This current was then passed through the calorimeter heater H by closing S and depressing a single lever T which simultaneously closed the circuit and started a stopwatch. Depression of T for the second time simultaneously opened the circuit and stopped the stopwatch. The watch was calibrated against the electronic timer in these laboratories and the time for which current had flowed through the heater could be read off to the nearest 0.02 seconds. An independent lever 'zeroed' the watch. The current and the potential drop across the heater and leads were measured on the milliammeter A and voltmeter V supplied by Sanamo Weston. These meters had previously been calibrated (Garden, Ph.D. thesis 1954).

To calculate the heat generated in the calorimeter it was necessary to know the resistance of the leads under experimental conditions. Three resistances were involved:-

R_1 = resistance of shielded cable at room temperature,

R_2 = resistance of silk covered copper wire at bath temperature

R_3 = resistance of the constantan wire of the internal leads at bath temperature.

These resistances were measured with a calibrated P.O. box at bath temperatures of 77°K. and 25°C. The function of the double heater lead PQR, was to facilitate the measurement of the resistance of the heater leads within the calorimeter, assuming that the resistance of these leads was equal to that of the double lead i.e. that the resistance of PQR equalled that of PQ + UZ. In fact P, R and V were situated just below the cooling cylinder of the calorimeter outer jacket. Actual resistances measured were KQL and MVN, where

$$KQL = R_1 + R_2 + R_3$$

and $$MVN = R_1 + R_2$$

Of the heat generated in the internal leads, one half was assumed dissipated in the gas phase and along the glass and the other half assumed to contribute to raising the temperature of the calorimeter Thus R_L, the resistance of the heater leads ineffective in raising the temperature of the calorimeter, equals the mean of the resistances of KQL and MVN.

$$R_L = R_1 + R_2 + \tfrac{1}{2}R_3.$$

From Fig. 11 two relationships are immediately obvious:

$$I_1 = I - I_2 \qquad (1)$$

$$I_2 R_V = E = I_1 R_{XN} \qquad (2)$$

where I is the ammeter reading in amperes

I_1 is the current through heater and leads

I_2 is the current through the voltmeter

E is the voltmeter reading in volts

R_V is the resistance of the voltmeter

From (1) and (2)

$$I_1 R_{XN} = R_V(I - I_1)$$

$$I_1 = \frac{IR_V}{R_V + R_{XN}}$$

Let V_{XY} be the potential difference across XY.

Then,

$$V_{XY} = E - I_1 R_L$$

$$= E - \frac{IR_V R_L}{R_V + R_{XN}}$$

The heat generated in the calorimeter is given by $I_1 V_{XY} t$ where t is the time for which current flows

$$W = I_1 V_{XY} t = \frac{IR_V}{R_V + R_{KN}} \left[E - \frac{IR_V R_L}{R_V + R_{KN}} \right] t$$

Now $R_{PK} = \frac{E}{I_1} = \frac{E}{I} - \frac{E}{R_V}$

Therefore

$$W = \left[I - \frac{E}{R_V} \right] Et - \left[I - \frac{E}{R_V} \right]^2 R_L t$$

$$= \frac{\left[I - \frac{E}{R_V} \right] Et}{4.184} - \frac{\left[I - \frac{E}{R_V} \right]^2 R_L t}{4.184} \text{ cals}$$

The second term in W is a correction term for the energy liberated in the leads. It never exceeds 2% of the total so that a value of R_L which is accurate to 10% would result in an error of only 0.2% in W.

CHAPTER III

TREATMENT OF OBSERVATIONS

3.1. Temperature Measurement

The temperature of the gas lines at room temperature was measured with the five 0-50°C thermometers distributed around the gas measuring system. These had been calibrated from 15-30°C against a 0-50°C N.P.L. thermometer as had two more 0-50°C thermometers used in the water and oil thermostats during water sorption determinations. The deviation from the standard was a maximum of 0.10°C and the appropriate corrections were therefore applied.

The temperature of the liquid nitrogen bath was measured by the oxygen vapour pressure thermometer described on p.44. The experimentally observed pressure was obtained by reading the position of the crown of the meniscus in each arm of the manometer and the height of the mercury column then reduced to that at 0°C. An accuracy of 0.2°C could be expected in the temperature so obtained.

3.2 Pressure Measurement

Pressure measurements relating to the gas phase during argon and nitrogen sorption runs were made on the precision manometer. The experimentally recorded readings were the positions of the crown and circumference of the mercury menisci. The crown readings were corrected for capillary depression using the data of Kistemaker (1945)

found by Laing (Ph.D. thesis 1953) to be in good agreement with the theoretical values of Gould and Vickers (1952).

The readings on the cathetometer were also corrected for the angle of the telescope caused by the fact that the cathetometer bar was not quite straight. The telescope did not, therefore, remain horizontal in all positions. At the side of the telescope was a spirit level, and the position of its bubble was calibrated in terms of a height correction. By observing the position of the bubble, a telescope levelling correction was applied to every reading from the cathetometer bar. This correction amounted to a maximum of 0.03 cms.

The height of the column of mercury measuring the pressure was also corrected to that at $0^{o}C$. This was done by dividing by the factor $1 + \alpha t$ where

$\alpha = 181.6 \times 10^{-6}$, the coefficient of volume expansion for mercury

t = the temperature in degrees Centigrade

The reading of the position of any crown could, in general, be reproduced to an average error of $\pm$ 0.002 cms. A pressure reading, requiring the determination of the postion of two crowns, thus had an average error of $\pm$ 0.004 cms.

3.3. Volume Measurement

The volume of gas sorbed in any increment was the difference between the volume at s.t.p. originally in the closer volume plus the calorimeter free space and the

volume remaining in the gas phase in the whole system at equilibrium.

3.3a The Doser Volume

The doser volume consisted of the gas burette and the line to the fixed mark of the manometer. The fundamental calibrated volume V_1 of the system was that of the gas burette from its lower fixed mark up to and including the bore of the tap leading from it. This was determined by four sets of mercury weighing with a mean deviation of 0.01%. All other volumes in the gas measuring system were determined by expansion of helium at known temperature and pressure from the gas burette using the ideal gas law. During these determinations all volumes had to be corrected to relate to the manometer fixed mark. The mercury level on the gas side was always set at some distance above the fixed mark and a correction applied for the volume occupied by the mercury. This volume was made up of (i) the volume of a cylinder of mercury of height h cm. and radius r cm. and (ii) the volume of the mercury meniscus. The former is simply $\pi r^2 h$, where r = 0.8 cms for 16 mm tubing and h is the height from the fixed mark to the circumference of the meniscus. The volume of the meniscus was calculated from the formula due to Kistemaker (1945) which for tubing of 16 mm. diameter reduces to

$$v = 256\ y\ (0.4948 + 0.0182\ y^{\frac{3}{2}})\ mms^3$$

where y is the meniscus height in mms. V_2 was the volume of the line from the gas burette to the manometer fixed mark.

3.3b. The Calorimeter Free Space

Beyond the calorimeter tap (T in Fig. 5) part of the system was at room temperature and part at the bath temperature. The determination of dead-space volumes was consequently more complex. With the entire line, including the trap U and the calorimeter G, at room temperature the total volume V_T beyond the calorimeter tap was determined by expansion of helium from the doser volume. This was done as rapidly as possible to avoid undue exposure of the calorimeter to mercury vapour. Experimental conditions were restored by replacing the liquid nitrogen around the trap and immersing the calorimeter in liquid nitrogen. Repetition of the helium expansion from the doser volume made it possible to calculate the part of V_T at liquid nitrogen temperature, V_3, and the volume at room temperature, V_4.

$$V_T = V_3 + V_4.$$

A number of determinations of each volume were performed. Table 1 summarises the results. The deviations quoted are mean deviations $\sum |d|/n$, where n is the number of observations.

Table 1

Total volume of burette V_1	29.849 ± 0.002 mls.
V_2	29.57 ± 0.03 mls.
V_T	97.14 ± 0.13 mls.
V_3	86.14 ± 0.06 mls.
V_4	11.00 ± 0.06 mls.

The figures quoted above for V_3 and V_4 are those when the trap and calorimeter Dewars had just been filled. By observation of the change in pressure with time after the Dewars had been filled the effect of the evaporation of the liquid nitrogen on the values of V_3 and V_4 could be calculated. Therefore during sorption runs the time at which the Dewar was filled was noted and the appropriate values of V_3 and V_4 were used.

3.3c. Gas Imperfection

In calculating gas volumes at low temperatures correction was made for the departure of the gas from ideality, using the Berthelot equation in the form

$$pV = RT\left\{1 + \frac{9}{128} \cdot \frac{Tc}{Pc} \cdot \frac{p}{T}\left(1 - \frac{6Tc^2}{T^2}\right)\right\}$$

The correction was negligible in the free space calculations, where the gas involved was helium, but in the case of argon and nitrogen it amounted to about 1% at 10 cms.

pressure when the temperature was 77°K. The correction was also negligible for water vapour at 25°C.

3.4. Gravimetric Measurement

The weight of water sorbed in an increment was measured by a gravimetric method combined with a small correction calculated volumetrically. Before admitting an increment of water to the sorbent the extension of the silica spring, D in Fig. 6, was measured with the cathetometer. Then with tap 2 closed, tap 1 was opened exposing the volume B to the sorbent. Tap 1 was now closed and tap 2 opened so that the system between taps 1 and 3 re-equilibrated by loss of water from the saturated solution of potassium bromide in E. The equilibration time was found to be at least four hours and whenever possible equilibration was allowed to continue overnight. Equilibration was assumed to be complete when no further change in the length of the spiral spring was observed for a period of about one hour. Since the temperature and relative humidity in the system was the same before and after admission of the increment, the adsorption of water on the glass walls could be assumed unchanged. Therefore the weight of water lost from E was equal to that which passed tap 1.

In general an increment amounted to about 2.5 mgms. of water which, for a sensitivity of 460 cms. per gm., was equivalent to a change in length of 1.15 cms. Since a cathetometer reading had an error of $\pm$ 0.002 cms the error

in measuring the extension was ± 0.004 cms. Measurement of the change of extension requiring two observations of the extension, was therefore subject to an error of ± 0.008 cms. or 0.7%. The conversion of this change of extension to loss in weight from the saturated solution which involved the use of the graph of deviation of calibration points from a straight line (Fig. 7) should not have introduced an error greater than 0.01 mgms. or 0.4%. Therefore the total error in the calculation of the weight which passed tap 1 is a maximum of just over 1%.

The weight sorbed in any increment was equal to the weight lost from E minus the increase in weight in the vapour phase. Calculation of the increased weight of water vapour in the line from tap 1 to the calorimeter and in the calorimeter free space was done volumetrically, the residual pressure being measured on the manometer C. This correction never amounted to more than 3% of the weight of a water increment.

3.5. Heat of Sorption Determinations

3.5a. Thermal Conductivity

The metal components of the calorimeter were designed to acheive rapid transfer of heat and were in good thermal contact. It was to be expected, however, that thermal contact between the kaolinite particles would be poor in the absence of a gas phase in the calorimeter. Therefore during calibration experiments it was necessary

to introduce c.a. 1 mm. of helium to the sorbent bed. Calibrations were shown to be unaffected by the pressure of helium by performing several calibrations with 10 20 cms. of helium present. A small pressure of helium was also introduced into the calorimeter before earlier sorption runs in case the residual pressure after the first few increments was too low to be effective in heat transfer. This was later found to be unnecessary. Garden, Kington and Laing (1955) have shown that heat of sorption determinations are not significantly affected by the presence of helium.

3.5b. Obtaining Traces

In order to obtain a trace, whether for calibration purposes or for a heat of sorption determination, the following sequence of operations was carried out:

(i) the calorimeter and cold junction were immersed in the bath (liquid nitrogen or oil thermostat) with a gas phase in the calorimeter and c.a. 2 mm. of helium in the outer jacket. The calorimeter was left for 1-2 hours to attain thermal equilibrium.

(ii) the galvanometer spotlight was switched on and, with the thermocouple circuit closed, absence of any drift was taken to be an indication that thermal equilibrium had been reached. The helium in the outer jacket was pumped out and the jacket pumped continuously during subsequent recording. The presence of a good vacuum in the

outer jacket was checked with the Macleod gauge.

(iii) with the camera loaded and the thermocouple circuit open trace recording was begun. After five minutes the circuit was closed giving rise to base lines A and B in Fig. 12.

(iv) after a further five minutes energy was generated in the calorimeter either by closing the calibration heater circuit or by admitting a gas increment. In the case of a gas increment, pressure and temperature readings were taken after 10 and 20 minutes to enable calculation of the volume sorbed as a function of time.

(v) the drum of the camera was allowed to rotate for about 30 minutes after which the circuit was opened and another open circuit base line C was recorded for five minutes.

(vi) the camera motor and light beam were switched off and the film developed, fixed, washed, and dried between sheets of blotting paper. Helium was admitted to the outer jacket to facilitate equilibration before the next recording.

In this manner a photographic trace was obtained which recorded the galvanometer deflection as a function of the distance x along the trace. Since the speed of the drum camera is known this distance can easily be converted into a function of time. In the case of a

Fig. 12.

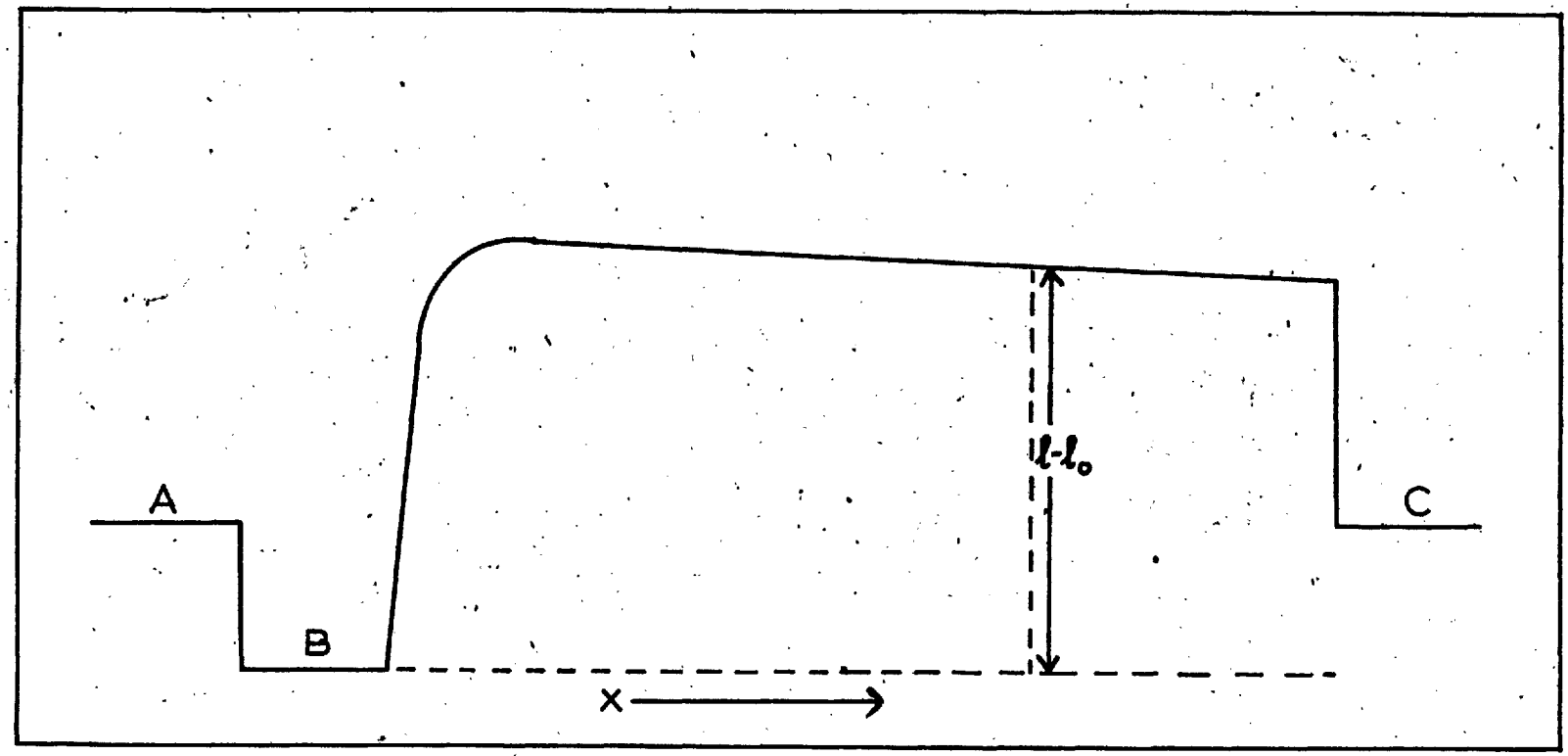

calibration trace the heat input corresponding to this deflection was known from the expression derived in 2.3b. The cooling characteristics of the calorimeter could therefore be determined and the trace adjusted to the equivalent of adiabatic conditions in the calorimeter.

3.5c. Trace Analysis

The thermodynamic treatment of processes in a non-adiabatic calorimeter containing a vapour phase and a condensed phase is discussed by Garden Kington and Laing (1955) and Garden (Ph.D. thesis 1954). Reference should be made to these authors for the derivation of formulae used in this section.

Calibration traces in the absence of a sorbed phase

The observed galvanometer deflection at any x value $(l - l_o)$ was corrected to the deflection $(l - l_o)_a$ which would have been observed under adiabatic conditions by means of the expression

$$(l - l_o)_a = (l - l_o) + k\int_0^x (l - l_o)\, dx$$

where k is a constant for any one calorimeter under given conditions and is defined by

$$k = - \frac{1}{(l - l_o)} \cdot \frac{d(l - l_o)}{dx}$$

In fact k defined the rate of cooling of the calorimeter, and since this depended partly on the vacuum in the outer jacket slight variations in k were to be expected. Since

the integral term was only about 10% of the total value of $(l - l_o)_a$ however, small variations in k had little effect on $(l - l_o)_a$.

The integral was evaluated by measuring the area under the curve with a planimeter. This is the area bounded by the closed circuit base line (drawn through B parallel to the line joining A and C), the ordinate $(l - l_o)$ at time t, and the trace.

$(l - l_o)$ was measured with an A. W. Faber Castell ruler graduated to 0.5 mm. Three values of $(l - l_o)$ were measured for each trace corresponding to 10, 15 and 20 minutes after energy input. In theory $(l - l_o)$ could have any value up to the width of the trace, about 12 cms. In practice a deflection of about 8 cms. was aimed at, in order to have a safety margin and small deflections were avoided because of the increased percentage error. $(l - l_o)$ could be measured with an error of + 0.04 cms. Analysis of several traces gave the value of k such that $(l - l_o)_a$ was constant for any one trace. In practice four or five calibrations were done before each sorption run and the value of k which resulted in the least variation in $(l - l_o)_a$ for each trace calculated for this group of calibrations.

The values of $(l - l_o)_a$ so obtained were then used to calculate the calibration factor K defined by

$$K = \left(\frac{W}{(l - lo)a} \right)_{n_s = 0}$$

where W is the electrical energy in calories generated in the calorimeter.

Values of K were obtained at 77°K and at 25°C and it was expected that these values would remain constant. However, at some stage during these experiments the value of K at 77°K changed. During runs 1 to 8 all of which had been investigations of the sorption of argon on the 'clean' sodium kaolinite surface, 13 calibration traces were analysed giving a value of 0.288 $\pm$ 0.004 calories per cm. Runs 9 and 10 were of water on sodium kaolinite at 25°C. After run 10 the two layers of water adsorbed at 25°C were frozen on to the surface at 77°K. Analysis of 11 calibration traces now gave a value of K of 0.262 $\pm$ 0.003 calories per cm. and this was unchanged when the water was removed. Analysis of 33 calibration traces done at 77°K after run 8 resulted in a value of 0.263 $\pm$ 0.004 calories per cm. The presence or absence of the water layers did not affect the results. The reson for this apparent decrease in the heat capacity of the system is not understood but it is clearly shown in Fig. 13, which demonstrates the linear relationship between the energy input W and the corrected deflection (l - lo)a. Values of k and K are summarised in Table 2.

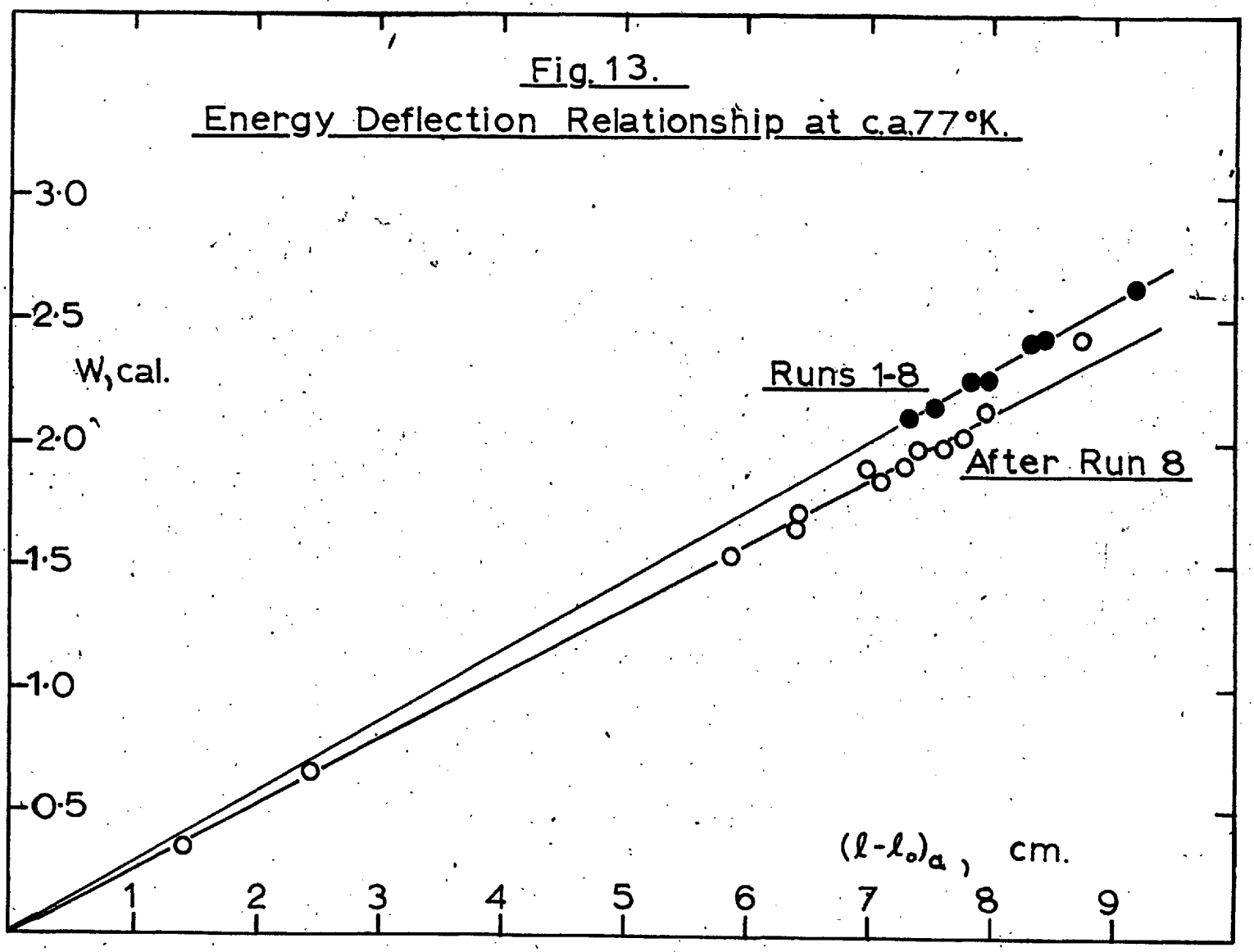
Fig. 13.
Energy Deflection Relationship at c.a. 77°K.
3·0
2·5
2·0
1·5
1·0
0·5
W, cal.
Runs 1-8
After Run 8
1
2
3
4
5
6
7
8
9
$(l-l_o)_a$, cm.

Table 2

	K cms./sq. cm.	K cal./cm.
Calorimeter at 77°K (up to run 8)	0.0051 ± 0.0003	0.288 ± 0.004
Calorimeter at 77°K (after run 8)	0.0051 ± 0.0003	0.263 ± 0.004
Calorimeter at 25°C	0.0195	0.293 ± 0.002

Six calibrations were done at 25°C. Deviations quoted are the mean deviations.

Calibration traces in the presence of a sorbed phase

It has been shown (Garden Ph.D. thesis 1954) that the calibration factor is unchanged by the presence of a sorbed phase provided that the heat capacity of the sorbed phase **plus** the gas phase in the calorimeter is negligible compared to the heat capacity of the calorimeter when $n_s = 0$. This was confirmed with the calorimeter at 77°K by the calibration results after run 8, which showed that K was unaffected by the presence of two layers (c.a. 90 mgms) of water. It was also confirmed at 25°C by ten calibration traces with increasing quantities of water sorbed. In this case a correction had to be applied for the heat of desorption. This correction,

$$\frac{(\bar{H}_g - \bar{H}_s) \times (n_{s_t} - n_{s_o})}{(1 - lo)_a}$$ where $(\bar{H}_g - \bar{H}_s)$ is the

heat of sorption and $(n_{s_t} - n_{s_o})$ is the number of moles desorbed after time t must be subtracted from the calculated values of K. The mean value obtained was then K = 0.290 ± 0.002 calories per cm. The calibration factor obtained at zero coverage could therfore be used throughout the entire sorbed phase concentration range.

Gas increment traces. From the analysis of a gas increment trace the isosteric heat of sorption was calculated as

$$(\bar{H}_g - \bar{H}_s) = K \frac{(l - l_o)_a}{(n_{s_t} - n_{s_o})} + K_1(C_g + C_{ns})\frac{(l - l_o)}{(n_{s_t} - n_{s_o})} - V_g\frac{(p_t - p_o)}{(n_{s_t} - n_{s_o})}$$

where K_1 is the constant relating the galvanometer deflection to the temperature change and is defined by $(T - T_o) = k_1 (l - l_o)$

C_g is the heat capacity of the gas phase,

C_{ns} is the heat capacity of the sorbed phase,

n_{s_o} is the number of moles sorbed at zero time,

n_{s_t} is the number of moles sorbed at time t,

p_o is the pressure at zero time,

p_t is the pressure at time t,

V_g is the volume available to the gas phase of the calorimeter,

K is evaluated as described above in the absence of a sorbed phase.

The second term in the expression is negligible in the present case. The third is the heat of compression

discussed by Kington and Aston (1951). It reaches a maximum where the isotherm is near horizontal, i.e. during the formation of the second sorbed layer. Its magnitude for a run with argon on sodium kaolinite is shown below.

Table 3

Correction for heat of compression

Volume Sorbed ml.s.t.p./gm.	θ	$(p_t - p_0)$ cm.	$(V_{st} - V_{s0})$ ml.s.t.p	$7.14 \cdot V_g \frac{(p_t - p_0)}{(V_{st} - V_{s0})}$ cal/mole	$\bar{H}_g - \bar{H}_s$ per cent
0.57	0.21	0.37	18.15	8	0.3
1.73	0.65	1.02	17.33	23	1.0
2.80	1.05	4.17	15.60	105	5.1
3.84	1.44	5.00	16.20	121	6.5
5.11	1.91	3.95	21.19	73	4.1
6.62	2.48	3.60	22.06	65	3.5
8.29	3.10	2.49	21.11	47	2.6

Vg was calculated from geometric considerations and checked by observation of the galvanometer deflection when a large increment of helium was admitted to the calorimeter, making the assumption that all the heat evolved was due to the heat of compression of helium. The observed deflection was very small however, and Vg may have been in error by as much as 20%. The value of Vg

used throughout was 55 ccs. A maximum error of 1.3% arises from this source in the above run. During a run with nitrogen, however considerably higher pressures were involved and the correction term reached a maximum of 500 calories per mole. This was about 30% of the heat of sorption and the error in the heat of sorption was therefore a maximum of 6% from the heat of compression term.

CHAPTER IV

RESULTS

The isosteric heats of sorption of argon, nitrogen and water were measured in the non-adiabatic calorimeter. The calorimeter contained 15.86 gms. of sodium kaolinite and the heats of sorption of argon and nitrogen were obtained on this sorbent and on the same sorbent with two layers of water frozen on to it at liquid nitrogen temperature. Heats of sorption of argon and nitrogen on this water-covered surface were also measured at liquid oxygen temperature. The larger pressures involved resulted in increased errors mainly due to the uncertainty in the heat of compression and these data at c.a. 90°K. have been tabulated but not further discussed. The isosteric heats of sorption of water on sodium kaolinite were measured at 25°C.

The data were corrected for gas imperfection and heats of compression. Kington and Aston (1951) have shown that the value of the calorimetric heat of sorption corrected for the adiabatic heat of compression is identical to the isosteric heat obtained from the Clapeyron equation. These heat data are listed in Tables 5 to 17 as a function of the amount sorbed and of θ, the number of molecular layers sorbed, calculated by application of the B.E.T. theory (Brunauer, Emmett and Teller, 1938). Actually, the value of $H_g - H_s$ obtained is the average slope of a

plot of energy evolved against the number of moles sorbed during the interval n_{so} to n_{st}. It is therefore tabulated as being the value at $n_{so} + \frac{1}{2}(n_{st} - n_{so})$, i.e. the total volume sorbed prior to the increment plus one-half of the increment.

After run 8, when it was realised that the presence of helium in the calorimeter was not necessary for thermal equilibrium during gas sorption runs (the gas-phase pressure associated with the first increment being sufficient), isotherm data were obtained at the same time as heat data. Isotherm data are recorded in Tables 18 to 26, equilibrium pressure being given as a function of amount sorbed and θ. For isotherm data the amount sorbed is the volume or weight sorbed at the end of the increment after equilibration and when the calorimeter has returned to bath temperature. A minimum equilibration time of about four hours was necessary and when possible equilibration was allowed to continue overnight. θ values are necessary when plotting comparative graphs of for example, argon on the 'clean' and the water-covered surface, the amount sorbed in a monolayer not being the same for these two surfaces.

4.1. Slow Processes

Two types of slow process were encountered. In the low concentration range, for the final 1% sorbed in some increments, the energy evolved during the time from

10 to 20 minutes after admitting the increment to the sorbent bed was much greater than that to be expected from the small amount sorbed during that time. Hence the three values of $\tilde{H}g - \bar{H}s$ obtained at 10, 15 and 20 minutes were increasing. This suggests an energetic rearrangement of sorbed molecules **not** accompanied by any detectable pressure change. The effect was most noticeable during water sorption.

At higher concentrations a slow process of gas sorption and simultaneous heat evolution was observed, the two balancing to give a constant $\tilde{H}g - \bar{H}s$ value for the increment. This effect was expected since the slight cooling of the calorimeter towards bath temperature during the time for which the trace was observed, would cause more gas to be sorbed which would reduce the rate of cooling by its accompanying heat evolution.

These slow processes are illustrated by the following data from the analyses of two water increments sorbed on sodium kaolinite at 25°C, and two nitrogen increments sorbed on sodium kaolinite at 77°K.

Table 4

Time min	(1 − lo)a cm.	Ws mgm. per total	$\tilde{H}g - \bar{H}s$ k.cal/mole
Increment 12/2			
10	8.96	2.87	16.48
15	9.25	2.87	17.01
20	9.52	2.87	17.51
Increment 12/10			
10	6.24	2.52	13.02
15	6.26	2.53	13.02
20	6.27	2.53	13.04
Time min	(1 − lo)a cm.	Vs ccs. s.t.p. per total	$\tilde{H}g - \bar{H}s$ k.cal/mole
Increment 18/1			
10	2.91	4.40	3.85
15	3.00	4.39	3.96
20	3.06	4.38	4.06
Increment 18/4			
10	5.07	12.10	2.33
15	5.07	12.13	2.32
20	5.13	12.16	2.34

4.2 Heat of Sorption Measurements

Heats of sorption of argon nitrogen, water and hydrogen on the 'clean' sodium kaolinite surface and of argon and nitrogen on the water covered surface were measured. So small a volume of hydrogen is sorbed on kaolinite at 77°K, however that these data were subject to considerable inaccuracy and have not been included.

4.2a Argon on 'Clean' Sodium Kaolinite

The first four heat runs were of argon on sodium kaolinite. They were however of an exploratory nature intended to familiarise the author with the apparatus and for the improvement of techniques to achieve greater accuracy. At first considerable scatter was observed and the heat data prior to run 5 have not therefore been used.

The differential heat of sorption falls rapidly from 3.1 k.cal/mole to 2.3 k.cal/mole when the monolayer is half completed. A small maximum due to a rise of 50 cal/mole in the heat values is observed and the heat of sorption then falls off steadily until the completion of the second molecular layer when it is 1.8 k.cal/mole slightly less than the heat of sublimation. The arithmetic average deviation of points from a smooth curve is ± 20 cal/mole.

4.2b Nitrogen on 'Clean' Sodium Kaolinite

Because of the effect of the nitrogen quadrupole the initial heats are considerably higher 4.0 k cal/mole, falling off rapidly during the formation of the monolayer and less steeply during the second layer. Final values in the third layer are about 1.5 k.cal/mole, approximately equal to the heat of sublimation. The mean deviation is ± 40 cal/mole.

4.2c Water on 'Clean' Sodium Kaolinite

The initial heat of sorption of water on this sorbent is 21 k.cal/mole. This falls off very rapidly to 13.5 k.cal/mole when the surface is half covered and there is a further decrease to 12 k.cal/mole at the completion of the monolayer. The second layer of water has a heat of sorption of 12 to 11 k.cal/mole between the heat of sublimation (12 k.cal/mole) and the heat of liquefaction (10.5 k.cal/mole). The mean deviation is ± 190 cal/mole.

4.2d Argon on Water covered Sodium Kaolinite

The heats at low coverage of both argon and nitrogen on the water covered surface are markedly lower than those on the clean surface. This is due to the removal of the heterogeneity of the sorbent by covering the high energy sites of the kaolinite with water. The differential heat of sorption of argon falls from 2.45 k.cal/mole to 2.05 k. cal/mole at the completion of the monolayer. This decrease

does not begin however, until the monolayer is almost half complete. In the second layer the heat of sorption falls to 1.8 K.cal/mole the same value as that finally reached on the clean surface. The mean deviation is ± 10 cal/mole.

4.2e Nitrogen on Water covered Sodium Kaolinite

The heat of sorption at low coverage is 3.3 K.cal/mole falling rapidly from θ - 0.2 to θ = 1.4, when it is 1.65 K.cal/mole. The value at the end of the second layer is about 1.7 K.cal/mole which is slightly higher than that on the clean surface and 200 cal/mole above the heat of sublimation. The mean deviation is ± 35 cal/mole.

4.3 Isotherm Measurements

Isotherm data for argon nitrogen and water on the 'clean' sorbent and for argon and nitrogen on the water-covered sorbent were measured, usually at the same time as the heat data. The oxygen vapour-pressure thermometer was introduced after run 10 so that for all isotherms carried out at liquid nitrogen temperature (except run 10) the observed pressure was corrected to that at 77.36°K by the integrated Clapeyron equation:

$$\ell n \frac{p_2}{p_1} = \frac{(\tilde{H}_g - \bar{H}_s)\,(T_2 - T_1)}{RT_1T_2}$$

where T_2 and p_2 are the higher temperature and pressure, and R is the gas constant.

Isotherm data for water were obtained at 25°C but

there was poor agreement between runs 9 and 12. However due to an error at increments 4 and 5 during run 9 the weight sorbed in these two increments (and therefore the total weight sorbed) was uncertain. The discrepancy could also have been due to a leakage of air into the system during run 9. After run 12 a check that no leakage had occurred was carried out by freezing the water on to the sorbent at liquid nitrogen temperature and measuring the residual gas phase pressure. This was negligible, thus excluding the possibility that a leak had occurred during run 12. This check was not carried out after run 9, however. Accordingly the isotherm data obtained from run 12 have been treated as the more accurate, and the value of the weight sorbed in a monolayer calculated by the B.E.T. theory from this isotherm has been used to calculate θ values for both heat runs.

Better agreement was obtained between runs 12 and 19, both of water on sodium kaolinite at 25°C but the latter being an isotherm run only. Even so a definite discrepancy was observed between the isotherms and B.E.T. plots of these two runs. Better agreement between the isotherms was obtained by applying the v_m value calculated from each run to that run only. This indicates that the difference in v_m calculated by the B.E.T. theory is a real difference and that some change in the kaolinite surface may have taken place between runs 12 and 19.

A discrepancy also appeared in the isotherms obtained

of nitrogen on the water-covered surface at c.a. 77°K. This was probably due to the difficulty of removing all the sorbed nitrogen between the two runs. The method used was to pump on the calorimeter at liquid nitrogen temperature for about 3 days. The pressure measured on the Macleod gauge could not be reduced below 2×10^{-5} mm Hg, although the same treatment for the removal of argon at liquid nitrogen temperature produced a better vacuum in a shorter time The conclusion must be reached that some nitrogen was already adsorbed before run 21 was begun. Only the isotherm from run 20 can therefore be considered accurate and only this isotherm has been shown in Fig. 20. Similarly only the v_m from run 20 has been used. Data from both runs have been tabulated.

4.4 Graphs

The data are presented in the form of a number of graphs, Figs. 14 to 21, which provide for the comparison of the heat data and the isotherm data of the three sorbate molecules on both surfaces.

Table 5

Argon on sodium kaolinite at c.a. 77°K

Heat runs 5, 6 and 7 V_m = 2.67 mℓ.s.t.p./gm.

Increment No.	Volume Sorbed mℓ.s.t.p./gm.	$\theta = V/v_m$	$\tilde{H}_g - \bar{H}_s$ k.cal./mole.
Run 5			
1	0.31	0.12	2.86
Run 6			
1	0.33	0.12	2.61
Run 7			
1	0.57	0.21	2.45
2	1.73	0.65	2.35
3	2.80	1.05	2.04
4	3.84	1.44	1.86
5	5.11	1.91	1.78
6	6.62	2.48	1.87
7	8.29	3.10	1.82

Table 6

Argon on sodium kaolinite at c.a. 77°K

Heat run 8 . v_m = 2.67 mℓ.s.t.p./gm.

Increment No.	Volums Sorbed mℓ.s.t.p./gm.	$\theta = V/v_m$	$\tilde{H}_g - \bar{H}_s$ k.cal./mole
1	0.28	0.10	2.77
2	1.17	0.44	2.32
3	2.21	0.83	2.21
4	3.10	1.16	1.92
5	3.96	1.48	1.89
6	4.74	1.78	1.78
7	5.42	2.03	1.81

Table 7

Argon on sodium kaolinite at c.a. 77°K

Heat run 14 v_m = 2.67 mℓ.s.t.p./gm.

Increment No.	Volume Sorbed mℓ.s.t.p./gm.	$\theta = V/v_m$	$\tilde{H}_g - \bar{H}_s$ k.cal./mole.
1	0.46	0.17	2.56
2	1.26	0.47	2.36
3	1.89	0.71	2.31
4	2.60	0.97	2.11
5	3.50	1.31	1.90
6	4.39	1.64	1.87
7	5.24	1.96	1.84
8	6.03	2.26	1.93

Table 8

Nitrogen on sodium kaolinite at c.a. 77°K

Heat run 17 v_m = 2.60 mℓ.s.t.p./gm.

Increment No.	Volume Sorbed mℓ.s.t.p./gm.	$\theta = V/v_m$	$\hat{H}_g - \bar{H}_s$ k.cal./mole.
1	0.21	0.08	3.75
2	0.94	0.36	2.87
3	1.84	0.70	2.42
4	2.42	0.93	1.97
5	2.77	1.06	1.90
6	3.13	1.20	1.71
7	3.51	1.35	1.64

Table 9

Nitrogen on sodium kaolinite at c.a. 77°K

Heat run 18 v_m = 2.60 mℓ.s.t.p./gm.

Increment No.	Volume Sorbed mℓ.s.t.p./gm.	$\theta = V/v_m$	$\tilde{H}_g - \bar{H}_s$ k.cal./mole.
1	0.14	0.05	3.96
2	0.54	0.21	3.20
3	1.24	0.48	2.62
4	2.06	0.79	2.33
5	2.59	1.00	2.07
6	2.90	1.12	1.85
7	3.22	1.24	1.83
8	3.55	1.37	1.73
9	3.96	1.52	1.63
10	4.43	1.70	1.57
11	4.84	1.86	1.67
12	5.19	2.00	1.63
13	5.52	2.12	1.57
14	5.88	2.26	1.73
15	6.25	2.40	1.63
16	6.88	2.65	1.49
17	7.22	2.78	1.53

Table 10

Water on sodium kaolinite at 25°C

Heat run 9 ω_m = 3.08 mgms./gm.

Increment No.	Weight Sorbed* mgms/gm.	$\theta = W/\omega_m$	$\tilde{H}_g - \bar{H}_s$ k.cal./mole.
2	0.27	0.09	15.74 - 17.00
3	0.44	0.14	15.77 - 16.40
9	1.62	0.53	13.29 - 13.76
11	2.02	0.66	13.12
13	2.39	0.78	12.61
15	2.74	0.89	12.26
17	3.13	1.02	11.58
20	3.60	1.17	11.71
22	3.88	1.26	12.10
24	4.21	1.37	11.60
26	4.59	1.49	11.62
28	4.90	1.59	11.42
30	5.19	1.69	11.01
31	5.30	1.72	11.08
33	5.55	1.80	11.22

*Because of an error at increments 4 and 5 some doubt exists in the values of the weight sorbed from incremnt 9 onwards. This error should not exceed 0.1 mgm./gm.

Table 11

Water on sodium kaolinite at 25°C

Heat run 12 ω_m = 3.08 mgms./gm.

Increment No.	Weight Sorbed mgms/gm	$\theta = W/\omega_m$	$\tilde{H}_g - \bar{H}_s$ k.cal./mole.
1	0.04	0.01	20.53 - 21.97
2	0.18	0.06	16.48 - 17.51
4	0.67	0.22	14.18 - 14.64
6	1.15	0.37	13.42
8	1.61	0.52	13.50
10	2.06	0.67	13.03
14	2.69	0.87	12.58
16	3.06	0.99	12.94
18	3.43	1.11	12.32
20	3.77	1.22	12.22

Table 12

Argon on water-covered sodium kaolinite at c.a. 77°K

Heat run 10 v_m = 2.39 mℓ.s.t.p./gm.

Increment No.	Volume Sorbed mℓ.s.t.p./gm.	$\theta = V/v_m$	$\tilde{H}_g - \bar{H}_s$ k.cal./mole.
1	0.29	0.12	2.42
2	0.84	0.35	2.44
3	1.26	0.53	2.24
4	1.79	0.75	2.20
5	2.48	1.04	1.87
6	3.29	1.38	1.80
7	4.25	1.78	1.81

Table 13

Argon on water-covered sodium kaolinite at c.a. 77°K.

Heat run 11. v_m = 2.39 mℓ.s.t.p./gm.

Increment No.	Volume Sorbed mℓ.s.t.p./gm.	$\theta = V/v_m$	$\tilde{H}_g - \bar{H}_s$ k.cal./mole.
1	0.32	0.13	2.45
2	1.12	0.47	2.31
3	1.97	0.82	2.14
4	2.67	1.12	1.92
5	3.48	1.46	1.83

Table 14

Nitrogen on water-covered sodium kaolinite at c.a. 77°K

Heat run 20 v_m = 2.45 mℓ.s.t.p./gm.

Increment No.	Volume Sorbed mℓ.s.t.p./gm.	$\theta = V/v_m$	$\tilde{H}_g - \bar{H}_s$ k.cal./mole.
1	0.36	0.15	3.32
2	1.21	0.49	2.62
3	1.98	0.81	2.25
4	2.42	0.99	1.81
5	2.82	1.15	1.81
6	3.35	1.37	1.59
7	3.91	1.60	1.69
8	4.42	1.80	1.63
9	4.89	2.00	1.85

Table 15

Nitrogen on water-covered sodium kaolinite at c.a. 77°K

Heat run 21 v_m = 2.45 mℓ.s.t.p./gm.

Increment No.	Volume Sorbed mℓ.s.t.p./gm.	$\theta = V/v_m$	$\tilde{H}_g - \bar{H}_s$ k.cal./mole.
1	0.13	0.05	3.30
2	0.60	0.24	2.94
3	1.23	0.50	2.63
4	1.74	0.71	2.26
5	2.14	0.87	2.02
7	2.93	1.20	1.64
8	3.44	1.40	1.66
9	3.87	1.58	1.69
10	4.22	1.72	1.75
11	4.47	1.82	1.64

Table 16

Argon on water-covered sodium kaolinite at c.a. 90°K

Heat run 16 $v_m^{*} \approx 2.34$ mℓ.s.t.p./gm.

Increment No.	Volume Sorbed mℓ.s.t.p./gm.	$\theta = V/v_m$	$\tilde{H}_g - \bar{H}_s$ k.cal./mole.
1	0.25	0.11	2.39
2	0.84	0.36	2.26
3	1.55	0.66	2.01
4	2.14	0.91	1.71
5	2.59	1.11	1.88
6	2.98	1.27	1.85

Table 17

Nitrogen on water-covered sodium kaolinite at c.a. 90°K

Heat run 15 $v_m^{*} \approx 2.30$ mℓ.s.t.p./gm.

Increment No.	Volume Sorbed mℓ.s.t.p./gm.	$\theta = V/v_m$	$\tilde{H}_g - \bar{H}_s$ k.cal./mole.
1	0.28	0.12	3.35
2	0.88	0.38	2.74
3	1.47	0.64	2.54
4	1.91	0.83	2.21
5	2.16	0.94	1.97

*These values of v_m are not accurate because of the presence of a small pressure of helium in the sorbent bed.

Table 18

Isotherm data for argon on sodium kaolinite at 77.36°K

Runs 13 and 14 v_m = 2.67 mℓ.s.t.p./gm.

Run and Increment No.	Volume Sorbed mℓ.s.t.p./gm.	$\theta = V/v_m$	Pressure cm. Hg.
13/1	0.65	0.24	0.12
13/2	1.74	0.65	0.52
13/3	2.78	1.04	2.72
13/4	3.16	1.18	4.42
13/5	3.45	1.29	5.77
13/6	3.61	1.35	6.51
14/1	0.92	0.34	0.19
14/2	1.60	0.60	0.46
14/3	2.19	0.82	1.03
14/4	3.04	1.14	3.85
14/5	4.01	1.50	8.20
14/6	4.87	1.82	10.81
14/7	5.73	2.15	12.56
14/8	6.42	2.40	13.83
14/9	7.02	2.63	14.70
14/10	7.51	2.81	15.45
14/11	7.94	2.97	15.95

Table 19

Isotherm data for nitrogen on sodium kaolinite at 77.36°K

Runs 17 and 18 v_m = 2.60 mℓ.s.t.p./gm.

Run and Increment No.	Volume Sorbed mℓ.s.t.p./gm.	$\theta = V/v_m$	Pressure cm. Hg.
17/1	0.43	0.16	0.01
17/2	1.44	0.55	0.21
17/3	2.25	0.86	1.55
17/4	2.60	1.00	5.12
17/5	2.95	1.13	10.80
17/6	3.35	1.28	17.58
17/7	3.73	1.43	23.56
18/1	0.28	0.11	0.01
18/2	0.81	0.31	0.04
18/3	1.67	0.64	0.33
18/4	2.46	0.95	3.28
18/5	2.73	1.05	7.16
18/6	3.09	1.19	13.85
18/7	3.39	1.30	18.71
18/8	3.77	1.45	24.94
18/9	4.22	1.62	30.04
18/10	4.68	1.80	36.33
18/11	5.07	1.95	40.95
18/12	5.38	2.07	44.81
18/13	5.72	2.20	48.62
18/14	6.14	2.36	51.59
18/15	6.75	2.60	52.71
18/16	7.11	2.73	55.43
18/17	7.41	2.85	57.58

Table 20

Isotherm data for water on sodium kaolinite at 25°C.

Run 9

Increment No.	Weight Sorbed* mgms./gm.	Pressure cm. Hg.
1	0.18	0.01
2	0.36	0.02
3	0.53	0.05
4	0.68	0.06
5	0.84	0.11
6	1.11	0.12
7	1.27	0.15
8	1.54	0.20
9	1.69	0.22
10	1.94	0.27
11	2.09	0.31
12	2.32	0.42
13	2.46	0.48
14	2.68	0.53
15	2.81	0.56
16	3.07	0.62
17	3.19	0.67
18	3.30	0.70
19	3.55	0.78
20	3.66	0.82
21	3.83	0.86
22	3.92	0.90
23	4.14	0.94
24	4.29	0.97
25	4.52	1.06
26	4.66	1.09
27	4.84	1.15
28	4.96	1.19
29	5.13	1.23
30	5.24	1.26
31	5.35	1.28
32	5.50	1.32
33	5.59	1.35

* Because of an error in increments 4 and 5 some doubt exists in the values of weight sorbed. This error should not exceed 0.1 mgm./gm.

Table 21

Isotherm data for water on sodium kaolinite at 25°C

Run 12 ω_m = 3.08 mgms./gm.

Increment No.	Weight Sorbed mgms./gm.	$\theta = W/\omega_m$	Pressure cm. Hg.
1	0.09	0.03	0.01
2	0.27	0.09	0.01
3	0.58	0.19	0.01
4	0.76	0.25	0.01
5	1.06	0.34	0.02
6	1.23	0.40	0.03
7	1.53	0.50	0.07
8	1.69	0.55	0.10
9	1.98	0.64	0.13
10	2.14	0.69	0.18
11	2.30	0.75	0.22
12	2.46	0.80	0.24
13	2.61	0.85	0.29
14	2.76	0.90	0.33
15	2.99	0.97	0.40
16	3.13	1.02	0.41
17	3.37	1.09	0.50
18	3.50	1.14	0.55
19	3.71	1.21	0.60
20	3.83	1.25	0.65
21	4.22	1.37	0.77

Table 22

Isotherm data for water on sodium kaolinite at 25°C

Run 19 ω_m = 2.94 mgms./gm.

Increment No.	Weight Sorbed mgms/gm.	$\theta = W/\omega_m$	Pressure cm. Hg.
1	0.89	0.30	0.02
2	1.82	0.62	0.14
3	2.67	0.91	0.35
4	3.54	1.20	0.63
5	4.49	1.53	0.92
6	5.44	1.85	1.13
7	5.77	1.96	1.22

Table 23

Isotherm data for argon on water-covered sodium kaolinite at c.a. 77°K*

Run 10 v_m = 2.39 mℓ.s.t.p./gm.

Increment No.	Volume Sorbed mℓ.s.t.p./gm.	$\theta = V/v_m$	Pressure cm. Hg.
1	0.58	0.24	0.15
2	1.10	0.46	0.37
3	1.43	0.60	0.67
4	2.17	0.91	2.39
5	2.83	1.18	5.24
6	3.82	1.60	9.22
7	4.76	1.99	11.71

* Temperature of liquid nitrogen bath not measured.

Table 24

Isotherm data for argon on water-covered sodium kaolinite at 77.36°K

Run 11 v_m = 2.39 mℓ.s.t.p./gm.

Increment No.	Volume Sorbed mℓ.s.t.p./gm.	$\theta = V/v_m$	Pressure cm. Hg.
1	0.65	0.27	0.16
2	1.61	0.67	0.89
3	2.35	0.98	3.02
4	3.01	1.26	6.10
5	4.02	1.68	9.86

Table 25

Isotherm data for nitrogen on water-covered sodium kaolinite at c.a. 77°K

Run 20 V_m = 2.45 mℓ.s.t.p./gm.

Increment No.	Volume Sorbed mℓ.s.t.p./gm.	$\theta = V/V_m$	Pressure cm. Hg.
1	0.72	0.29	0.03
2	1.72	0.70	0.66
3	2.25	0.92	3.69
4	2.61	1.07	8.83
5	3.08	1.26	16.97
6	3.69	1.51	25.89
7	4.21	1.72	32.64
8	4.73	1.93	39.56
9	5.15	2.10	44.76

Table 26

Isotherm data for nitrogen on water-covered sodium kaolinite at c.a. 77°K

Run 21

Increment No.	Volume Sorbed* mℓ.s.t.p./gm.	Pressure cm. Hg.
1	0.26	0.01
2	0.93	0.10
3	1.54	0.63
4	1.96	2.48
5	2.34	7.16
6	2.67	12.77
7	3.23	21.97
8	3.72	28.90
9	4.12	34.08
10	4.41	37.93
11	4.64	40.81

* Some doubt exists in the volume sorbed because of incomplete degassing of the sorbent prior to this run.

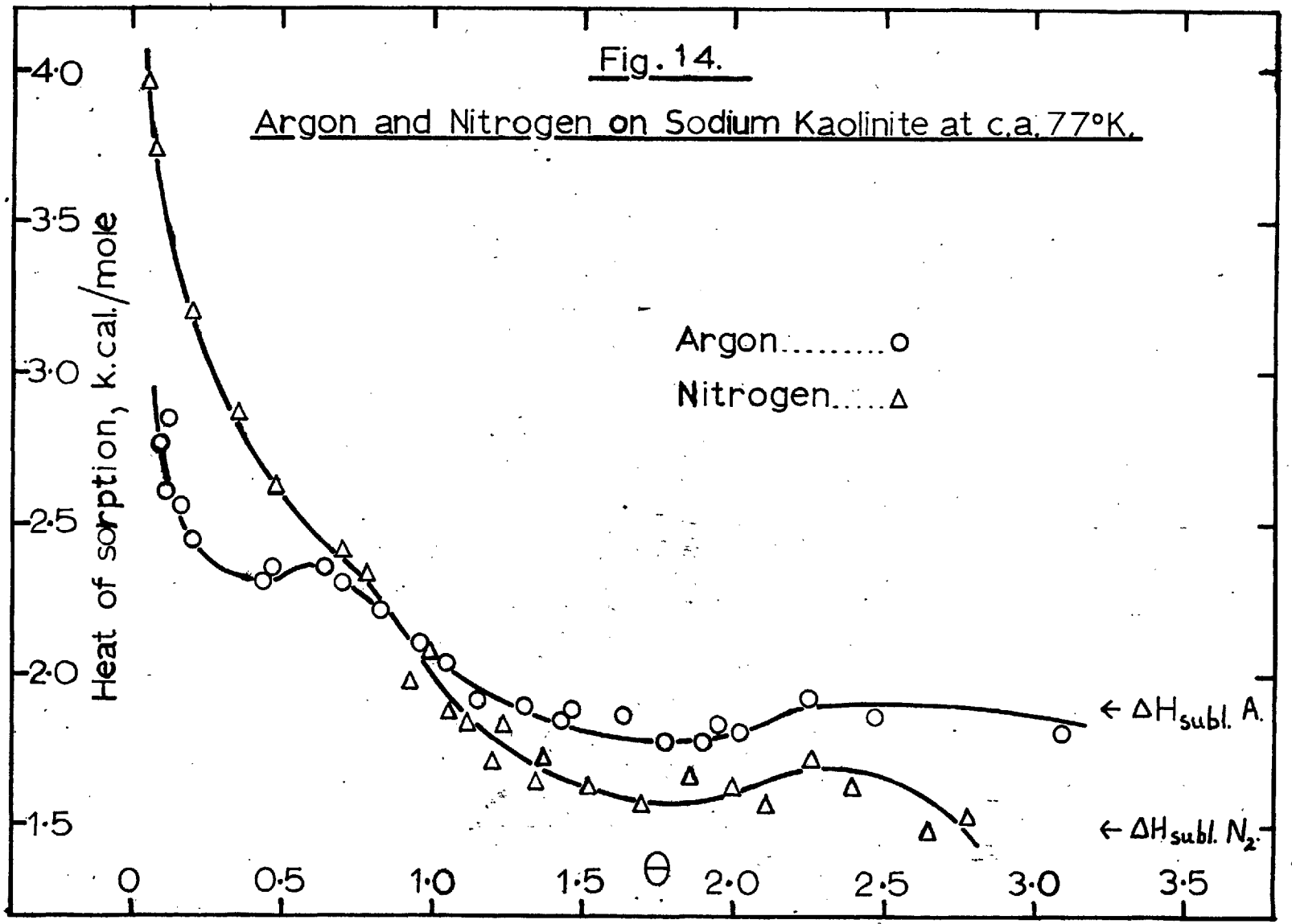
Fig. 14.
Argon and Nitrogen on Sodium Kaolinite at c.a. 77°K.
Heat of sorption, k.cal./mole
4·0
3·5
3·0
2·5
2·0
1·5
Argon.....o
Nitrogen.....Δ
← ΔH subl. A.
← ΔH subl. N2.
0
0·5
1·0
1·5
θ
2·0
2·5
3·0
3·5

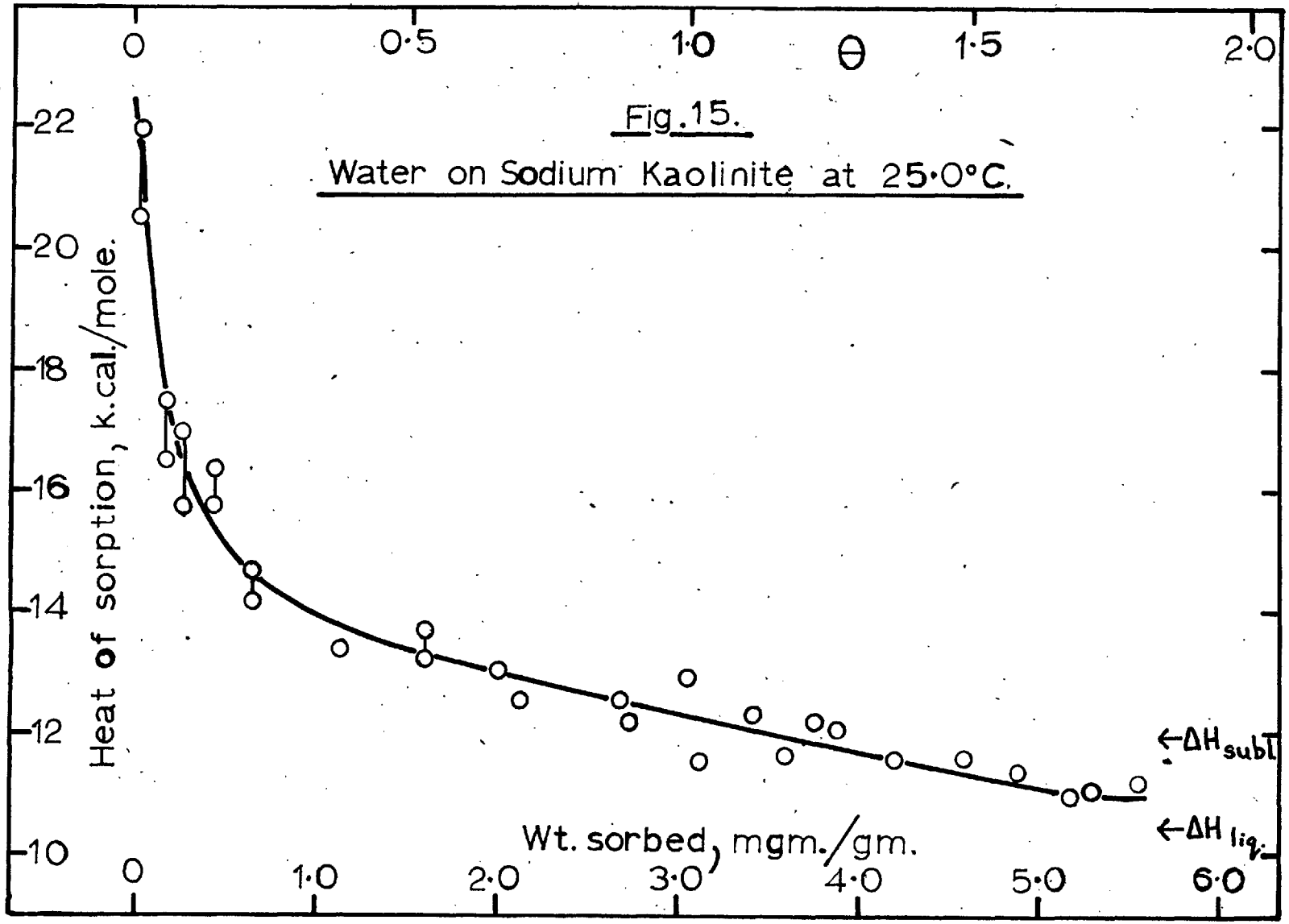

Fig. 15.

Water on Sodium Kaolinite at 25·0°C.

Fig. 16.

Argon, Nitrogen and Water on Sodium Kaolinite

Argon at c.a.77°K.....o

Nitrogen at c.a.77°K.....Δ

Water at 25°C.....●

Heat of sorption, k.cal./mole.

H_2O scale

Heat of sorption, k.cal./mole.

θ

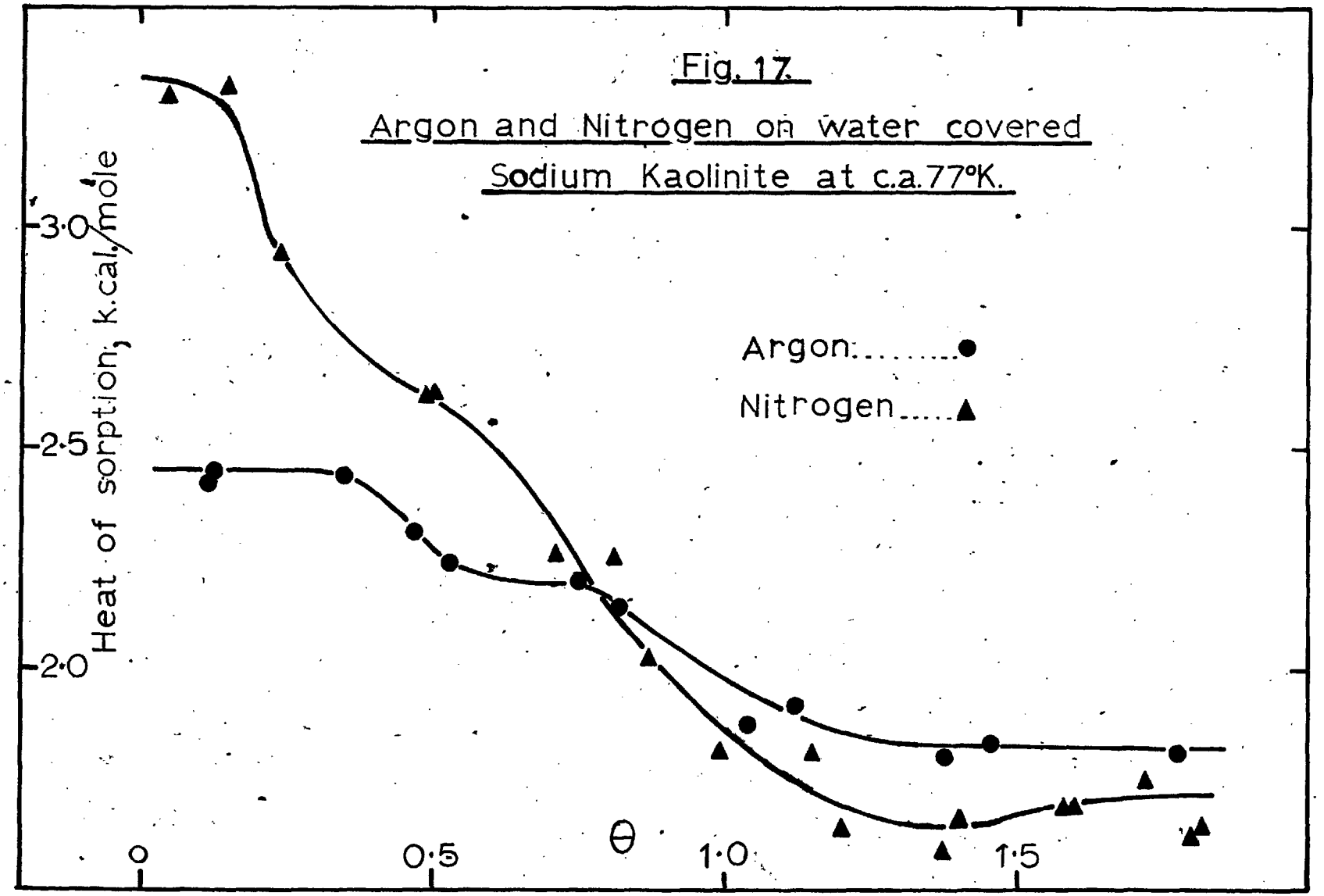
Fig. 17.
Argon and Nitrogen on water covered Sodium Kaolinite at c.a. 77°K.
Heat of sorption, k.cal./mole
3·0
2·5
2·0
Argon
Nitrogen
0
0·5
θ
1·0
1·5

Fig. 18a.

Argon on clean and water covered Sodium Kaolinite at c.a.77°K.

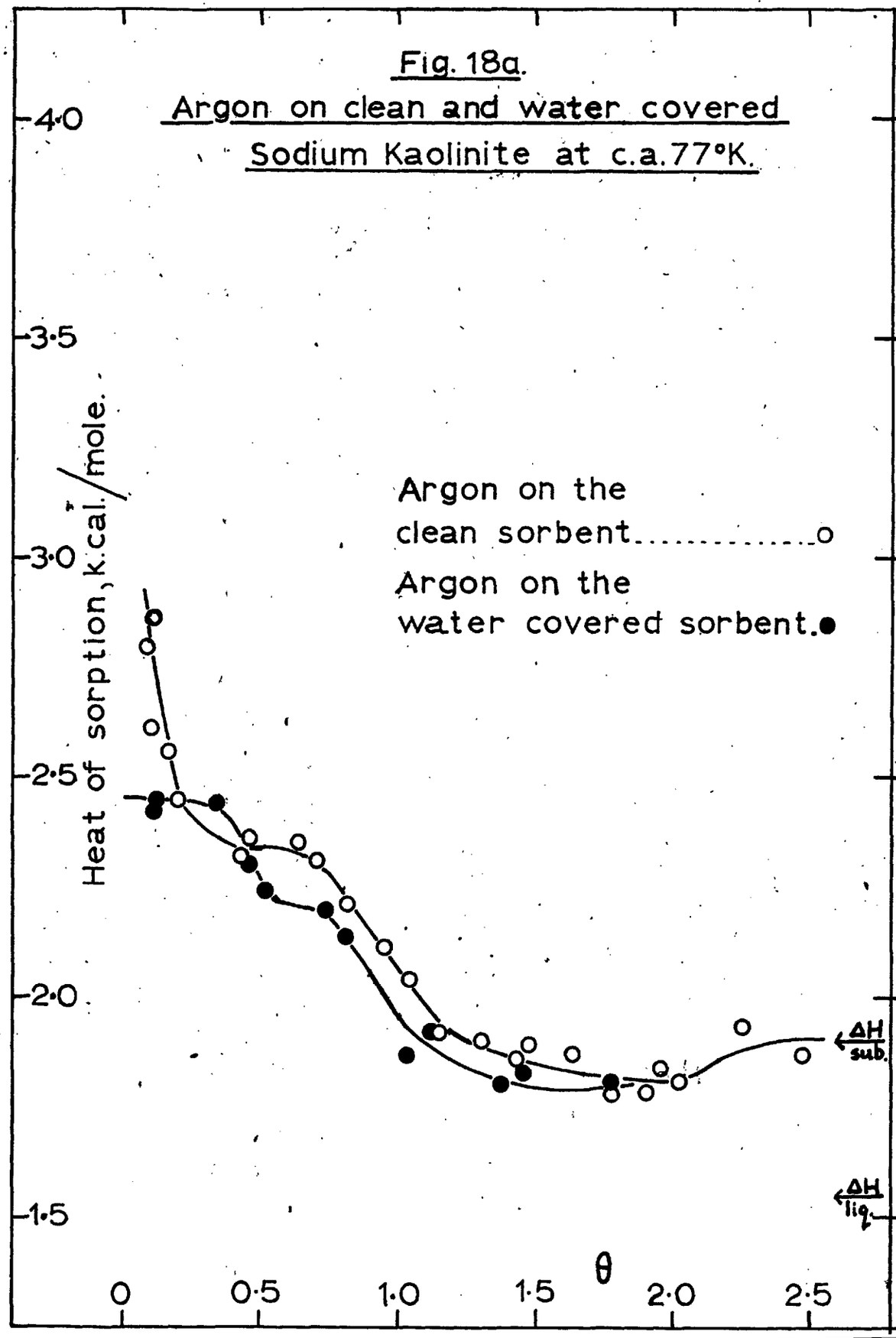

Fig. 18b.

Nitrogen on clean and water covered Sodium Kaolinite at c.a.77°K.

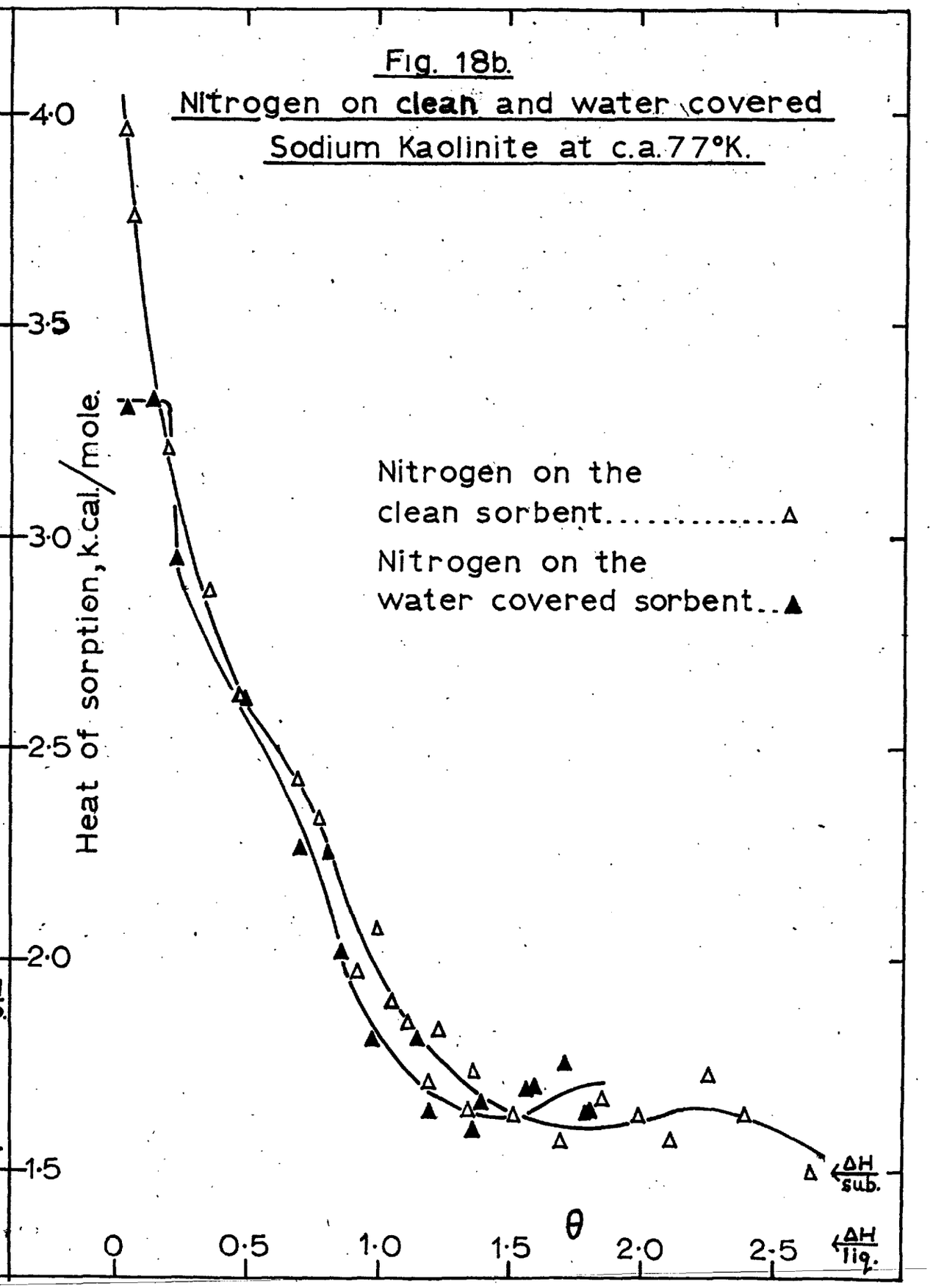

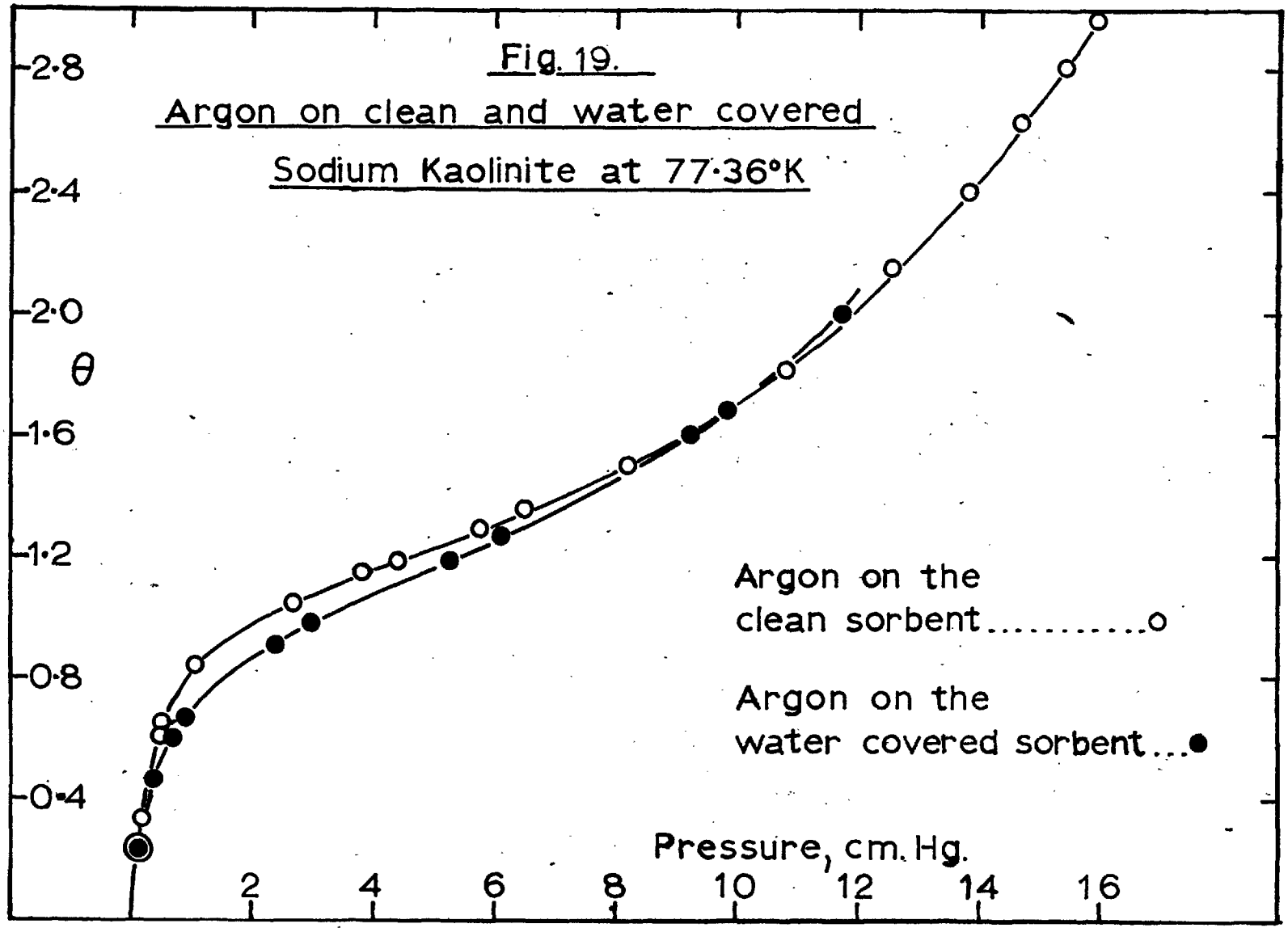
Fig. 19.
Argon on clean and water covered
Sodium Kaolinite at 77·36°K
2·8
2·4
2·0
θ
1·6
1·2
0·8
0·4
Argon on the
clean sorbent.....o
Argon on the
water covered sorbent...●
Pressure, cm. Hg.
2
4
6
8
10
12
14
16

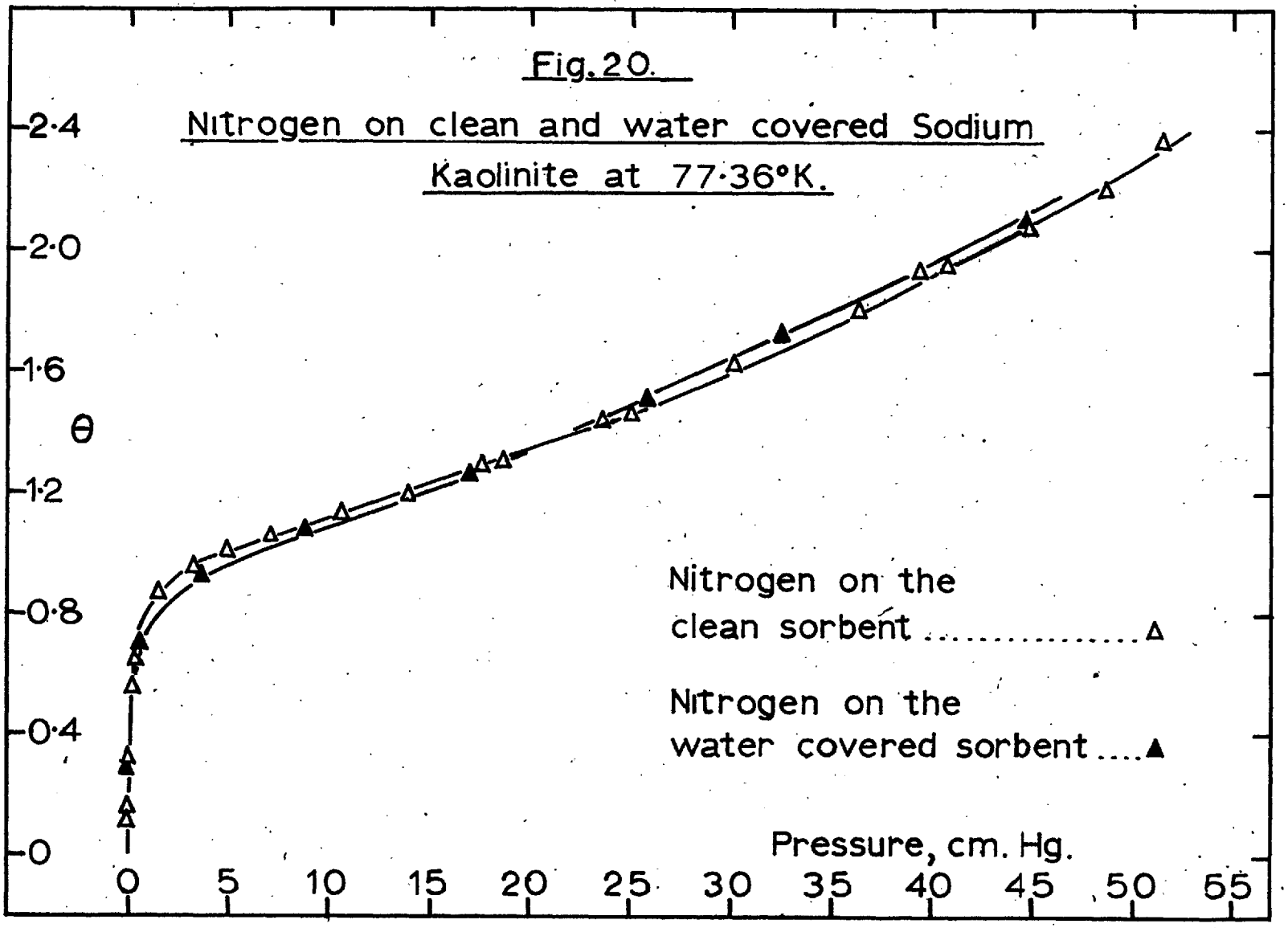
Fig. 20.
Nitrogen on clean and water covered Sodium Kaolinite at 77·36°K.
2·4
2·0
1·6
θ
1·2
0·8
0·4
0
0
5
10
15
20
25
30
35
40
45
50
55
Pressure, cm. Hg.
Nitrogen on the clean sorbent .....Δ
Nitrogen on the water covered sorbent ....▲

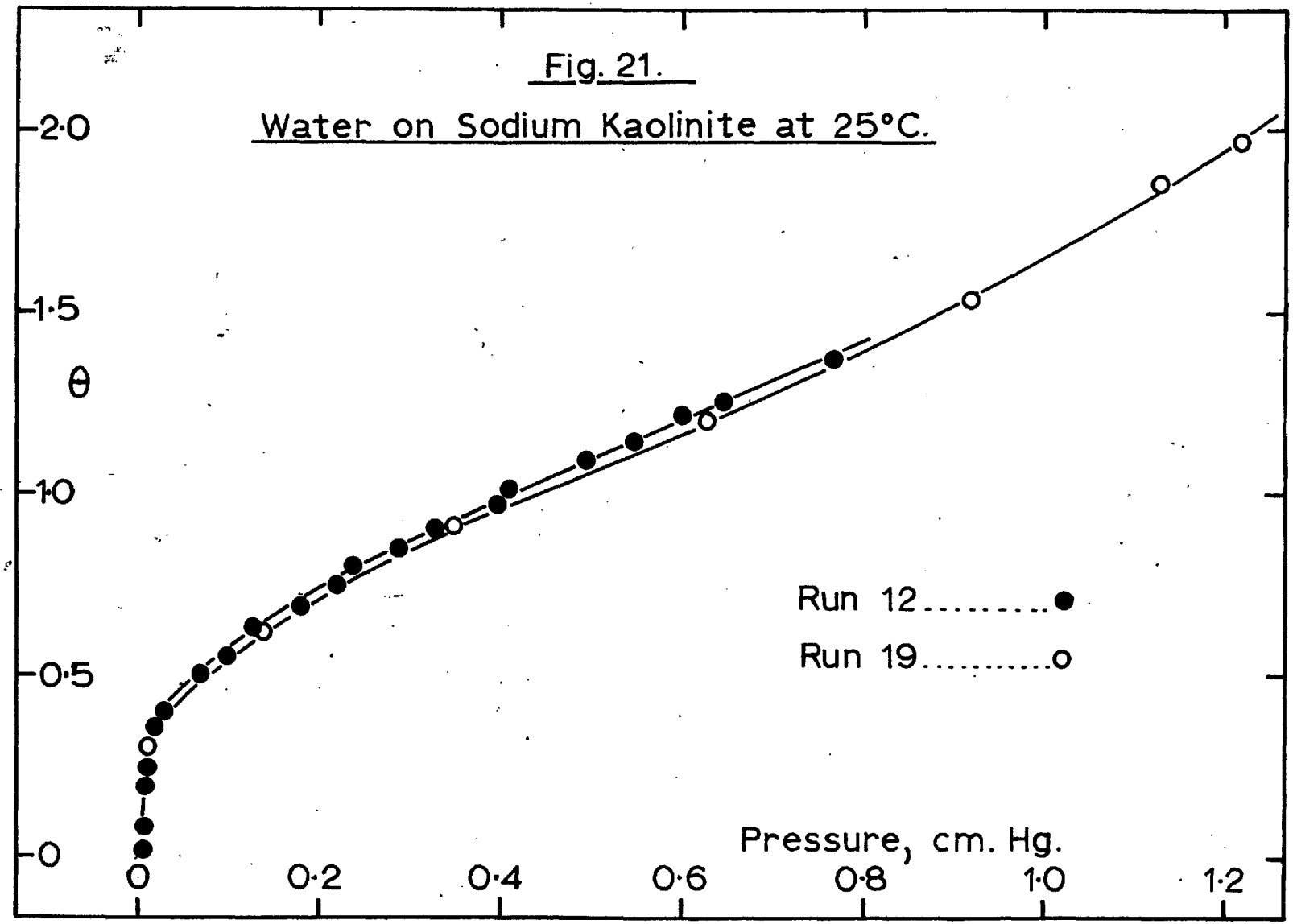
Fig. 21.
Water on Sodium Kaolinite at 25°C.
2·0
1·5
θ
1·0
0·5
0
0
0·2
0·4
0·6
0·8
1·0
1·2
Pressure, cm. Hg.
Run 12.....●
Run 19.....o
1101

CHAPTER V

DISCUSSION

5.1. The B.E.T. Treatment of Isotherms.

The theory of physical adsorption of Brunauer, Emmett and Teller (1938) was the first, and is still probably the best and most useful theory covering the complete pressure range. It is not fully satisfactory, and the assumptions of the theory are very crude, but they are sufficiently good to contain a number of the important qualitative features observed experimentally. Especially after the confirmatory work of Harkins and Jura (1944), it now seems clear that the determination of surface areas by the B.E.T. theory is the best method available at the present time.

The volume sorbed in a monolayer, v_m, is calculated from the equation

$$\frac{p}{v(p_o - p)} = \frac{1}{v_m c} + \frac{c-1}{v_m c}\cdot\frac{p}{p_o}$$

for adsorption on a free surface. In this equation

p = equilibrium pressure,

v = volume sorbed,

p_o = saturation pressure of the sorbate at the temperature of the experiment.

For values of p/p_o between 0.05 and 0.35 the plot

of the function $p/v(p_o - p)$ against p/p_o is linear if the theory is obeyed. The intercept of the straight line is $1/v_m c$ and the slope is $(c - 1)/v_m c$, so that v_m can readily be calculated from the experimental data.

The B.E.T. theory was applied to the isotherm data listed in Tables 18 to 26 and the plot of $p/v(p_o - p)$ against p/p_o was linear in each case, as can be seen from Figs. 22 to 24.

The values of the saturation vapour pressure for nitrogen at its boiling point and for water at 25°C presented no difficulty.

The question arose, however, whether p_o for argon at 77.36°K should be the value for the solid or the extrapolated value for the liquid. Argon has a melting point of 84.0°K, and at first sight it would appear that at 77.36°K the saturation vapour pressure of the solid (20.6 cm) should be used. However, a number of investigators have reported evidence, based on various properties of the adsorbed films, which indicates an abnormally low freezing point of argon in the adsorbed phase.

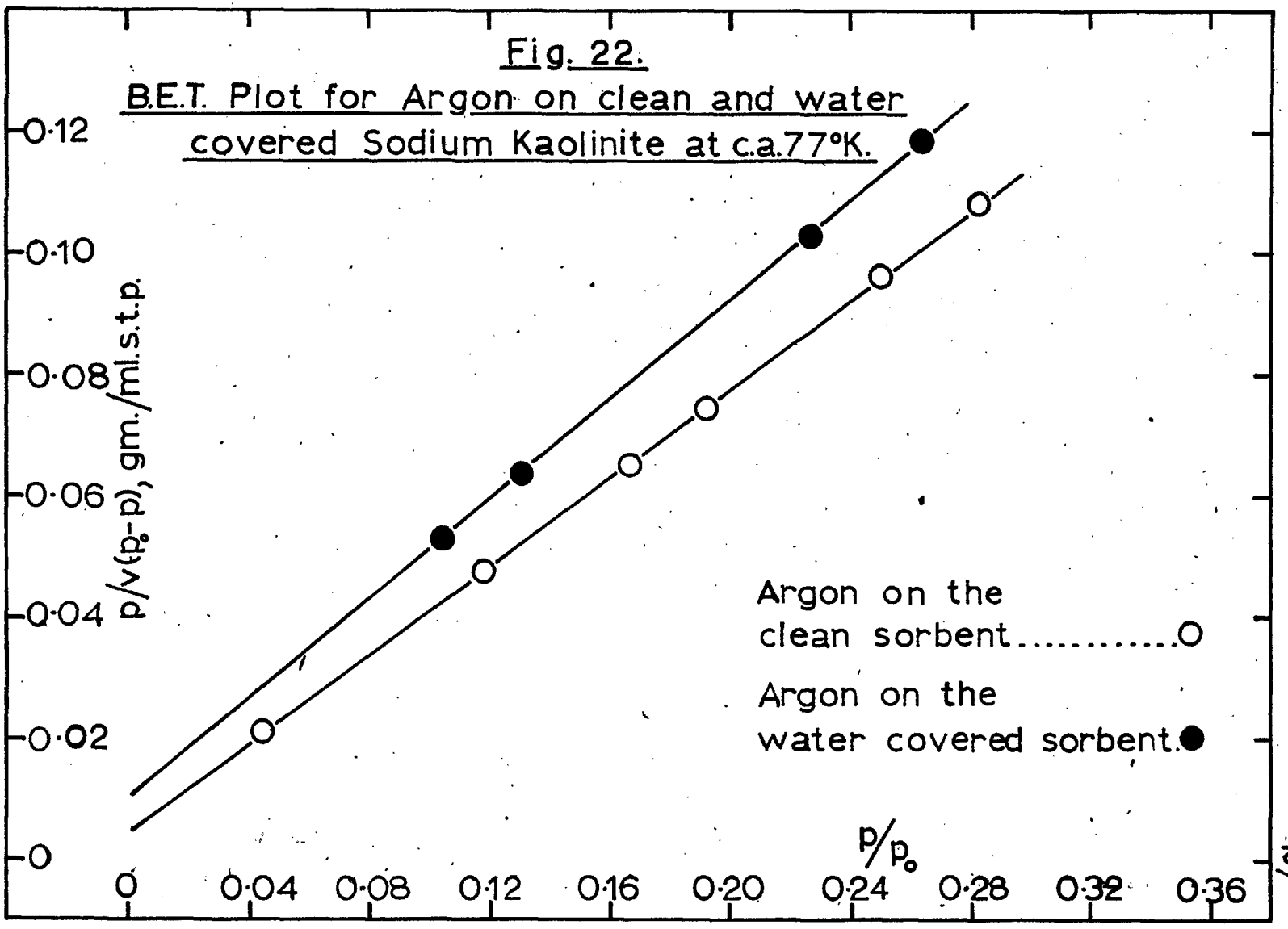
Fig. 22.
B.E.T. Plot for Argon on clean and water covered Sodium Kaolinite at c.a.77°K.
0·12
0·10
0·08
0·06
0·04
0·02
0
p/v(p₀-p), gm./ml.s.t.p.
0
0·04
0·08
0·12
0·16
0·20
0·24
0·28
0·32
0·36
p/p₀
Argon on the clean sorbent.....O
Argon on the water covered sorbent.●
107

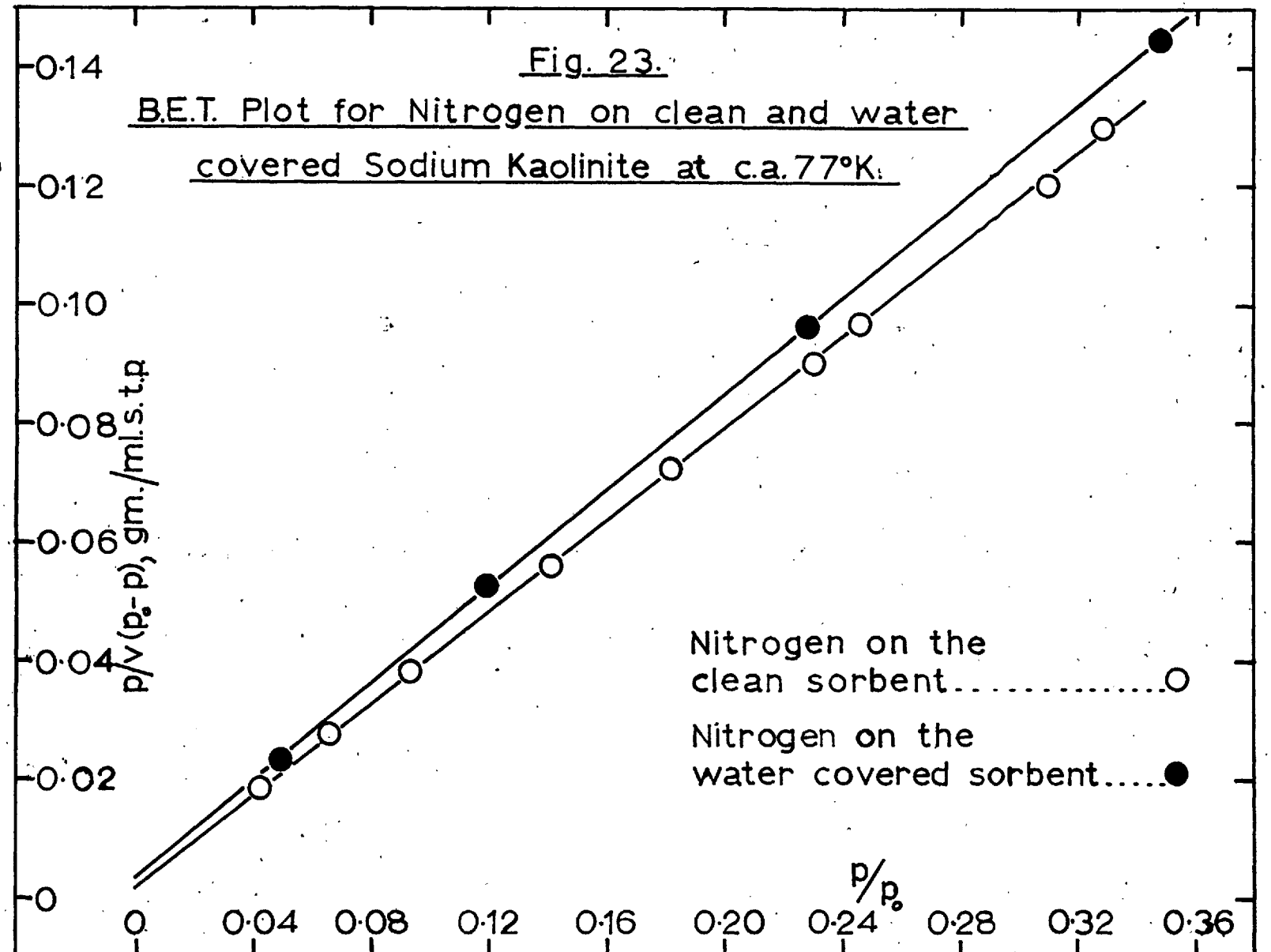
Fig. 23.
B.E.T. Plot for Nitrogen on clean and water covered Sodium Kaolinite at c.a. 77°K.
0·14
0·12
0·10
0·08
0·06
0·04
0·02
0
p/v(p₀-p), gm./ml.s.t.p
0
0·04
0·08
0·12
0·16
0·20
0·24
0·28
0·32
0·36
p/p₀
Nitrogen on the clean sorbent.....O
Nitrogen on the water covered sorbent.....●
801

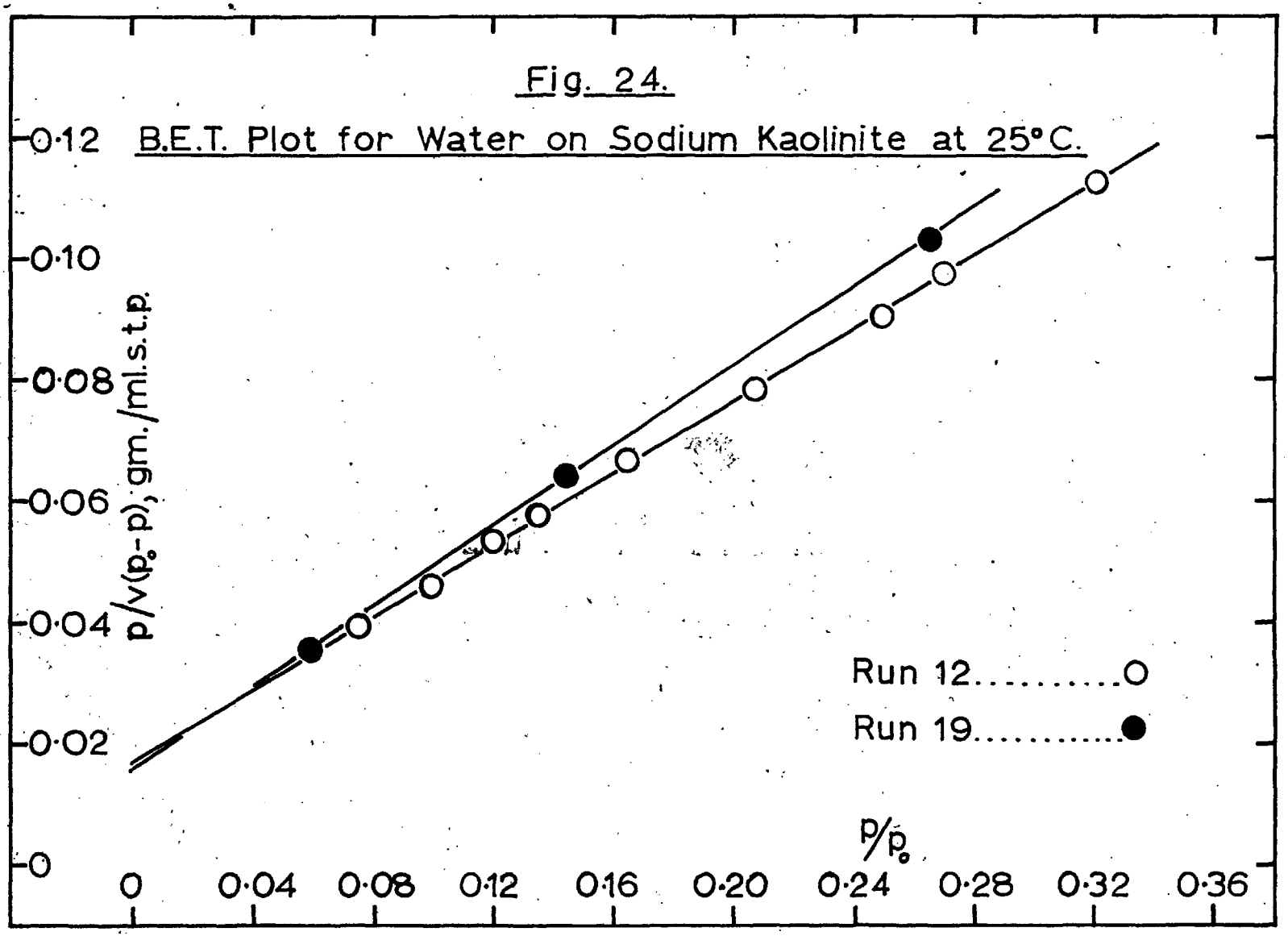
Fig. 24.
B.E.T. Plot for Water on Sodium Kaolinite at 25°C.
0·12
0·10
0·08
0·06
0·04
0·02
0
p/v(p₀-p), gm./ml.s.t.p.
Run 12.....O
Run 19.....●
p/p₀
0
0·04
0·08
0·12
0·16
0·20
0·24
0·28
0·32
0·36

Boobe, Millard and Cynarski (1953), in their investigations of argon on graphitised carbon at liquid nitrogen temperatures, observe that the heats of sorption fall to a minimum between the heat of sublimation and the heat of liquefaction, at the beginning of the second layer. They suggest that the adsorbed argon may approach the state of a liquid film but as the second layer nears completion there may be an increased order resulting in a solid film with correspondingly higher heats of adsorption. Morrison and Drain(1951) have obtained definite evidence that the freezing point of adsorbed argon on non-porous rutile is lowered by several degrees. Direct evidence that the extrapolated saturation vapour pressure of the supercooled liquid should be used for sorbed argon at $78^{\circ}K$ comes from a recent publication of Daneš and Nováková (1958). They have shown that sorption isotherms of argon at $78^{\circ}K$ and $90^{\circ}K$ on several adsorbents, porous and non-porous, only agree if the liquid value for p_o is used. Both argon and nitrogen isotherms were obtained at $78^{\circ}K$ and the use of the liquid value for p_o in the former case also resulted in better agreement between the surface area and pore diameter values.

In these experiments, the use of the value of p_o for the solid gave the unlikely result that on the sodium kaolinite surface the argon atom occupied a larger area

than the nitrogen molecule. Use of the extrapolated liquid value for p_o (23.2 cm) reverses this result. The latter value was therefore used in each case to calculate v_m for argon. The values of p_o for argon were calculated from Tables of Thermal Properties of Gases, U.S. Nat. Bur. of Standards Circular 564 (1955).

A summary of the values obtained for the volume sorbed in a monolayer is given below.

Table 27

Sorbate	Sorbent	Temperature	p_o cm.Hg.	v_m nℓ.s.t.p/gm
A	'clean'	77.36°K	23.2	2.67
A	water-covered	"	"	2.39
N_2	'clean'	"	76.0	2.60
N_2(run 20)	water-covered	"	"	2.45
				mgm./gm
H_2O(run 12)	'clean'	25.0°C	2.376	3.08
H_2O(run 19)	'clean'	"	"	2.94

The discrepancy between the isotherms of nitrogen on the water covered surface and that between the water isotherms were discussed in 4.3.

5.2. The Areas Occupied by Sorbed Molecules.

In their original paper, Emmett and Brunauer (1937)

suggested obtaining cross-sectional molecular areas for the various adsorbates by means of the equation

$$\text{Molecular area} = 4(0.866)\left[\frac{M}{4\sqrt{2}Ld}\right]^{\frac{2}{3}}$$

where M is the molecular weight of the adsorbate, L is Avogadro's number and d is the density of the solidified or liquefied adsorbate. The equation was derived on the assumption that the molecules have cross-sectional areas equivalent to those possessed in the liquid or solid forms, and that they are close packed on the surface of the adsorbent. It has been shown that this procedure gives very satisfactory agreement between areas obtained for molecules having similar boiling points, (e.g. N_2, CO and O_2). In general however, using the molecular areas calculated from the above equation the specific surface of any sorbent is slightly larger when nitrogen is used to determine it than with any other sorbate. The reason for this discrepancy is not understood.

The cross sectional area of nitrogen from this equation is 16.2 $Å^2$ and this is generally accepted as the value for sorbed nitrogen at its boiling point. Using the value of v_m for nitrogen on 'clean' sodium kaolinite listed in Table 19, the surface area of the sorbent could therefore be calculated as 11.3 metres^2/gm. Now, using the B.E.T. values of v_m for argon and water on the same

surface in conjunction with this surface area, the areas occupied by these sorbate molecules was calculated.

The same procedure was applied to calculate the cross sectional area of argon adsorbed on the ice surface. However the ice surface when the argon isotherms and when the nitrogen isotherms were done may not have been quite identical The water run prior to the argon isotherms on the ice surface was run 9 whereas the water run prior to the nitrogen isotherms on the ice surface was run 19, in which about 3 per cent more water was adsorbed and subsequently frozen. This difference in the sorbent may have been a contributory factor in obtaining an apparently larger cross-sectional area for argon when adsorbed on the ice surface. The values of the cross sectional areas obtained are listed in Table 28.

Table 28

Sorbate	Sorbent	Temperature	Molecular Area $\AA^2$	Molecular Area from Liquid close Packing $\AA^2$
N_2	'Clean'	77.36°K	-	16.2
A	Sodium Kaolinite	77.36°K	15.7	14.0
H_2O(run12)	Surface area	25.0° C	11.0	10.8
H_2O(run19)	11.3 m^2/gm.	25.0° C	11.5	10.8
N_2	Water covered Sodium Kaolinite	77.36°K	-	16.2
A	Surface area 10.7 m^2/gm.	77.36°K	16.7	14.0

A considerable amount of discussion exists in the literature on the nature of water adsorbed on clays. Hendricks and Jefferson (1938), Macey (1942) and Barshad (1949) have all proposed that the adsorbed water layer is in the form of a hexagonal network (see p. 7).

Hendricks and Jefferson suggested that the water layer is composed of water molecules joined into hexagonal groups of an extended hexagonal net. The stability of the layer of water molecules was said to arise from its geometrical relationship to the oxygen ions or hydroxyl groups of the silicate framework and the resultant formation of hydrogen bonds. If the separation of the oxygen atoms of the water layer is 3.0 $\mathring{A}$ in projection, the net has just the dimensions of the silicate layer minerals. There are then four molecules of water per molecular layer per unit cell of the clay mineral, each water molecule occupying an area of 11.7 $\mathring{A}^2$.

Macey's concept of the water layer, based on the similarity between the structure of ice and the oxygen ions at the surface of clay minerals, was that the initially adsorbed water has the structure of ice. This being so the area occupied by each water molecule would be 17.7 $\mathring{A}^2$.

Barshad suggested another concept of the nature of the adsorbed water on the basis of careful dehydration determinations with montmorillonite. He suggested that the

area occupied by the water molecule is reduced from 11.2 to 5.6 Å^2 because of changes in the packing of the water molecules on the surface as the clay mineral becomes more hydrated. The above theories are based almost entirely on a geometrical fit of the proposed water layer to the silicate lattice and supported by little experimental evidence relating to the area occupied by sorbed molecules. Clearly, in the light of the cross-sectional area for an adsorbed water molecule calculated from these experiments to be 11.0 - 11.5 Å^2, Macey's ice like structure is unacceptable on the basis of molecular area, as is the configuration at high states of hydration proposed by Barshad.

There has been considerable criticism of all three theories because they neglect the probable influence of exchangeable cations. Hendricks, Nelson and Alexander (1940) suggested that cations which can coordinate six molecules of water may stabilize the hexagonal array, but Williamson (1951) has pointed out that such a cation draws the molecules into closer packing and distorts rather than stabilizes the hexagonal network.

Williamson considers that water is physically associated with clay minerals in one or both of the following ways, (a) adsorbed on the surface of the clay

mineral proper, (b) as water of hydration of the base exchangeable cations. There is good evidence that the latter is inadequate in amount to account for all the adsorbed water of clay (see, for example, Walker, 1949). From the data obtained during these experiments it has been shown in 5.3. and 5.3a. that only about 20 per cent of the water monolayer is adsorbed in such a position that it is influenced by a cation. It is not possible therefore that in a hexagonal array of six water molecules all six molecules are equally associated with a cation.

5.3. Heats of Adsorption on Sodium Kaolinite.

The heat data on the sodium kaolinite surface (Fig. 16) show that about 20 per cent of the molecules in the monolayer are adsorbed with considerably higher heats than the remaining 80 per cent. This is especially noticeable in the case of water, where 20 per cent of the water monolayer is adsorbed with heats between 22 and 15 K.cal./mole and 80 per cent with heats between 15 and 12.5 K.cal./mole. Though less pronounced, a similar effect is observed with argon and nitrogen. It can therefore be concluded that in general, about 20 per cent of the kaolinite surface is considerably more active with regard to physical adsorption.

If this high activity was associated with high interaction energy resulting from dispersion forces then the

effect would be approximately the same for argon, nitrogen and water, since the dispersion forces associated with these molecules are of the same order of magnitude. This, however, is not the case and the difference in magnitude of the heats of adsorption of argon, nitrogen and water in the first 20 per cent of the monolayer indicates that the higher activity originates in electrostatic forces.

This conclusion is further supported by consideration of the heterogeneity in the first 20 per cent of the monolayer i.e. in those active sites.

Table 29

Sorbate	$\tilde{H}_g - \bar{H}_s$ at $\theta \approx 0$ k.cal./mole	$\tilde{H}_g - \bar{H}_s$ at $\theta = 0.2$ k.cal./mole	Change in $\tilde{H}_g - \bar{H}_s$ $\theta = 0 \rightarrow 0.2$ cal./mole.
A	2.9	2.4	500
N_2	4.0	3.2	800
H_2O	22	15	7,000

If the heterogeneity originated in sites of different dispersion energy then the decrease in heat values from $\theta = 0$ to $\theta = 0.2$ would be approximately the same for all three adsorbates. If, on the other hand, the heterogeneity originated in the electrostatic field at the surface, the change in heat of sorption with surface coverage would be

different for the three adsorbates because of the difference in their polar character. It is therefore evident that about 20 per cent of sites on the kaolinite surface are energetically more active in physical adsorption because of the higher electrostatic field associated with these sites.

5.3a. The Position of Exchangeable Cations

It is now suggested that the active sites on kaolinite are related to the exchangeable cations on the surface, in this case sodium ions. From the exchange capacity of the kaolinite used, 3.00 m.equivs. Na^+ per 100 gms., and the weight of water sorbed in a monolayer, 2.94 → 3.08 mgm./gm., it is readily calculated that there are 5.4 → 5.7 water molecules per cation. About 20 per cent of these water molecules are adsorbed on highly energetic sites, so that it can be concluded that only one water molecule can be adsorbed in a position where it is being influenced by a cation, assuming that all the cations are in such a position on the surface that close approach of adsorbed molecules is possible.

Keenan, Mooney and Wood (1951) have suggested, from considerations of ionic diameters and the kaolinite lattice, that the cations are probably situated in the centre of the hexagonal arrays of oxygen atoms which occur on one of the the basal surfaces of kaolinite.

However, calculations in this department on the electrostatic field above the kaolinite lattice (Broggazi, private communication) have shown that a positive ion would be repelled from this position and that therefore this cannot be the position adopted by exchangeable cations. These calculations are still going on and it is hoped, when they are further developed, to be able to predict the position of the cations in the kaolinite lattice.

It is now possible to postulate an adsorbed water phase in which about 20 per cent of the water molecules are adsorbed in close proximity to a cation and therefore experience a high interaction energy. The remaining 80 per cent of the monolayer interacts with the oxygen and hydroxyl ions of the rest of the kaolinite surface and the heats of sorption are only slightly above the heat of sublimation of water, as would be expected if water was adsorbed on to a surface similar in nature to water itself. In addition, there is no evidence for heats of sorption greater than the heat of sublimation in the second and higher layers, and no evidence that large numbers of layers of water are adsorbed at pressures substantially lower than the saturation pressure, as has been reported for silver iodide. This would require that the forces operating at the surface must be sufficiently long range to affect the outer layers.

In fact, Jaeger (1938) and Spiel (1940) have suggested that the thickness of adsorbed water at optimum plasticity for kaolinite is of the order of several hundred angstroms. However, De Wit and Arens (1950), by measurements of the density of hydrated kaolinite particles, have concluded that the thickness of adsorbed water held by kaolinite should be measured in a very few molecular layers, a finding which agrees with the data on water sorption in the present study.

5.4 Heats of Sorption on Water Covered Sodium Kaolinite.

If the high initial heats of sorption of argon and nitrogen on sodium kaolinite are due to the electrostatic heterogeneity of the exchangeable cations in the kaolinite lattice, then covering this surface with two layers of water (afterwards frozen at c.a. $77^{\circ}K$) would be expected to remove the effect of these active sites. As can be seen from Figs. 18a and 18b, this is exactly what was observed experimentally.

It should be noted that the first point in calorimetric measurements represents an integral heat from zero coverage so that the effect of energetic sites which represented only a small proportion of the total surface would still be detectable. In fact, on the water covered surface, high heat values for $\theta = 0 \rightarrow 0.2$ are entirely absent and the graphs for the 'clean' and water covered sorbents cross

at about $\theta = 0.2$, i.e. the high energy cation sites must have been covered by water.

For the range $\theta = 0.2 \rightarrow 1.0$ heats of sorption of both argon and nitrogen are approximately the same on ice as on sodium kaolinite, thus confirming the theory outlined above that 80 per cent of the kaolinite surface consists of oxygen and hydroxyl ions energetically very similar to the ice surface.

5.4a. The Effect of the Nitrogen Quadrupole.

The heats of sorption of nitrogen on sodium kaolinite are greater than those for argon on this surface until about 90 per cent of the monolayer has been filled. This can be attributed to the contribution of the nitrogen quadrupole in the field gradients occurring at the surface of kaolinite (this being inhomogeneous), and which occur at any ionic surface. However it is also found that the heats of sorption of nitrogen on the ice surface are substantially higher than those for argon on this surface, although the ice surface is considerably more homogeneous than kaolinite. Initially the nitrogen heats are some 900 cal/mole greater than the argon heats. This is presumably due to the interaction of the nitrogen quadrupole with the field due to the two layers of water dipoles. A more detailed discussion will be undertaken after consideration of the electrostatic field above a plane of water dipoles.

5.4b. Lateral Interaction between Adsorbed Molecules.

Although the ice surface is much more uniform than the kaolinite surface, in neither case is there any tendency for the argon or the nitrogen heat values to increase as $\theta \rightarrow 1.0$. The effect of mutual interactions between adsorbed argon atoms is discussed in 5.5c, but the same treatment of adsorbed nitrogen molecules is complicated by the presence of the nitrogen quadrupole and by the dependence of the interactions between quadrupoles on their orientation.

Macleod (Ph.D. thesis, 1958) has dealt in detail with the quadrupole-quadrupole interaction of nitrogen sorbed in natural chabazite. He considered the mutual interaction to be expected from a system of non-rotating linear quadrupoles and calculated the interaction energy between two molecules in four basic orientations. Taking the value of the nitrogen quadrupole to be $Q_s = 2.58 \times 10^{-26}$ e.s.u., Macleod calculated that the attractive interaction energy due to dispersion and repulsive forces is between 50 and 260 cal./mole at separations of $4.1 \rightarrow 4.5$ Å. He states, however, that the lower value is probably near zero because the calculation of the repulsive energy in this particular orientation leads to a value which is too small. Drain (1953) calculated that at a separation of 4.44 Å the interaction

energy of a complete monolayer of nitrogen molecules forming a square lattice, with the quadrupoles parallel to one side of the square, was about 100 cal/mole compared to an attraction of 400 cal./mole due to dispersion forces.

It cannot therefore be concluded that the absence of a maximum as $\theta \rightarrow 1.0$ in the nitrogen heat curve on the water surface is attributable to the quadrupole-quadrupole repulsive forces. The most that can be said is that the magnitude of any vander Waals attraction between the sorbed molecules would certainly be reduced by these repulsive forces. The actual magnitude of the quadrupole-quadrupole interaction depends largely on the orientation of the molecules, about which little is known.

Beebe, Millard and Cynarski (1953) measured the heats of sorption of argon on two carbon black adsorbents, Graphon and Spheron. On Graphon, which has the more homogeneous surface an increase of c.a. 400 cal./mole is observed from $\theta = 0.5 \rightarrow 1.0$, and this is attributed to lateral interaction between the adsorbed molecules. On Spheron this increase is not observed and it is suggested that the heterogeneity of the Spheron surface may smear out the effect of lateral interaction. This may also occur at the kaolinite surface.

Maxima in the isosteric heat values in the region $\theta = 0.5 \rightarrow 1.0$ have also been reported by other authors,

e.g. Orr (1939a) for argon, nitrogen and oxygen on potassium chloride and caesium iodide, and Rhodin(1950) for nitrogen on single crystal faces of copper. Detailed discussion on the absence of a maximum in the heat values of argon on the water surface is reserved for 5.5c.

5.5. The Electrostatic Field above the Water Covered Kaolinite Surface.

In order to achieve a fuller understanding of the observations outlined in 5.4a and 5.4b it is necessary to consider the field above two layers of water molecules adsorbed on to the kaolinite lattice. However, calculations in this department by Bregazzi (private communication) have shown that the electrostatic field above the kaolinite lattice falls to zero at a distance of about 6 $\mathring{A}$ from the oxygen or hydroxyl layer at the kaolinite surface. Therefore, the electrostatic field at any point above two layers of water molecules would be unaffected by the field associated with the kaolinite.

For the calculation of the field, the water layer was assumed to consist of an infinite plane of water dipoles in a close packed hexagonal array each a distance 'd' apart. Two dipole arrays were considered, (i) all dipoles orientated perpendicular to the surface, (ii) all dipoles oriented parallel to the surface. For case (i) all the dipoles were assumed to be oriented perpendicular to the

plane and in the same sense. Then the field perpendicular to the plane at any point A, due to one dipole of strength μ, is given by the equation

$$Fx' = \frac{\mu}{a^3}(1 - 3\cos^2\theta)$$

where 'a' is the distance between A and the dipole centre, and θ is the angle between the polar axis and the line joining A and the dipole centre. The field parallel to the plane is zero.

The total field was calculated at various heights (a) above the centre of one triangle of dipoles, and (b) directly above one dipole. A summation of the twelve rings of nearest neighbours (63 dipoles) was followed by an integration from the thirteenth ring to infinity and the total field for an infinite plane thereby obtained. The calculation is given in detail in Appendix I.

The same calculation above the centre of one triangle of dipoles was repeated for an infinite plane of dipoles all oriented parallel to the plane and in the same sense. In this case the field perpendicular to the plane of polar centres is zero and the field parallel to the plane is given by the equation

$$Fx'' = \frac{\mu}{a^3}(1 - 3\cos^2\theta)$$

The value of Fx' for any one dipole differs from that of

F_x'' since θ will be altered by 90° because of the change in orientation of the dipole. In fact, for the position above a triangle of dipoles, the field above the plane of dipoles which have orientation (ii) is half the field at the same point above the plane of dipoles oriented perpendicular to the surface (see Appendices I and II). The calculations are summarised in the following table and in Fig. 25.

Table 30

Height above the plane of dipole centres	Field directly above a dipole due to a plane of dipoles with orientation (i)	Field above the centre of a triangle of dipoles due to a plane of dipoles orientation (i)	orientation (ii)
0.4 d		6.24 μ/d^3	
0.5 d	-10.07 μ/d^3	3.41 "	1.65 μ/d^3
0.6 d	- 4.51 "	1.79 "	
0.8 d		0.456 "	
1.0 d	- 0.25 "	0.117 "	0.014 "
1.5 d	- 0.026 "	0.014 "	0 "
2.0 d	- 0.014 "	0 "	0 "

It can be seen that the values in column 4 are not exactly half the values in column 3. This discrepancy is due to the limitation of the summation and integration method used and would disappear if a sufficiently large number of dipoles

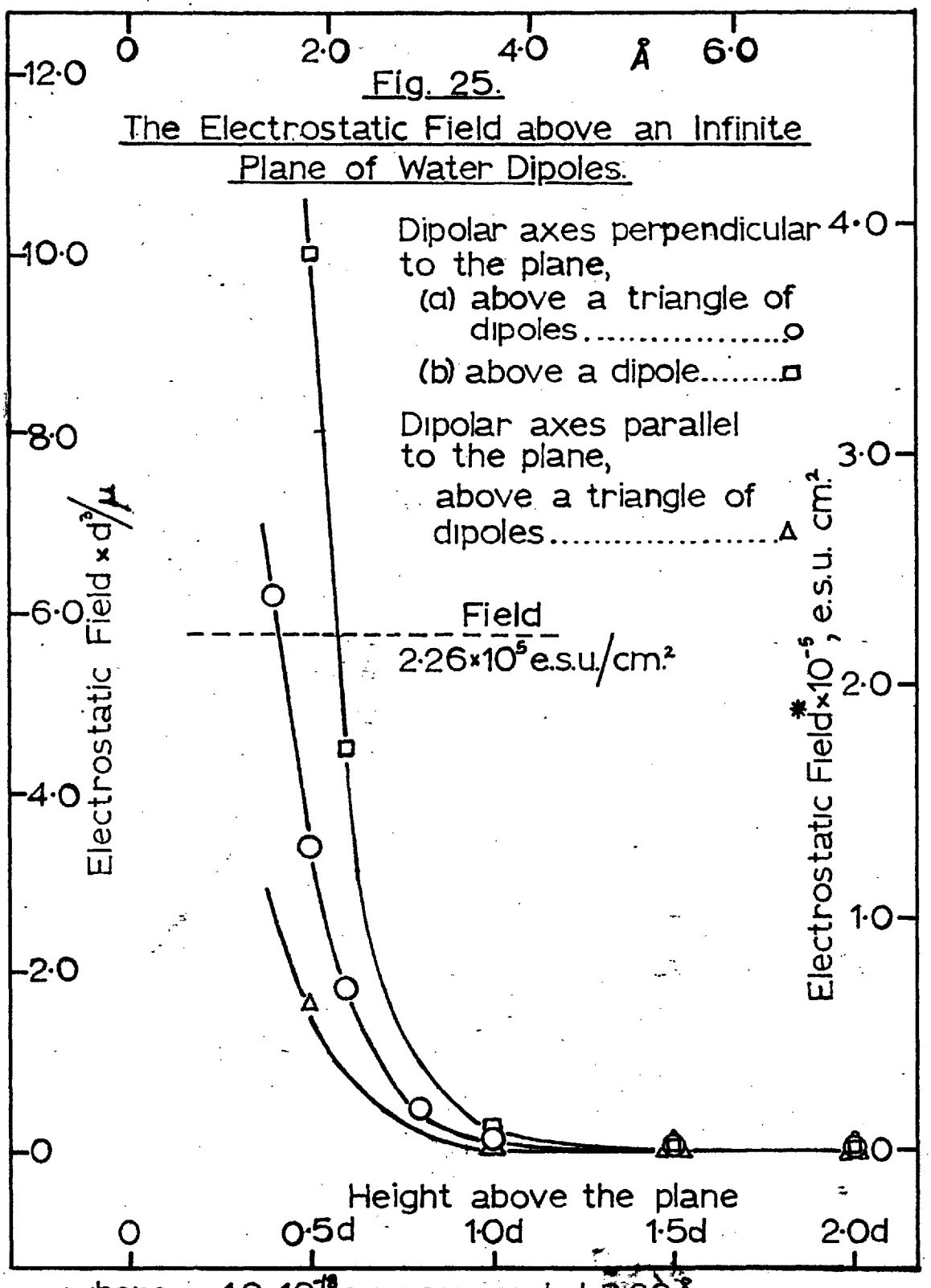

Fig. 25.

The Electrostatic Field above an Infinite Plane of Water Dipoles.

* where $\mu = 1{\cdot}8 \times 10^{-18}$ e.s.u. cm., and d = 3·60 Å.

were considered for the summation.

During the course of these calculations it was found that above the centre of a triangle of dipoles, the field due to the nearer neighbours only was opposite in sign to the total field. In other words, the direction of the field at this point is opposite to that which might be expected at first sight, and a layer of dipoles with their positive ends outwards would attract a positive charge to this position. Roberts (1939) observes the same effect in his calculation of the electrostatic field above the 100 plane of a body centred ionic crystal, which is analogous to the plane of water dipoles when all the dipoles are oriented perpendicular to the plane since in both cases, if the dipoles are not treated as point charges but as rods of small but finite length, there are two parallel planes opposite in sign.

As can be seen from Table 30, the effect of the underlying layer of water molecules on the field at a point above the second layer is negligible since the distance to the plane of dipole centres of the underlying layer must be greater than 'd'.

5.5a. The Interaction of Nitrogen with the Field above the Water Surface.

The fact that the heats of sorption of nitrogen are greater than those of argon on the water surface has

been attributed to the effect of the nitrogen quadrupole. The energy of interaction of any quadrupole with an electrostatic field is given by the equation

$$\mathcal{E} = \frac{Q}{4}\left(\frac{\partial F}{\partial t}\right)$$

where Q is the quadrupole moment and $\partial F/\partial t$ the field gradient.

The energy of interaction of a nitrogen quadrupole with the field above a layer of water dipoles all oriented perpendicular to the surface was therefore considered. The field gradient was calculated from Fig. 25 at various distances from the plane of dipole centres. In these calculations 'd', the separation of the water molecules, was taken to be 3.60 Å (calculated from the nitrogen specific surface and the B.E.T. values of the water monolayer), μ, the water dipole, as 1.8×10^{-18} e.s.u. cm. and Q, the quadrupole moment of a non rotating nitrogen molecule, as 3.0×10^{-26} e.s.u. cm^2 (Hill and Smith, 1951). The calculations are summarised in the following table and Fig. 26.

The experimental results have shown that the initial heat of sorption of nitrogen on the water surface is c.a. 900 cal./mole greater than that for argon on the same surface. It can be seen from Fig. 26 that, if this heat is attributed to the interaction of the nitrogen quadrupole with the field, and if the nitrogen molecule is

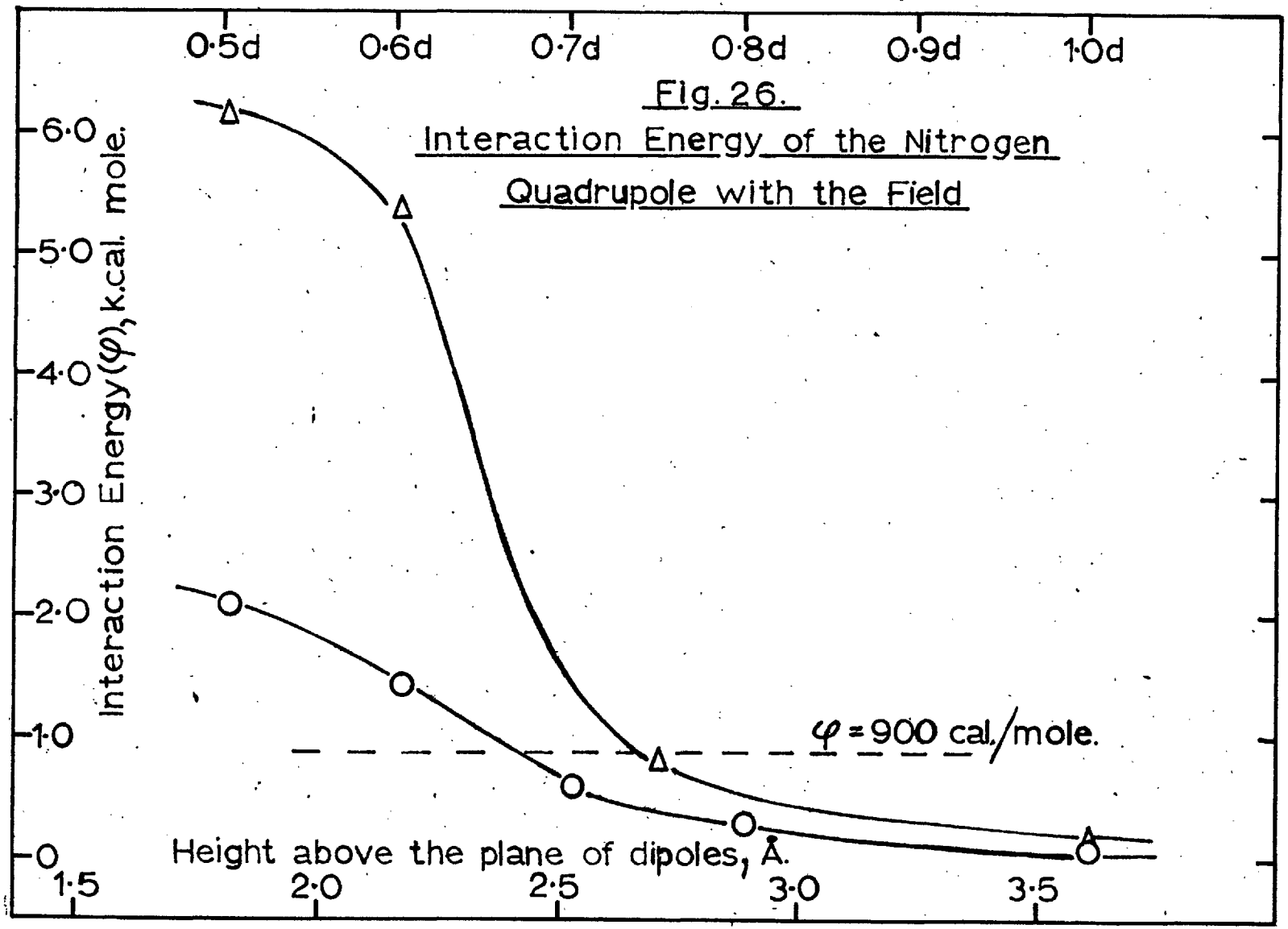
0·5d
0·6d
0·7d
0·8d
0·9d
1·0d
Fig. 26.
Interaction Energy of the Nitrogen Quadrupole with the Field
Interaction Energy(φ), k.cal. mole.
6·0
5·0
4·0
3·0
2·0
1·0
0
φ = 900 cal./mole.
Height above the plane of dipoles, Å.
1·5
2·0
2·5
3·0
3·5

Table 31

Distance above the plane, t.	Interaction with the field above a triangle of dipoles $\frac{\partial F}{\partial t}$ e.s.u./cm^3 x10^{-12}	φ, cal/mole	Interaction with the field directly above a dipole $\frac{\partial F}{\partial t}$ e.s.u./cm^3 x10^{-12}	φ, cal/mole
0.50d (1.80 Å)	19.5	2,100	56.9	6,140
0.60d (2.16 Å)	13.5	1,450	49.7	5,370
0.70d (2.52 Å)	5.7	620		
0.75d (2.70 Å)			7.7	830
0.80d (2.88 Å)	3.1	330		
1.00d (3.60 Å)	0.96	104	1.3	140

(a) above the centre of a triangle of dipoles, the quadrupole centre must be 2.40 Å above the plane of polar centres of the water layer, (b) directly above a dipole, the quadrupole centre must be 2.68 Å above the plane of polar centres of the water layer. Consideration of the dipole orientation in which the polar axes are parallel to the surface would give similar values of the field gradient to those in column 2 of Table 31, and would result in a slightly smaller separation to correspond with an interaction energy of 900 cal./mole. This case has not been calculated in full.

Both calculated values of the separation are, in fact, fairly small in view of the radii of the molecules involved,

but they are more acceptable if it is allowed that the polar centre of the water molecule may be displaced from the molecular centre. Burnelle and Coulson (1957) have shown that the main part of the dipole moment of water comes from the lone pair electrons of the oxygen atom, so that the polar centre is likely to be displaced in the direction of the oxygen atom. The radius of the water molecule is about 1.4 Å, and the minimum radius of the nitrogen molecule about 1.7 Å. Therefore, the expected separation would be about 3.1 Å. However, bearing in mind the limitations of the method used, the values of 2.40 Å and 2.68 Å derived from Fig. 26 can be accepted as support for the theory that the 900 cal/mole by which the nitrogen heats are in excess of the argon heats is due to the quadrupole-field interaction.

5.5b. The Interaction of Argon with the Field above the Water Surface.

The data obtained for argon on both surfaces have shown that the heat of sorption of argon on two layers of water is some 600 cal./mole greater than that of argon on two other layers of argon. In both cases the distance of the third layer from the kaolinite lattice prevents the latter playing any part (see p. 124). Therefore, the difference can be attributed to the interaction of the induced dipole of the argon atom and the field due

to the water surface.

Within the limitations discussed below, the energy of interaction is given by the expression

$$\varphi = -\tfrac{1}{2} \alpha F^2$$

where $\alpha = 1.63 \times 10^{-24}$ c.c./molecule the polarizability of argon, and F is the field. Therefore when $\varphi = 600$ cal./mole, $F = 2.26 \times 10^5$ e.s.u./cm^2. This is the field in which the argon atom must be situated in order to produce a heat of sorption by dipole induction of 600 cal./mole. From Fig. 25 it is therefore possible to say that, for the orientation in which the polar axes are perpendicular to the surface, the induced dipole centre must be 1.5 Å or 2.1 Å above the plane of water dipoles, depending on the position adopted by the argon atom. Consideration of the radius of the water molecule (c.a. 1.4 Å) and of the argon atom (c.a. 1.9 Å) indicates that these separations are impossibly small, but the discussion below shows that the use of the equation $\varphi = -\frac{1}{2}\alpha F^2$ is likely to yield a value smaller than the true value.

The argon atom adsorbed on the water surface is situated in a steep field gradient and, furthermore, the field close to the dipoles is large. Both these facts make it doubtful whether the value of α quoted above can legitimately be used in this calculation.

Lenel (1933) calculated the heats of adsorption of argon on ionic crystals (a system very similar to argon on the water surface) and obtained good agreement between his calculated and his measured heats. He considered that in calculating the ion-induced dipole interaction the mean polarizability of argon could not be used because the field of the ionic lattice is very inhomogeneous. Lenel, in fact, did not calculate the total field above the ionic lattice but assumed that practically the entire effect depended on that part of the adsorbed atom which was close to the ion. He calculated the interaction energy accordingly by means of an equation derived by Teller.

Orr (1939b) has dealt with the electrostatic field above the ionic lattice in a much more thorough manner. He evaluated the field by a direct summation of 88 - 96 ions and calculated the remaining contributions by integration but went on to calculate the interaction energy by using the mean polarizability of argon without commenting on the justification for using it when the adsorbed atoms experience a large field gradient.

Coulson, Maccoll and Sutton (1952) have shown that the static polarizability increases with high field strengths of the order of 10^8 V./cm., which are experienced in the neighbourhood of an ion or dipole, the induced dipole may be as much as twice that calculated from the expression

$\mu_i = \alpha F$, this having been derived on the assumption that F is small, and α being the 'small field' polarizability.

The above factors all imply that the simple calculation of the separation of the induced dipole from the plane of permanent dipoles is likely to result in a value which is too small. Although the radii for water and argon stated above imply that a separation of about 3.3 Å should be anticipated, the separation may actually be smaller than that if allowance is made for the displacement of the polar centre of both molecules from the molecular centre.

5.5c. Lateral Interaction between Adsorbed Argon Atoms.

Consideration of the magnitude of the van der Waals attractive forces between molecules leads one to expect that the heat curve of argon on a homogeneous surface would show a considerable maximum (of the order of 1 K.cal./mole) as the second half of the monolayer was filled, assuming that the sorbed atoms adopted a separation at or near their equilibrium separation. This has been observed by Beebe et al (1953) for argon on Graphon, but does not occur during the sorption of argon on the water surface studied during these experiments.

The magnitude of the induced dipole-induced dipole repulsion between argon atoms was found to be insufficient

to outweigh the van der Waals attraction at separations near the equilibrium separation as can be seen in Fig. 27.

It has already been shown that, in order to satisfy the heat data, the argon atom must be situated in a field of strength 2.26×10^5 e.s.u./cm.^{2}, although this is probably closer to the value of the average field in which the atom lies than to the field at the centre of the induced dipole. From a knowledge of the field the value of the induced dipole can be calculated from the equation $\mu_i = \alpha F$, where α is the polarizability of argon. The value of μ_i is then 0.37×10^{-18} e.s.u. cm. The heats of adsorption arising from the mutual repulsion of induced dipoles, for a random distribution of particles over the surface, can now be calculated for various separations from the equation (Miller, 1949)

$$\varphi_{(R)} = \frac{9\mu_i^2 \,(2 + 9\alpha\theta/r^3)}{2r^3\,(1 + 9\alpha\theta/r^3)^2}$$

where 'r' is the separation of the atoms. The values calculated were those at the maximum interaction, i.e. at $\theta = 1.0$, and are given in Table 32.

The van der Waals attraction of argon atoms at various separations was calculated from the well known Lennard-Jones potential

$$\phi(r) = \epsilon \left[\left(\frac{r_e}{r}\right)^{12} - 2\left(\frac{r_e}{r}\right)^{6} \right]$$

where ϵ = 233.2 cal./mole, r_e = 3.84 Å } from second virial coefficient data.

The values in Table 32 for the van der Waals attractive forces are for 6 $\phi(r)$ since in the close packed array each at. has six nearest neighbours. All values were calculated for θ = 1.0 i.e. at the completion of the monolayer.

Table 32

Atomic Separation Å	Induced Dipole Repulsion cal./mole	van der Waals Attraction cal./mole
3.0	371	
3.2	332	4,120
3.4	301	229
3.45		- 171
3.5		- 637
3.55		- 884
3.6	270	-1,089
3.8	240	
4.0	216	-1,333
4.2	193	
4.4	174	- 963
4.6	156	
4.8	141	- 637
5.0	127	
5.2	115	- 417
5.6	95	- 276
6.0	79	- 185

As well as the absence of a maximum in the argon heat curve a distinct decrease of some 200 cal./mole occurs at about θ = 0.5. At this coverage lateral

Fig. 27.

The Induced Dipole Repulsion and the van der Waals Attraction between Adsorbed Argon Atoms

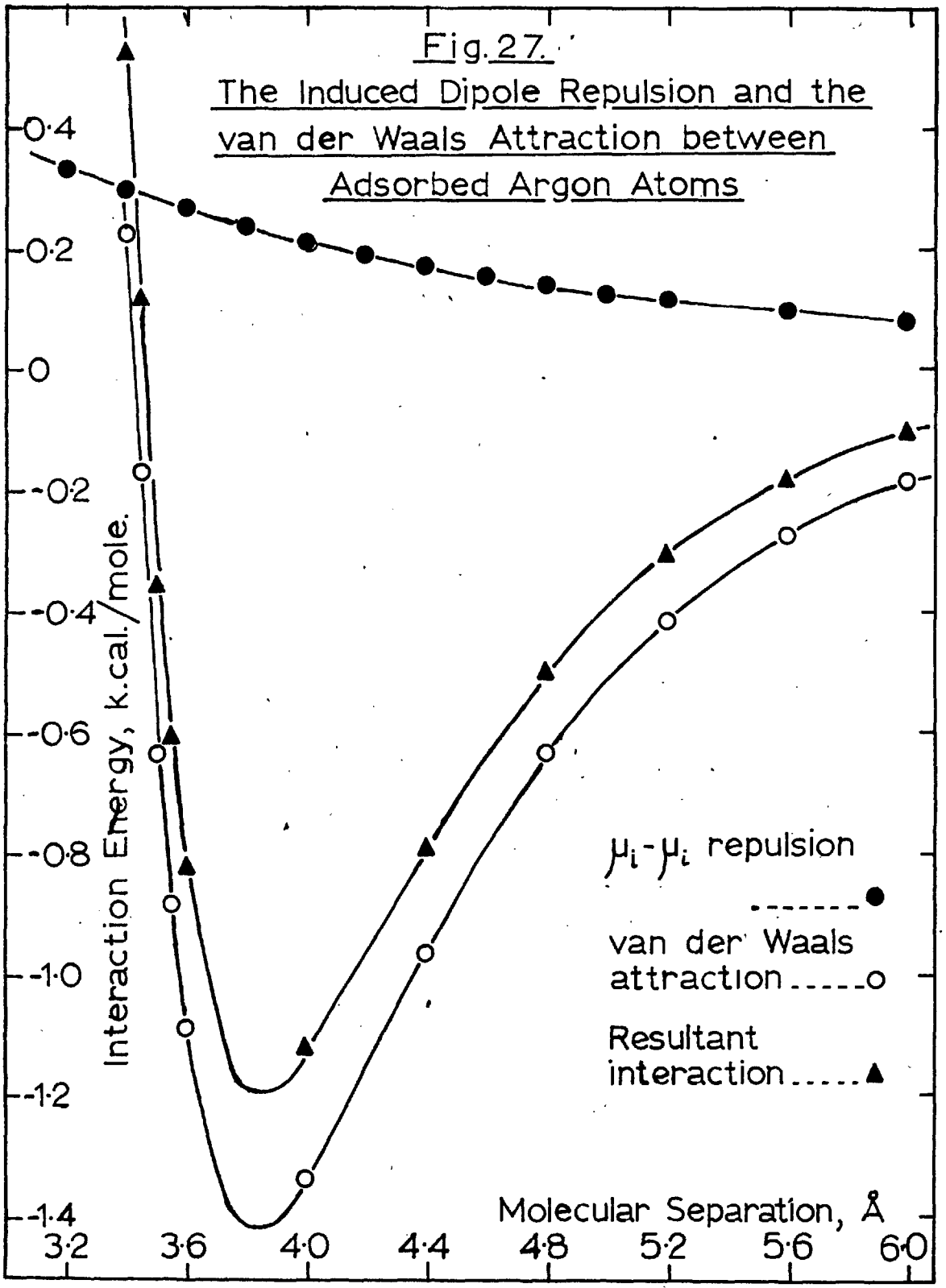

interactions between adsorbed molecules begin to be important and this fall of 200 cal./mole in the heat values can only be attributed to a repulsion between the adsorbed argon atoms. As can be seen from Fig. 27, a repulsion of this magnitude can only be explained if the sorbed atoms are substantially closer together than the equilibrium separation. In fact, allowing for the induced dipole-induced dipole repulsion the separation must be 3.44 Å. This would require that the sorbed atoms be squeezed together in the sorbed phase. However, it seems reasonable to suppose that the most likely position for the argon atoms to adopt on the water surface, i.e. the position of minimum potential energy, would be above the centre of a group of three water molecules. The argon atoms would then have a separation equal to that of the water molecules i.e. 3.56 → 3.64 Å, which, considering the inaccuracy of the B.E.T. theory and the fact that the water has afterwards been frozen at 77°K, is in good agreement with the value of 3.44 Å required.

Even without the mutual interaction of the induced dipoles, a repulsion of 200 cal./mole would occur because of van der Waals forces if the atoms had a separation of 3.40 Å. Therefore no firm conclusion can be drawn that the orientation of the water dipoles is perpendicular to the surface, which would be required for the maximum

repulsive energy from the induced dipole-induced dipole interaction. The data can be explained more readily however if this orientation is accepted.

5.6. Evaluation of the Entropy of the Sorbed Phase from Experiment 1 Data.

From a knowledge of the isotherm and heats of sorption of any one system the differential entropy of the sorbate may be calculated. Garden, Kington and Laing (1955) have shown that the differential entropy is given by

$$\bar{S}_s = \tilde{S}_{g_0} + R\ell n\,(p_o/p) - \alpha p - \frac{(\tilde{H}_g - \bar{H}_s)}{T}$$

where $\tilde{S}_{g_0}$ is the molar entropy of the ideal gas at a standard pressure p_o at the temperature T of the experiment. The choice of p_o is entirely arbitrary but 1 atm. is usually chosen. α is a correction for non-ideality of the gas phase and is introduced by the use of the Berthelot equation of state

$$\alpha = \frac{27}{32} \cdot \frac{R}{P_c} \cdot \frac{T_c^3}{T^3}$$

where T_c and P_c are the critical temperature and pressure of the bulk phase. The molar entropy of the ideal gas must be determined either by calculation from theoretical considerations or from experimental data available in the literature.

5.6a. The Differential Entropy of Adsorbed Argon at 77.36K

For monatomic molecules the molar entropy of the ideal

gas can be calculated from the Sackur-Tetrode equation

$$\tilde{S}_{g0} = R(\tfrac{3}{2}\ln M + \tfrac{5}{2}\ln T - \ln P + K_{SP})$$

where M is the molecular weight of the gas. If P = 1 atm., K_{SP} = -1.157 (Mayer and Mayer, 1940). This equation gave a value of 30.30 e.u. for $\tilde{S}_{g0}$, and the differential entropies of sorbed argon at 77.36°K on sodium kaolinite and on the water surface were calculated from the equation stated in 5.6. The experimentally measured isotherm points were used in the calculation and the corresponding values of $\tilde{H}_g - \bar{H}_s$ read off from the heat curve. αp, the correction term for non-ideality of the gas phase, amounts to 0.03 e.u. at a pressure of 10 cm. and can therefore be considered negligible for all lower pressures. The data are given in Tables 33 and 34.

5.6b. The Differential Entropy of Adsorbed Water at 25°C

In this case the molar entropy of the ideal gas was obtained from Kelley (1948). When p_0 = 76 cm., $\tilde{S}_{g0}$ = 45.13 ± 0.03 e.u. The correction term for the non-ideality of water at 25°C is again negligible, αp amounting to only 0.002 e.u. at a pressure of 2 cm. As in the case of argon the experimental isotherm points were used and the corresponding heat values interpolated from the heat curve. Because of the uncertainty in the isotherm of run 9, only the isotherm points from run 12 were used in conjunction with the heat curve. The data

Table 33

Differential Entropy of Argon

on Sodium Kaolinite at 77.36°K

Run and Increment No.	Volume Sorbed mℓ. s.t.p./gm.	$\theta = V/v_m$	$\bar{S}_s$(exp.) e.u.
13/1	0.65	0.24	12.05
13/2	1.74	0.65	9.81
13/3	2.78	1.04	10.53
13/4	3.16	1.18	10.93
13/5	3.45	1.29	10.99
13/6	3.61	1.35	11.01
14/1	0.92	0.34	12.05
14/2	1.60	0.60	9.89
14/3	2.19	0.82	10.09
14/4	3.04	1.14	10.83
14/5	4.01	1.50	11.03
14/6	4.87	1.82	10.78
14/7	5.73	2.15	10.03
14/8	6.42	2.40	9.00

Table 34

Differential Entropy of Argon on Water Covered Sodium Kaolinite at 77.36°K.

Run and Increment No.	Volume Sorbed m.ℓ.s.t.p./gm.	$\theta = V/V_m$	$\bar{S}_s$(emp.) e.u.
10/1	0.58	0.24	11.10
10/2	1.10	0.46	10.87
10/3	1.43	0.60	11.13
10/4	2.17	0.91	10.68
10/5	2.83	1.18	11.50
10/6	3.82	1.60	11.15
10/7	4.76	1.99	10.75
11/1	0.65	0.27	10.94
11/2	1.61	0.67	10.78
11/3	2.35	0.98	11.25
11/4	3.01	1.26	11.47
11/5	4.02	1.68	11.03

Table 35

Differential Entropy of Water on Sodium Kaolinite at 25°C

Increment No.	Weight Sorbed mgms/gm	$\theta = W/\omega_m$	$\bar{S}_s$(exp.) e.u.
1	0.09	0.03	2.06
2	0.27	0.09	7.28
3	0.58	0.19	11.72
4	0.76	0.25	16.65
5	1.06	0.34	16.04
6	1.23	0.40	15.84
7	1.53	0.50	14.17
8	1.69	0.55	13.66
9	1.98	0.64	13.04
10	2.14	0.69	12.50
11	2.30	0.75	12.24
12	2.46	0.80	12.29
13	2.61	0.85	12.43
14	2.76	0.90	12.86
15	2.99	0.97	13.24
16	3.13	1.02	14.03
17	3.37	1.09	14.13
18	3.50	1.14	14.68
19	3.71	1.21	14.68
20	3.83	1.25	14.60
21	4.22	1.37	14.27

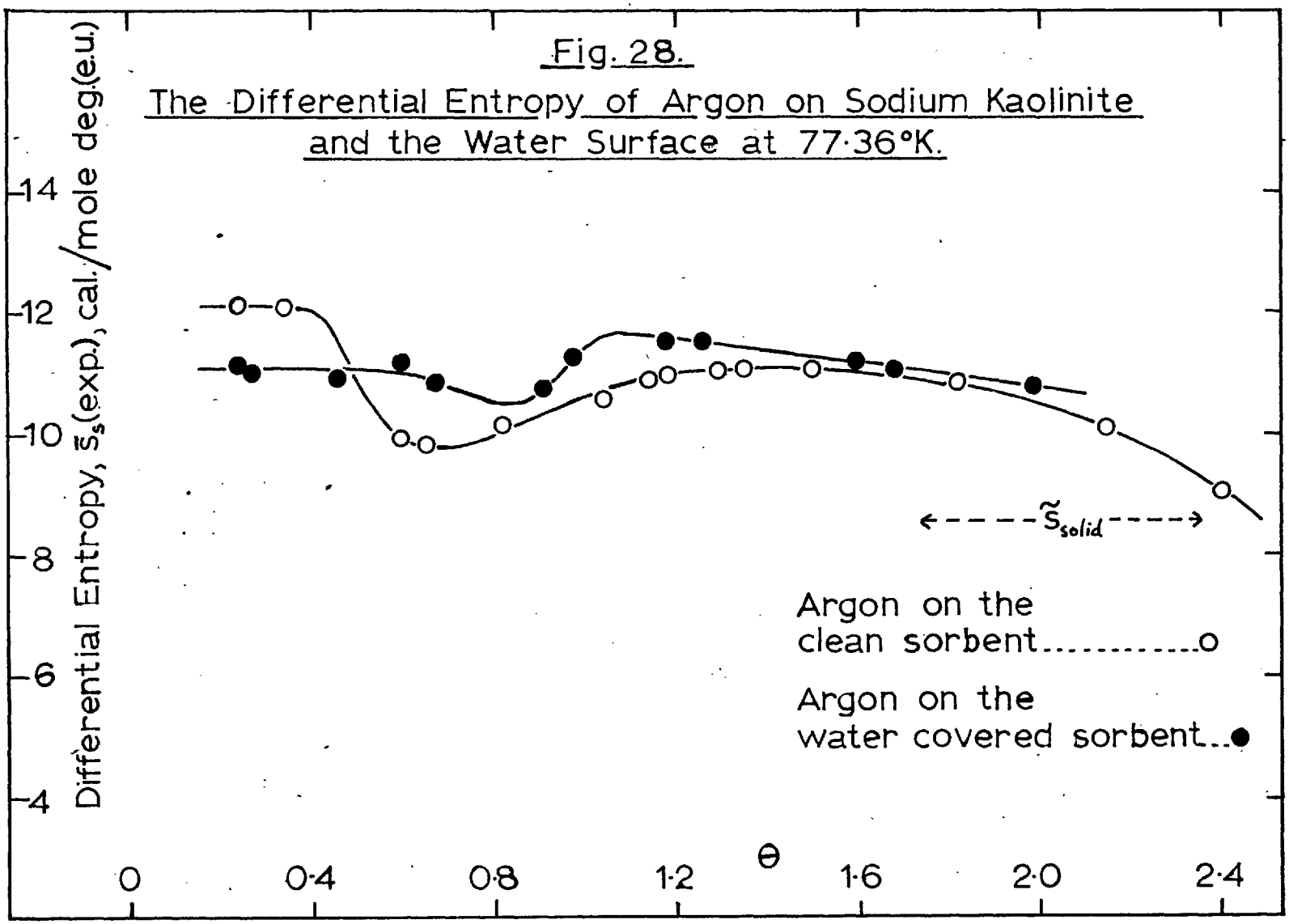
Fig. 28.
The Differential Entropy of Argon on Sodium Kaolinite and the Water Surface at 77·36°K.
Differential Entropy, $\bar{s}_s$(exp.), cal./mole deg.(e.u.)
14
12
10
8
6
4
0
0·4
0·8
1·2
θ
1·6
2·0
2·4
$\tilde{s}_{solid}$
Argon on the clean sorbent.....o
Argon on the water covered sorbent...●

145

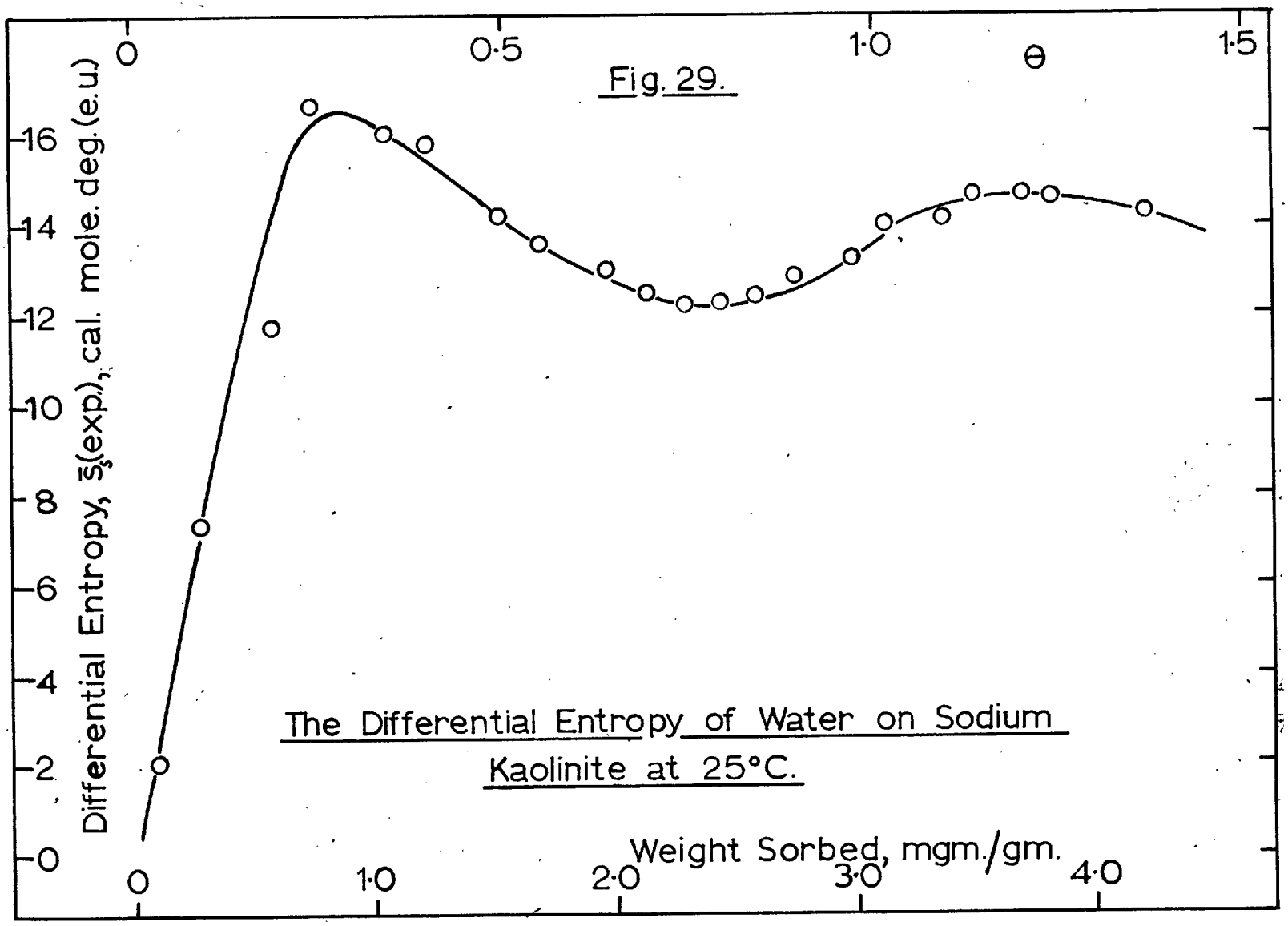
Fig. 29.
Differential Entropy, $\bar{s}_s$(exp.), cal. mole. deg.(e.u.)
0
2
4
6
8
10
12
14
16
0
0·5
1·0
1·5
θ
0
1·0
2·0
3·0
4·0
Weight Sorbed, mgm./gm.
The Differential Entropy of Water on Sodium Kaolinite at 25°C.

are given in Table 35.

5.7. The Nature of the Sorbed Phase.

A monolayer on the exterior of a solid may be considered as being either mobile or localized, depending on the magnitude of the thermal energy of the sorbate compared with the surface-energy barriers. If the sorbed molecules encounter potential barriers on the surface greater than their thermal energy then they will tend to be confined to one region of the solid and the phase will be localized. Alternatively with lower potential barriers or at higher temperatures, the molecules may possess considerable translational freedom.

The concept of a sorbed phase being either completely localized or completely mobile is obviously oversimplified, and there is the possibility that a localized-mobile transition could occur. For example, a phase which is completely mobile at low sorbate concentrations must become localized at high concentrations. The caging action of neighbouring molecules will result in a free translation passing over to a vibration of progressively decreasing amplitude with increasing concentration of sorbed molecules.

Gorden and Kington(1956) have considered the entropy of a localized phase on an energetically homogeneous set of sites. The solid is assumed to be unperturbed by the sorbate and the system is treated as a

one component phase of sorbate in the presence of a field provided by the sorbent.

(i) No mutual interactions homogeneous surface.

The entropy of a localized phase may conveniently be separated into two parts

$$\bar{S}_s = \bar{S}_{therm} + \bar{S}_{conf.}$$

The thermal entropy will include entropy originating from the electronic states of the molecule vibrations about chemical bonds, rotations and restricted rotations, and vibrations about a mean position on a site. The configurational entropy arises from the number of distinguishable arrangements of N molecules on N_s sites, and the expression for the differential configurational entropy deduced by Garden and Kington (1956) was

$$\bar{S}_{conf.} = R \ln \left(\frac{1}{\theta} - 1\right)$$

$\bar{S}_{conf.}$ from this equation is plotted as a function of θ in Figs. 30 and 31

(ii) Mutual interactions, homogeneous surface.

Everett (1950) has shown that the differential configurational entropy, taking into account the effect of mutual interactions may be obtained from the partition function of Fowler and Guggenheim (1939) as

$$\bar{S}_{conf.} = R \ln \left(\frac{1}{\theta} - 1\right) - zR \ln \frac{2(1 - \theta)}{(\beta + 1 - 2\theta)} + \frac{W}{T} \frac{(\beta - 1 + 2\theta)}{\beta}$$

where z is the number of nearest neighbours of any site and β

is given by

$$\beta = \left\{1 - 4\theta(1 - \theta)\left[1 - \exp\left(2\omega/zkT\right)\right]\right\}^{\frac{1}{2}}$$

Garden and Kington (1956) have shown that the effect of introducing mutual interactions for the system argon in chabazite is small in the range $\theta = 0.1$ to 0.9. In any case $\bar{S}_{conf.}$ is zero at $\theta = 0.5$.

(iii) Heterogeneous surface.

For a heterogeneous surface the treatment of Drain and Morrison (1952) following Hill must be used. In a later communication, Drain and Morrison (1953) have shown that at $\theta = 0.5$ the difference between the values of the configurational entropy for the homogeneous and the heterogeneous surfaces is very small.

By confining our considerations to entropy values at $\theta = 0.5$ it is therefore fully sufficient to use the simple localized theory on a homogeneous surface.

5.8. The Thermal Entropy of Argon and Water on Sodium Kaolinite.

In general, the thermal entropy can be obtained by subtracting the values of the configurational entropy, calculated by means of the equation in paragraph (i) above, from the experimentally observed differential entropy

$$\bar{S}_{therm} = \bar{S}_{s} - \bar{S}_{conf.}$$

The values of $\bar{S}_{therm.}$ are given in Tables 36 to 38 and plotted in Figs. 30 to 33.

Now, in the case of argon, the thermal entropy consists of the entropy of the three vibrational degrees of freedom associated with the movement of the molecule about its mean position on a site.

$$\bar{S}_{therm.} = 3\bar{S}_v$$

From Fig. 30 it can be seen that at $\Theta = 0.5$

$$\bar{S}_{s(exp)} = \bar{S}_{therm.} = 3\bar{S}_v = 10.8 \text{ e.u.}$$

$$\therefore \; {}_1S_v = 3.60 \text{ e.u.}$$

assuming that the three vibrational entropies are equal.

Consider the entropy of an harmonic oscillator at $77.36^{\circ}K$ (Mayer and Mayer, 1940)

$$u = \frac{h\nu}{kT} = \frac{\Theta}{T}$$

where $h = 6.626 \times 10^{-27}$ erg. sec., Planck's constant,

$k = 1.3804 \times 10^{-16}$ erg./deg., the Boltzmann constant,

and ν = the vibrational frequency

$$\therefore \; u = \frac{4.800 \times 10^{-11}\nu}{77.36} = 0.6205 \times 10^{-12}\nu$$

Table 36

The Configurational and Thermal Entropies of Argon on Sodium Kaolinite at 77.36°K

Run and Increment No	Volume Sorbed $m\ell$.s.t.p./gm	$\theta = V/V_m$	$\bar{S}_{conf}$ e.u.	$\bar{S}_s - \bar{S}_{conf} = \bar{S}_{therm}$ e.u.
13/1	0.65	0.24	2.29	9.76
13/2	1.74	0.65	-1.23	11.04
14/1	0.92	0.34	1.32	10.73
14/2	1.60	0.60	-0.81	10.70
14/3	2.19	0.82	-3.01	13.10

Table 37

The Configurational and Thermal Entropies of Argon on Water Covered Sodium Kaolinite at 77.36°K.

Run and Increment No	Volume Sorbed $m\ell$.s.t.p./gm.	$\theta = V/V_m$	$\bar{S}_{conf}$ e.u	$\bar{S}_s - \bar{S}_{conf} = \bar{S}_{therm}$ e.u.
10/1	0.58	0.24	2.29	8.81
10/2	1.10	0.46	0.32	10.55
10/3	1.43	0.60	-0.81	11.94
10/4	2.17	0.91	-4.60	15.28
11/1	0.65	0.27	1.98	8.96
11/2	1.61	0.67	-1.41	12.19
11/3	2.35	0.98	-7.74	18.99

Table 38

The Configurational and Thermal Entropies of Water on Sodium Kaolinite at 25°C.

Increment No.	Weight Sorbed gms/gm	$\theta = W/\omega_m$	$\bar{S}_{conf}$ e.u.	$\bar{S}_s - \bar{S}_{conf} = \bar{S}_{therm}$ e.u.
1	0.09	0.03	6.91	-4.85
2	0.27	0.09	4.60	2.68
3	0.58	0.19	2.88	8.84
4	0.76	0.25	2.18	14.47
5	1.06	0.34	1.32	14.72
6	1.23	0.40	0.81	15.03
7	1.53	0.50	0	14.17
8	1.69	0.55	-0.40	14.06
9	1.98	0.64	-1.14	14.18
10	2.14	0.69	-1.59	14.09
11	2.30	0.75	-2.18	14.42
12	2.46	0.80	-2.76	15.05
13	2.61	0.85	-3.45	15.88
14	2.76	0.90	-4.37	17.23
15	2.99	0.97	-6.91	20.15

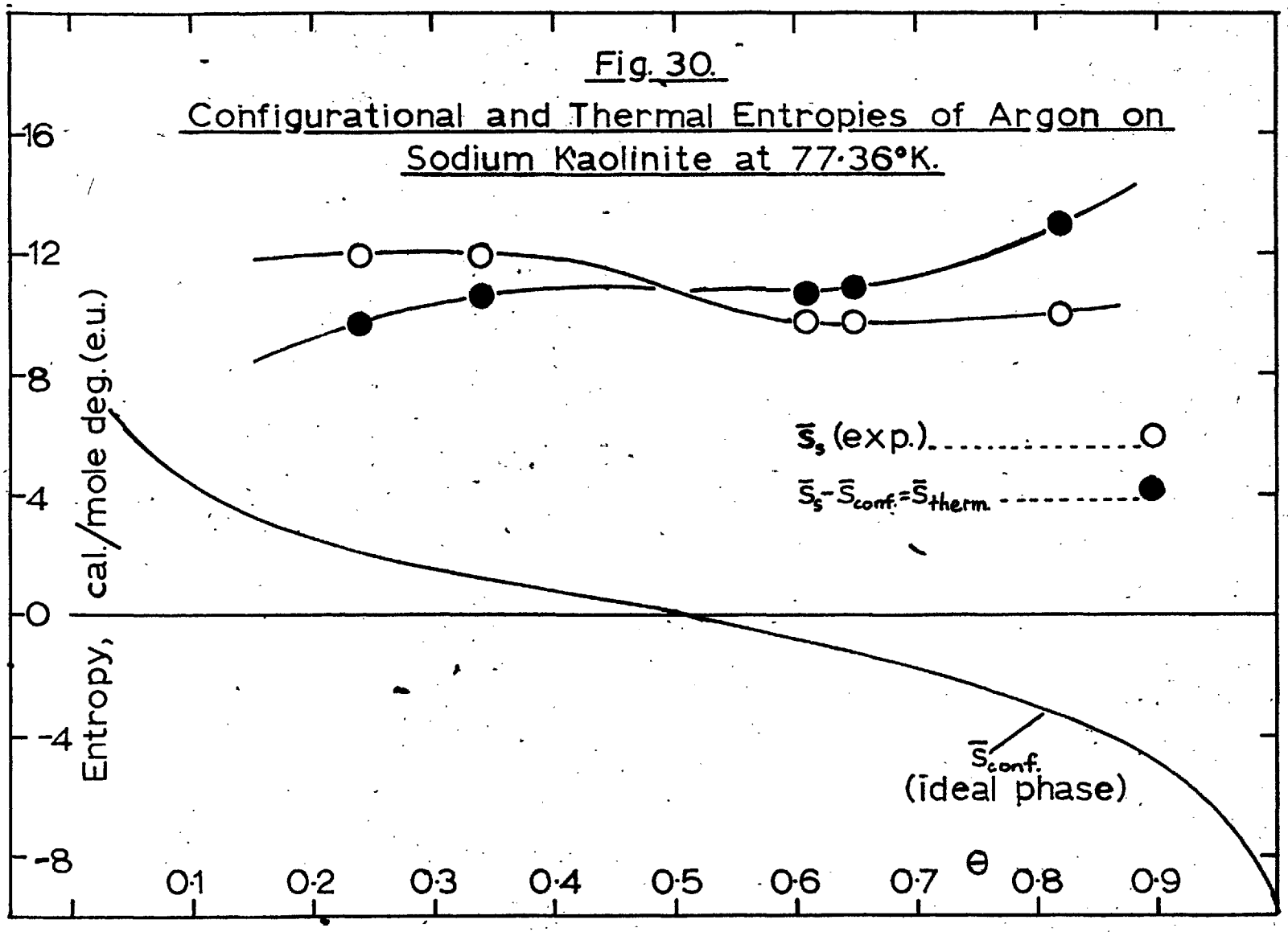
Fig. 30.
Configurational and Thermal Entropies of Argon on Sodium Kaolinite at 77·36°K.
16
12
8
4
0
-4
-8
Entropy, cal./mole deg. (e.u.)
$\bar{S}_s$ (exp.)
$\bar{S}_s - \bar{S}_{conf.} = \bar{S}_{therm.}$
$\bar{S}_{conf.}$ (ideal phase)
0·1
0·2
0·3
0·4
0·5
0·6
0·7
θ
0·8
0·9

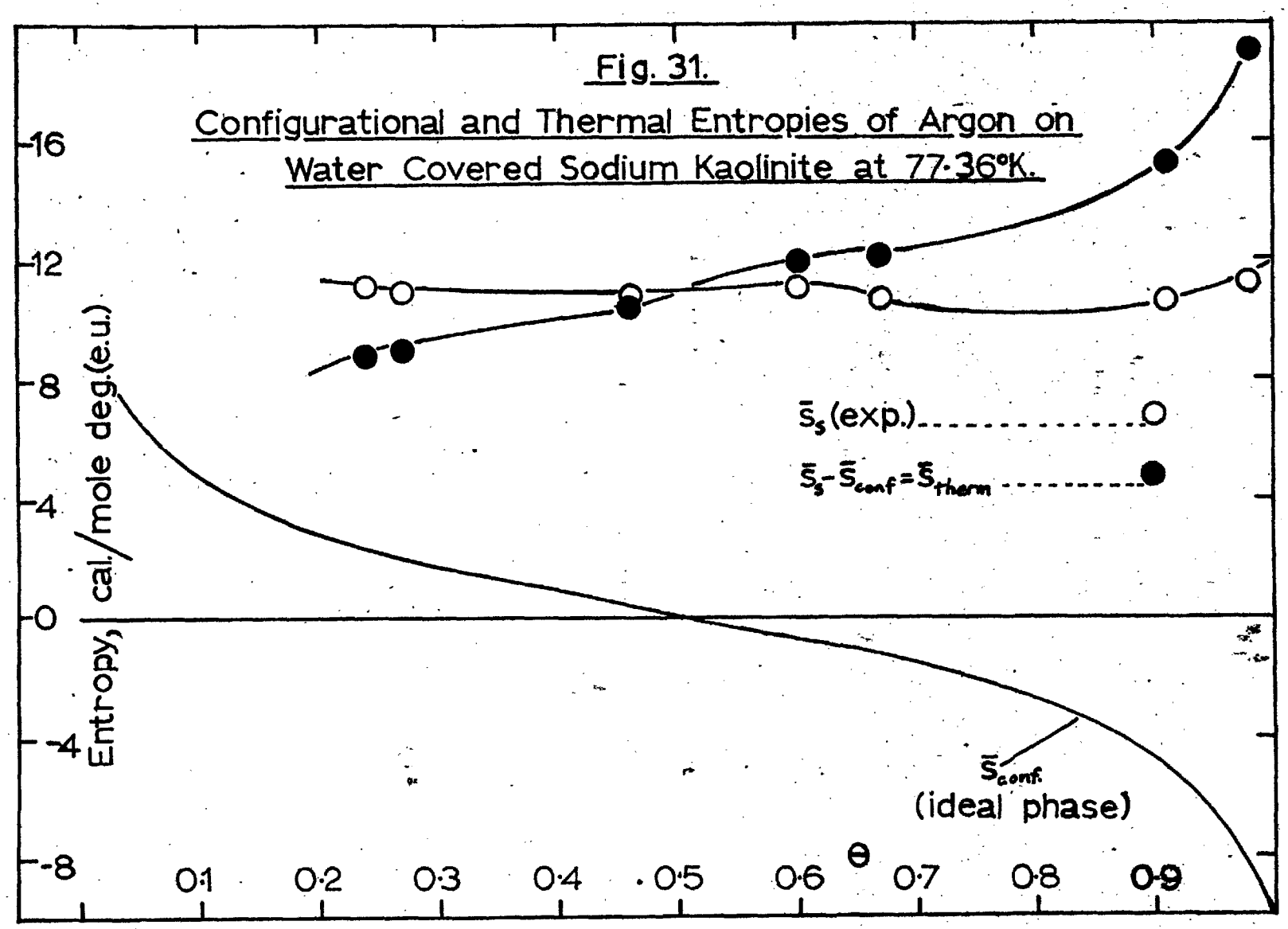
Fig. 31.
Configurational and Thermal Entropies of Argon on Water Covered Sodium Kaolinite at 77·36°K.
16
12
8
4
0
-4
-8
Entropy, cal./mole deg.(e.u.)
$\bar{S}_s$(exp.)
$\bar{S}_s - \bar{S}_{conf} = \bar{S}_{therm}$
$\bar{S}_{conf.}$
(ideal phase)
0·1
0·2
0·3
0·4
0·5
0·6
θ
0·7
0·8
0·9

Fig. 32.

Thermal Entropy of Argon on Sodium Kaolinite and the Water Surface at 77·36°K.

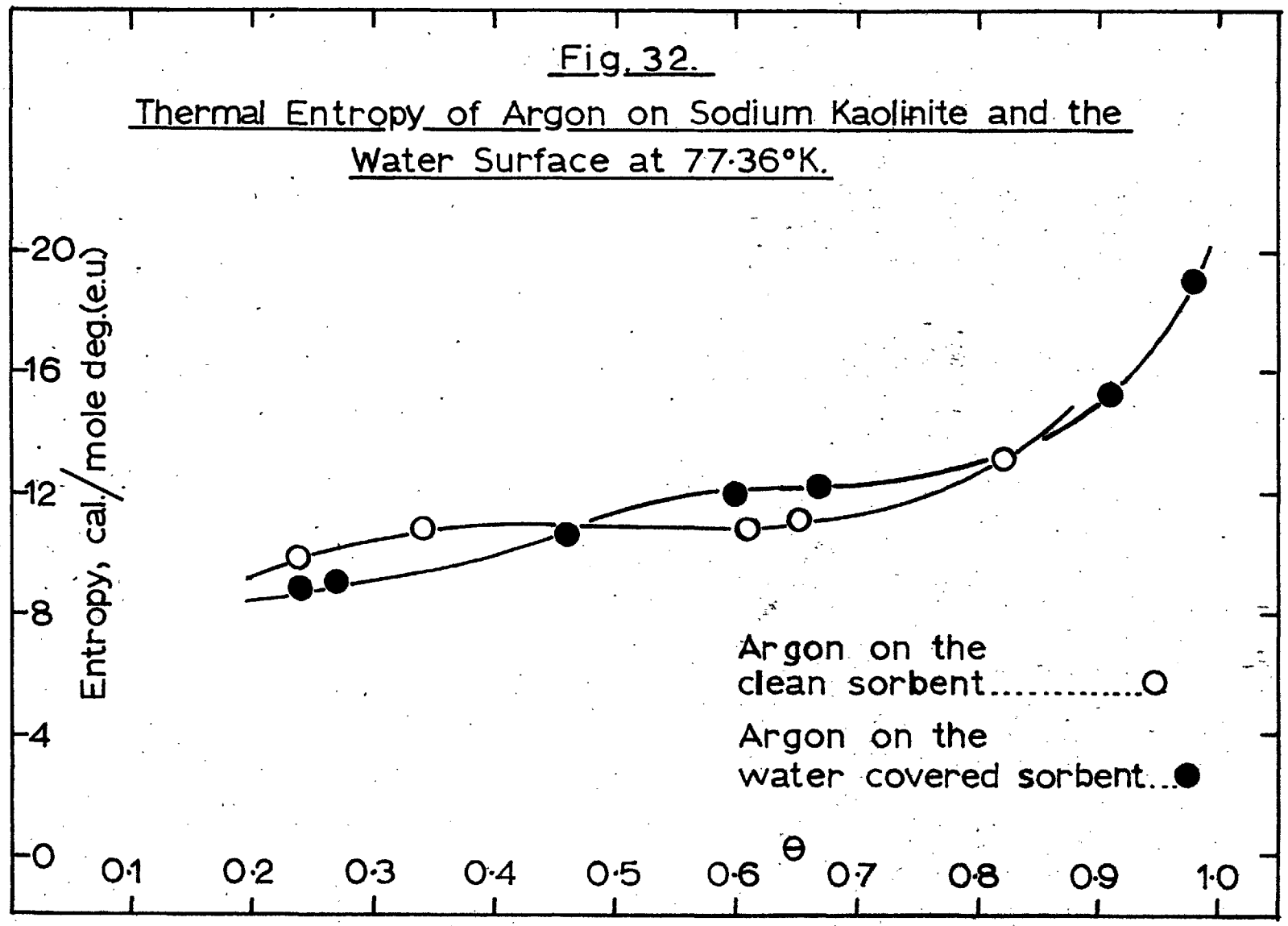

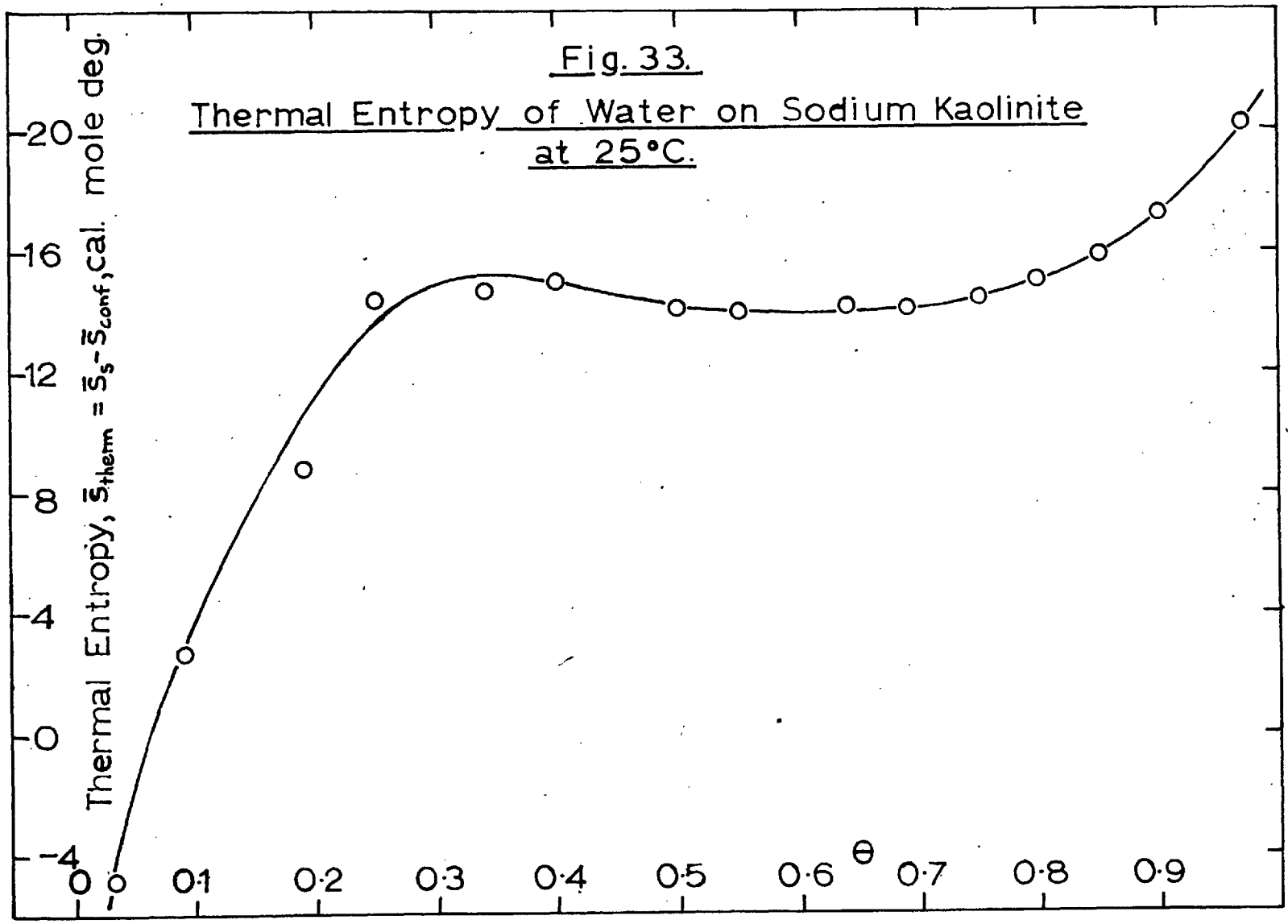
Fig. 33.
Thermal Entropy of Water on Sodium Kaolinite at 25°C.
Thermal Entropy, $\bar{S}_{therm} = \bar{S}_s - \bar{S}_{conf}$, cal. mole deg.
20
16
12
8
4
0
-4
0
0·1
0·2
0·3
0·4
0·5
0·6
θ
0·7
0·8
0·9

Now ν can be calculated for various values of u, and corresponding values of S/R and therefore ${}_1S_V$, can be obtained from the Tables in Mayer and Mayer.

u	ν (sec^{-1})	S/R	${}_1S_V$ (e.u.)
0.40	0.645×10^{12}	1.923	3.82
0.45	0.725×10^{12}	1.807	3.59
0.50	0.806×10^{12}	1.703	3.38

Interpolating, when ${}_1S_V = 3.60$ e.u.

$$\nu = 0.72 \times 10^{12} \text{ sec}^{-1}$$

Orr (1939b) calculated the vibrational frequencies of argon above various points on the potassium chloride lattice. He obtained values for ν of from 0.81 to 1.00×10^{12} sec^{-1}.

Using the above argon data we can estimate the vibrational frequency of water

$$\nu \propto \sqrt{f/m}$$

where f is the restoring force and m the mass of the molecule. Therefore, assuming that

$$\nu \propto \sqrt{q_{st}/m}$$

where q_{st} is the heat of sorption and m is the molecular weight

$$\frac{\nu_{H_2O}}{\nu_A} = \sqrt{\frac{g_{H_2O}}{g_A} \cdot \frac{m_A}{m_{H_2O}}}$$

$$= \sqrt{\frac{13.4}{2.35} \cdot \frac{39.94}{18.02}} = 3.555$$

$$\therefore \quad \nu_{H_2O} = 3.555 \times 0.72 \times 10^{12}$$

$$= 2.56 \times 10^{12} \text{ sec}^{-1}$$

Now consider the entropy of an harmonic oscillator at 25°C

$$u = \frac{h\nu}{kT} = \frac{4.800 \times 10^{-11}\nu}{298.16}$$

$$= 0.161 \times 10^{-12}\nu$$

As before, ν can be calculated for various values of u, and corresponding values of S/R and therefore ${}_1S_V$, can be obtained from the tables in Mayer and Mayer.

u	ν (sec^{-1})	S/R	${}_1S_V$ (e.u.)
0.35	2.17×10^{12}	2.055	4.08
0.40	2.48×10^{12}	1.923	3.82
0.45	2.80×10^{12}	1.807	3.59

Therefore when $\nu_{H_2O} = 2.56 \times 10^{12}$ sec^{-1}

$${}_1S_V = 3.76 \text{ e.u.}$$

$$\therefore \quad {}_3S_V = 11.28 \text{ e.u.}$$

$$\nu_{H_2O} = 2.56 \times 10^{12} \text{ sec}^{-1}$$

$$\equiv \frac{2.56 \times 10^{12}}{3 \times 10^{10}} = 85 \text{ cm}^{-1}$$

From Fig. 33 it can be seen that the thermal entropy of water on sodium kaolinite when $\theta = 0.5$ is

$$\bar{S}_{therm} = 14.5 \text{ e.u.}$$

Now, for water

$$\bar{S}_{therm} = {}_3\bar{S}_V + {}_3\bar{S}_R + \bar{S}_{int.\ vib.}$$

where ${}_3\bar{S}_R$ is the entropy associated with free rotation or libration. The entropy associated with internal vibrations is negligible at 25°C. Therefore

$$\begin{aligned} {}_3\bar{S}_R &= \bar{S}_{therm.} - {}_3\bar{S}_V \\ &= 14.50 - 11.28 \\ &= 3.22 \text{ e.u.} \end{aligned}$$

Moelwyn-Hughes (1957a) has shown that the rotational entropy of water at 25°C is 10.48 e.u. Therefore, the possibility of free rotation for the sorbed phase of water on sodium kaolinite can obviously be ruled out.

5.9 The Frequency of Libration of Adsorbed Water at 25°C

Assuming all the libration frequencies to be equal

$${}_1S_L = \frac{3.22}{3} = 1.07 \text{ e.u.}$$

From the relationship for the entropy of an harmonic oscillator at 25°C

$$u = 0.161 \times 10^{-12}\nu$$

ν for various values of u can again be calculated and the corresponding values of S/R obtained from Mayer and Mayer

u	ν (sec^{-1})	S/R	${}_1S_L$ (e.u.)
1.75	10.87×10^{12}	0.559	1.11
1.80	11.18×10^{12}	0.537	1.07
1.85	11.49×10^{12}	0.516	1.03

Therefore when ${}_1S_L = 1.07$ e.u.

$$\nu_L = 11.18 \times 10^{12} \text{ sec}^{-1}$$

$$\equiv \frac{11.18 \times 10^{12}}{3 \times 10^{10}} \text{ cm}^{-1}$$

$$= 373 \text{ cm}^{-1}$$

5.9a. Comparison of the Vibrational and Librational Frequencies of Solid, Liquid and Adsorbed Water.

Values of the vibrational frequency of ice and water have been obtained by Cartwright (1936) by direct observation of the infra red spectrum. Also by direct observation, Giguere and Harvey (1956) have obtained values for the librational frequency of ice and water. These are listed in the following table, together with the values for adsorbed water calculated from this study of water on sodium kaolinite.

Table 39

	Frequency, ν (cm^{-1})		
	Ice	Liquid Water	Adsorbed Water
Vibrational	160	160	85
Librational	800	710	400

It can therefore be seen that:

(i) the vibrational frequency, i.e. the vibration about the mean position on a site is considerably smaller in adsorbed water than in either bulk phase. The frequency calculated as the frequency of vibration of the adsorbed water is in fact the mean of one vibration normal to the surface and two vibrations parallel to the surface. Since the heat of sorption is greater than the heat of liquefaction or sublimation, the frequency normal to the surface must be <u>greater</u> than the vibrational frequency of the bulk state. It must therefore be concluded that the transverse vibrations about the adsorption site are of lower frequency than in the bulk phase. This conclusion is entirely feasible since the restoring forces in this direction will be lower in the adsorbed phase.

(ii) the libration frequency is lower than in the bulk phase. Since the restoring forces for librational motion in the sorbed phase are smaller than those in the

bulk phase, this result is again perfectly reasonable.

The above conclusions regarding both vibrational and librational frequencies are in agreement with the results of Frohnsdorff (Ph.D. thesis, 1959) who, in his study of water sorbed in sodium A showed that the heat capacity of the sorbed water was greater than that of liquid water, after suitable correction had been made for the declustering effect.

5.10. Summary of Conclusions.

(i) The area occupied by a water molecule in the first layer on sodium kaolinite is 11.0 to 11.5 $Å^2$. This eliminates Macey's theory that the adsorbed water has the structure of ice.

(ii) 20 per cent of the kaolinite surface is substantially more active in physical adsorption of argon, nitrogen and water than the remaining 80 per cent. This activity is identified with the electrostatic field at the surface rather than with dispersion forces. There is one active site for water adsorption for every Na^+ ion on the surface.

(iii) The heat of adsorption of water in the second and higher layers is between the heat of sublimation and the heat of vaporization and there is no evidence of any long range effect emanating from the kaolinite lattice.

(iv) Calculations of the electrostatic field over

two positions on the ice covered kaolinite surface show that the usual simple expression $\frac{1}{2}\alpha F^2$ for the induction energy is unable to account for the difference between the heat of adsorption of argon on this surface and the heat of sublimation.

(v) The non-appearance of a maximum in the differential heat curve of argon at high concentrations on the uniform ice surface cannot be explained in terms of repulsion between induced dipoles. An explanation in terms of close packing of the argon atoms is advanced.

(vi) The differential heats of adsorption of nitrogen show that the contribution from the interaction of the quadrupole with the surface field gradient is of importance both on the dipolar surface of water molecules and on the kaolinite surface, which is more ionic in nature.

(vii) At $\theta = 0.5$ the mean vibrational frequency of an adsorbed water molecule about its site position is c.a. 85 cm^{-1}. Free rotation of the water molecules is not permitted but a librational motion with a mean frequency of c.a. 400 cm^{-1} is required by the entropy data. Both frequencies are lower than in the bulk phase of ice or liquid water and suggest that the restoring force for any lateral motion on the surface is smaller than the corresponding forces in the bulk phase.

APPENDIX I

The Calculation of the Electrostatic Field above an Infinite Plane of Dipoles Oriented Perpendicular to the Plane

For this calculation the layer of water molecules on the kaolinite surface was assumed to consist of a close packed hexagonal array extended in an infinite plane. The water molecules were a distance 'd' apart and the polar axes were all oriented in the same sense and perpendicular to the plane.

The field at any point due to one dipole of strength μ is given by the equations (Moelwyn-Hughes, 1957b)

$$F_x = \frac{\mu}{a^3}(1 - 3\cos^2\theta)$$

$$F_y = -\frac{3\mu}{a^3}\sin\theta\cos\theta$$

where 'a' is the distance between the dipole centre and the point considered and θ is the angle between the polar axis and the line joining the polar centre to this point. F_x is the field parallel to the polar axis and Fy is the field perpendicular to the polar axis.

In this case for an infinite plane of dipoles, the total field perpendicular to the polar axes is zero. Consider therefore F_x due to <u>one</u> dipole at any point

A above the plane of dipoles.

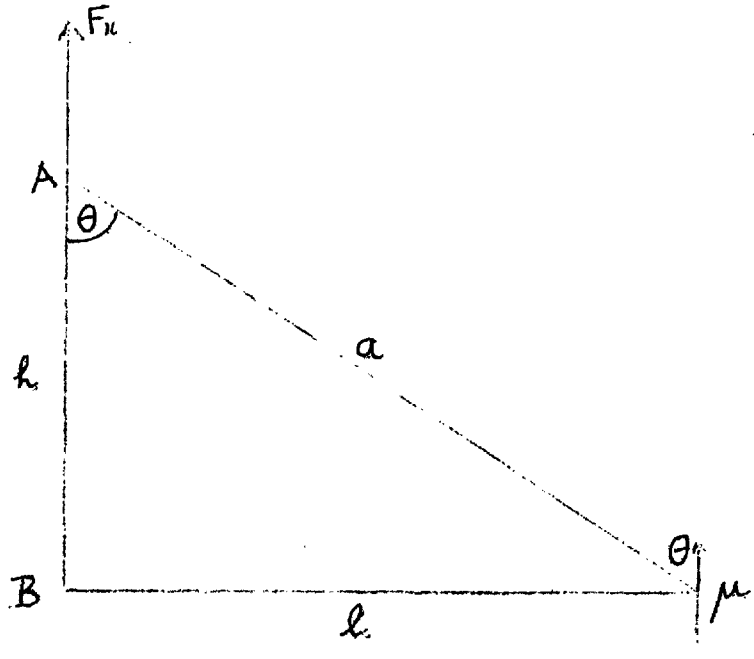

B is the point in the plane of dipole centres directly below A.

$$F_x = \frac{n}{a^3}(1 - 3\cos^2\theta)$$

$$a^2 = h^2 + \ell^2$$

$$\text{and } \cos\theta = \frac{h}{a} = \frac{h}{(h^2 + \ell^2)^{\frac{1}{2}}}$$

$$\therefore F_x = \frac{n}{(h^2 + \ell^2)^{\frac{3}{2}}}\left[1 - \frac{3h^2}{(h^2 + \ell^2)}\right]$$

Let $h = xd$ and $\ell = fd$

where 'd' is the distance between the water dipoles.

Then,

$$Fx = \frac{u}{d^3(x^2 + f^2)^{\frac{3}{2}}} \left[\frac{f^2 - 2x^2}{x^2 + f^2} \right]$$

$$= \frac{\mu}{d^3} \left[\frac{f^2 - 2x^2}{(x^2 + f^2)^{\frac{5}{2}}} \right] \longrightarrow (1)$$

The total field at point A due to an infinite plane of dipoles was calculated by means of a summation for the 63 or 73 dipoles nearest to point B, followed by an integration to infinity for the remaining contribution.

The summation was performed by calculating the values of f from the geometry of the plane of dipoles, giving x various values from 0.4 to 2.0 and substituting in equation (1). The field due to the 63 or 73 nearest neighbours was thereb obtained (in terms of μ/d^3) as a function of the height above the plane of dipole centres.

The equation for the integration was derived as follows.

Consider the field at point A at a perpendicular distance h from an infinite layer of dipoles each of strength u. Each dipole is perpendicular to the plane, and the density of dipoles is ρ per cm^2. All the F_y components will cancel out so that the total field at A

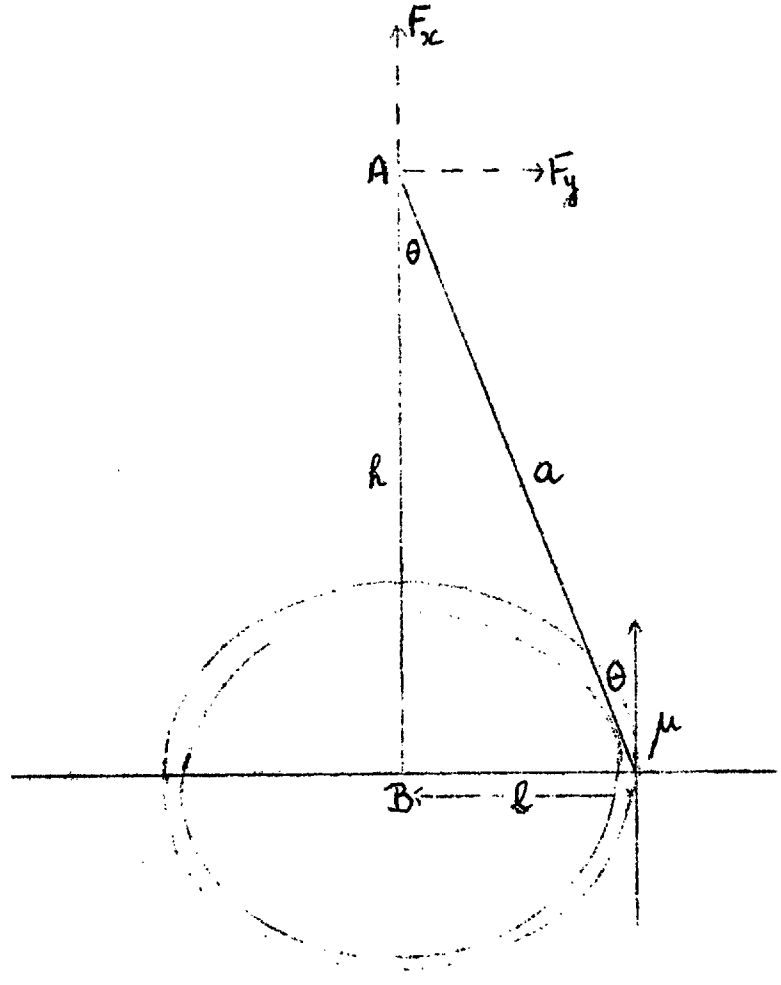

will be due only to the F_x components. B is the point in the plane of dipole centres directly below A.

The field component at A due to one dipole is

$$F_{x_i} = \frac{\mu}{a^3} (1 - 3 \cos^2 \theta)$$

Therefore the field at A due to all dipoles in the annulus of radius ℓ and width $d\ell$ is

$$F_{x_A} = \int . 2\pi\ell . d\ell \frac{u}{a^3} (1 - 3\cos^2\theta)$$

Therefore, the field at A due to all dipoles between ℓ_1 and ∞ is

$$F_x(\ell_1 \to \infty) = \int_{\ell_1}^{\infty} (2\pi\rho_u) \frac{\ell}{a^3} (1 - 3\cos^2\theta) d\ell$$

$$= 2\pi\rho_u \int_{\ell_1}^{\infty} \frac{\ell}{a^3} (1 - 3\cos^2\theta . d\ell$$

Now $\cos\theta = \frac{h}{a}$, $\therefore \frac{1}{a^3} = \frac{\cos^3\theta}{h^3}$

$\tan\theta = \frac{\ell}{h}$, $\therefore \ell = h\tan\theta$

$$\frac{d\ell}{d\theta} = h\sec^2\theta$$

$$d\ell = \frac{h}{\cos^2\theta} d\theta$$

$$\therefore F_x \text{ (integration)} = \frac{2\pi\rho_u}{h} \int_{\theta_1}^{\pi/2} (1 - 3\cos^2\theta)\sin\theta \, d\theta$$

$$= \frac{2\pi\rho_u}{h} \left[. \cos\theta \right]_{\theta_1}^{\pi/2} - \frac{2\pi\rho_u}{h} \left[- \cos^3\theta \right]_{\theta_1}^{\pi/2}$$

$$= \frac{2\pi\rho_u}{h} \left\{ \cos\theta_1 - \cos^3\theta_1 \right\}$$

However $\cos\theta = \frac{h}{a}$

and, as above when considering the summation, let

$$h = xd \text{ and } \ell = fd.$$

Each dipole occupies an area of $\frac{\sqrt{3}}{2} d^2$

$$\therefore \rho = \frac{2}{\sqrt{3d^2}}$$

$$\therefore F_x(\text{integration}) = \frac{2\pi \cdot 2\mu}{\sqrt{3}d^2 \cdot xd}\left[\frac{h}{a} - \frac{h^3}{a^3}\right]$$

$$= \frac{4\pi}{\sqrt{3}}\left(\frac{\mu}{d^3}\right)\frac{1}{x}\left[\frac{h}{(h^2+\ell^2)^{\frac{1}{2}}} - \frac{h^3}{(h^2+\ell^2)^{\frac{3}{2}}}\right]$$

$$= \frac{4\pi}{\sqrt{3}}\frac{\mu}{d^3}\left[\frac{f^2}{(x^2+f^2)^{\frac{3}{2}}}\right] \longrightarrow (2)$$

The contribution to F_x from all dipoles not included in the summation was therefore obtained by substituting in equation (2) the value of f for the nearest dipole to point B (excluding those taken in the summation by means of equation (1)), and values of x between 0.5 and 2.0. The total value of the field at any given x value was then the total from the summation plus the contribution from the integration. The total field as a function of the height above the plane of dipole centres is shown in Fig. 25. The calculation was performed for two positions above the dipole array, (i) where point B coincides with a dipole centre and (ii) where point B is at the centre of a triangle of dipoles.

APPENDIX II

The Calculation of the Electrostatic Field above an Infinite Plane of Dipoles Oriented Parallel to the Plane

For this calculation the layer of water molecules on the kaolinite surface was assumed to consist of a close packed hexagonal array extended in an infinite plane. The water molecules were a distance 'd' apart and their polar axes were all oriented in the same sense and parallel to the plane.

The field at any point due to one dipole of strength μ is given by the equations (Hoelwyn Hughes, 1957b)

$$F_x = \frac{\mu}{a^3}(1 - 3\cos^2\theta)$$

$$F_y = -\frac{3\mu}{a^3}\sin\theta\cos\theta$$

where 'a', F_x and F_y are as defined in Appendix I. For an infinite plane of dipoles the total field perpendicular to the polar axes is zero. Therefore only the F_x components need be considered. Consider, therefore, F_x due to one dipole at any point A above the plane of dipoles. Take first the plane ACD in which CD is drawn in the plane of polar centres and parallel to the polar axes. Angle $\hat{ACD}$ is a right angle.

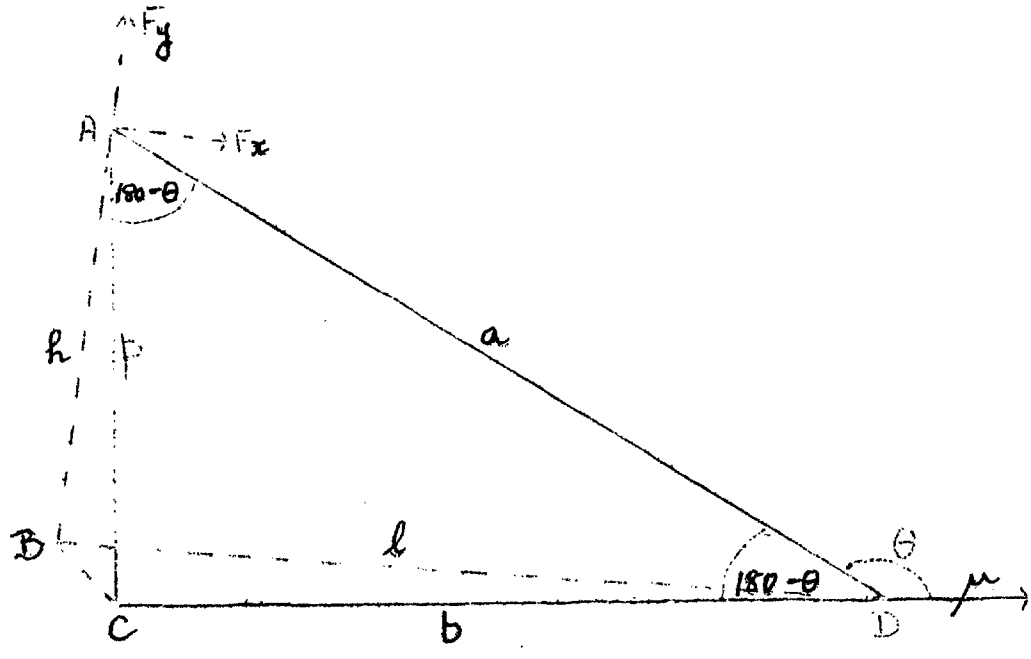

θ is the angle in the AOD plane between AD and the polar axis.

Therefore $\cos(180 - \theta) = -\cos\theta = \frac{b}{a}$

$$\cos^2\theta = \frac{b^2}{a^2}$$

ABD is the plane perpendicular to the plane of polar centres, angle $\hat{ABD}$ being a right angle

$$a^2 = h^2 + \ell^2$$

$$\therefore F_x = \frac{u}{(h^2 + \ell^2)^{\frac{3}{2}}}\left(1 - \frac{3b^2}{h^2 + \ell^2}\right)$$

Defining all distances in terms of 'd' as in Appendix I, let

$$h = xd$$

$$\ell = fd$$

and $$b = gd$$

$$\therefore F_x = \frac{\mu}{(x^2 + f^2)^{\frac{3}{2}} d^3} \left(1 - \frac{3g^2}{x^2 + f^2}\right)$$

$$= \frac{\mu}{d^3} \frac{1}{(x^2 + f^2)^{\frac{3}{2}}} \left(\frac{x^2 + f^2 - 3g^2}{x^2 + f^2}\right)$$

$$F_x = \frac{\mu}{d^3}\left[\frac{x^2 + f^2 - 3g^2}{(x^2 + f^2)^{\frac{5}{2}}}\right] \longrightarrow \quad (1)$$

The total field at point A due to an infinite plane of dipoles was calculated by means of a summation for the 54 dipoles nearest to point B, followed by an integration to infinity for the remaining contribution.

The summation was performed by calculating the values of f and g from the geometry of the plane of dipoles, giving x various values from 0.5 to 2.0 and substituting in equation (1). The field due to the 54 nearest neighbours was thereby obtained (in terms of μ/d^3) as a function of the height above the plane of dipole centres.

For this particular model in the expression

$$F_x = \frac{\mu}{a^3}(1 - 3\cos^2\theta)$$

θ and 'a' are variables. In order to integrate for all dipoles fr . $a = a_1 \rightarrow \infty$ we therefore proceed as follows.

Consider first the integration of the expression for the electrostatic field due to a circle of dipoles each a radius ℓ from point B. In this case 'a' and ℓ are constants.

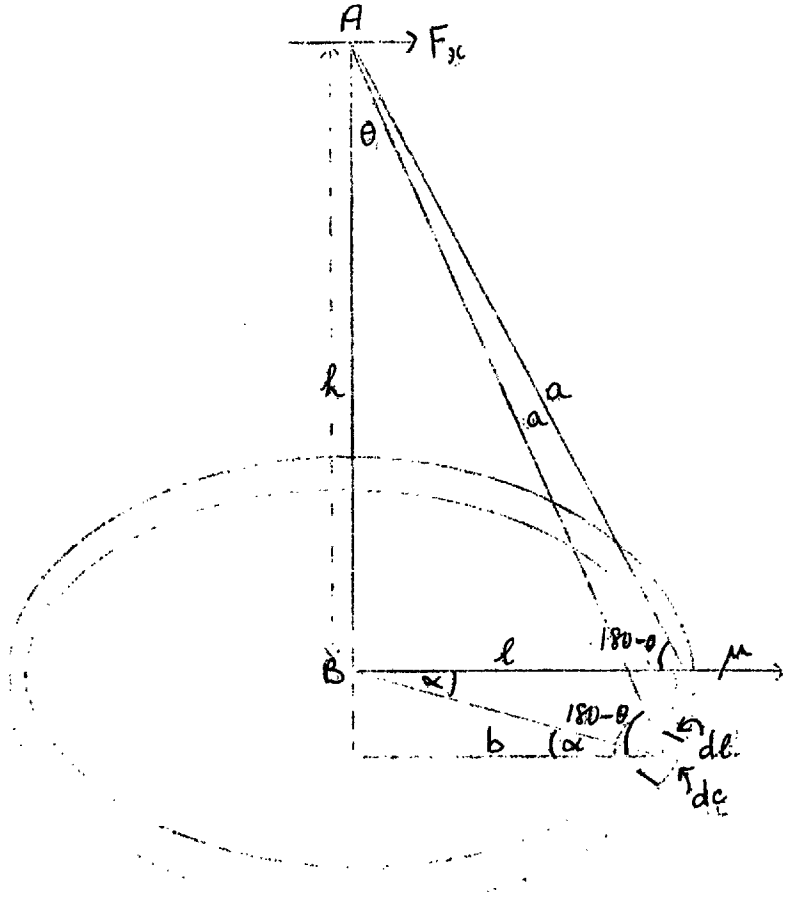

Take a small element of area $dc.d\ell$. Let ρ = the number of dipoles per cm.^{2}

Then $$F_x = \int_{\alpha=0}^{2\pi} \frac{\mu}{a^3}(1 - 3\cos^2\theta \; d\ell . dc . \rho$$

$$= \frac{\mu\rho d\ell}{a^3} \int_{\alpha=0}^{2\pi} (1 - 3\cos^2\theta)\, dc.$$

Now $\cos(180 - \theta) = -\cos\theta = \frac{b}{a}$

and $\cos\alpha = \frac{b}{\ell}$

$\therefore \quad -a\cos\theta = \ell\cos\alpha$

$\cos\theta = -\frac{\ell}{a}\cos\alpha$

Also $dc = \ell d\alpha$

$$\therefore F_x = \frac{\mu\rho d\ell}{a^3} \int_{\alpha=0}^{2\pi} (1 - 3\frac{\ell^2}{a^2}\cos^2\alpha)\ell d\alpha$$

$$= \frac{\mu\rho\ell d\ell}{a^3} \int_{\alpha=0}^{2\pi} d\alpha - \frac{3\mu\rho\ell^3}{a^5} \int_{\alpha=0}^{2\pi} \cos^2\alpha d\alpha$$

$$= \frac{\mu\rho\ell d\ell}{a^3} \left[\alpha - \frac{3\ell^2}{a^2} \left(\frac{\alpha}{2} + \frac{\sin 2\alpha}{4} \right) \right]_0^{2\pi}$$

$$= \frac{\mu\rho\ell d\ell}{a^3} \left[2\pi - \frac{3\ell^2}{a^2}\pi \right]$$

This expression must now be integrated for values of $\ell = \ell_1 \to \infty$, i.e. $\beta = \beta_1 \to \frac{\pi}{2}$

$$\tan\beta = \frac{\ell}{h}$$

$$\therefore \ell = h \tan\beta$$

$$d\ell = h.d\tan\beta$$

$$\frac{d\ell}{d\beta} = \frac{h}{\cos^2\beta}$$

$$\therefore d\ell = \frac{h}{\cos^2\beta}.d\beta$$

$$\cos\beta = \frac{h}{a}$$

$$\therefore \frac{1}{a^3} = \frac{\cos^3\beta}{h^3}$$

Therefore

$$F_x = \mu\rho.h\tan\beta.\frac{\cos^3\beta}{h^3}\left[2\pi .. \frac{3h^2\tan^2\beta.\cos^2\beta.\pi}{h^2}\right] d\ell$$

$$= \frac{\pi\mu\rho}{h^2}\int_{\beta=\beta_1}^{\pi/2}\left[2\sin\beta\cos^2\beta - 3\sin^3\beta\cos^2\beta\right]\frac{h}{\cos\beta}d\beta$$

$$= \frac{\pi\mu\rho}{h}\int_{\beta=\beta_1}^{\pi/2}\left[2\sin\beta - 3\sin^3\beta\right]d\beta$$

$$= -\frac{2\pi\mu\rho}{h}\left[\cos\beta\right]_{\beta_1}^{\pi/2} - \frac{3\pi\mu\rho}{h}\left[\frac{\cos^3\beta}{3} - \cos\beta\right]_{\beta_1}^{\pi/2}$$

$$= \frac{\pi\mu\rho}{h}\left\{\cos\beta - \cos^3\beta\right\}_{\beta_1}^{\pi/2}$$

$$\therefore \quad F_x = \frac{\pi\mu\rho}{h}\left[\cos^3\beta_1 - \cos\beta_1\right]$$

In the model under consideration one dipole occupies an area of $\sqrt{3}d^2/2$.

$$\therefore \rho = 2/\sqrt{3}d^2.$$

Also $\quad h = xd$

$$\ell = fd$$

and $\quad a^2 = \ell^2 + h^2 = (f^2 + x^2)d^2$

$$\therefore \quad F_x = \pi\mu \cdot \frac{2}{\sqrt{3}d^2 \cdot xd}\left[\cos^3\beta_1 - \cos\beta_1\right]$$

$$= \frac{2\pi\mu}{\sqrt{3}d^3} \cdot \frac{1}{x}\left[\frac{h^3}{a^3} - \frac{h}{a}\right]$$

$$= \frac{2\pi\mu}{\sqrt{3}d^3} \cdot \frac{xd}{x}\left[\frac{x^2d^2 - (f^2 + x^2)d^2}{(f^2 + x^2)^{\frac{3}{2}} \cdot d^3}\right]$$

$$\therefore F_x \text{ (integration)} = \frac{2\pi}{\sqrt{3}}\left(\frac{\mu}{d^3}\right)\left[\frac{f^2}{(f^2 + x^2)^{\frac{3}{2}}}\right] \longrightarrow \quad (2)$$

The contribution to F_x from all dipoles not included in the summation was therefore obtained by substituting in equation (2) the value of f for the nearest dipole to point B (excluding those considered in the summation by means of equation (1)), and values of x

between 0.5 and 2.0. The total value of the field at any given x value was then the total from the summation plus the contribution from the integration. The total field as a function of the height above the plane of dipole centres is shown in Fig. 25. The calculation was performed for the position above the dipole array where point B is at the centre of a triangle of dipoles.

REFERENCES

Barshad (1949). Amer. Mineral. 34, 675.

Boobo Millard and Cynarski (1953). J.A.C.S. 75, 839.

Brindley (1951). X-ray Identification and Crystal Structures of Clay Minerals. The Mineralogical Society.

Brindley and Robinson (1946a). Mineral. Mag. 27, 242.

Brindley and Robinson (1946b). Trans. Far. Soc. 42B, 198.

Brunauer, Emmett and Teller (1938). J.A.C.S. 60, 309.

Burnelle and Coulson (1957). Trans. Far. Soc. 53, 403.

Cartwright (1936). Phys. Rev. 49, 470.

Coulson, Maccoll and Sutton (1952). Trans. Far. Soc. 48, 106

Danes and Nováková (1958). Chem. listy 52, 382.

De Wit and Arons (1950). Trans. 4th Intern. Congr. Soil Sci. 2, 59.

Drain (1953). Trans. Far. Soc. 49, 650.

Drain and Morrison (1952). Trans. Far. Soc 48, 316.

Drain and Morrison (1953). Trans. Far. Soc. 49, 654.

Emmett and Brunauer (1937). J.A.C.S. 59, 1553.

Everett (1950). Trans. Far. Soc. 46, 942.

Fowler and Guggenheim (1939). Statistical Thermodynamics, p. 429. Camb. Univ. Press.

Garden and Kington (1956). Proc. Roy Soc. A234, 24.

Garden, Kington and Laing (1955). Trans. Far. Soc. 51, 1558.

Giguere and Harvey (1956). Can. J. Chem. 34, 798.

Goates and Bennett (1957). Soil Sci. 83, 325.

Gould and Vickers (1952). J. Sci. Inst. 29, 85.

Gregg, Parker and Stephens (1953). Clay Min. Bull. 2, 34.

Grim (1947). Am. Mineral. 32, 493.

Grim and Cuthbert (1945). J. Am Ceram. Soc. 28, 90.

Grimshaw, Heaton and Roberts (1945). Trans. Brit. Ceram. Soc. 44, 69.

Gruner (1932). Z. Krist. 83, 75.

Harkins and Jura (1944). J.A.C.S. 66, 1362.

Hendricks and Jefferson (1938). Am. Mineral. 23, 863.

Hendricks, Nelson and Alexander (1940). J.A.C.S. 62, 1457.

Hill and Smith (1951). Phys. Rev. 82 451.

Jaeger (1938). Verhandel. Koninkl. Nederland. Akad. Wettensch. Afdell. Natuurk. Sec. II, 16.

Johnson and Norton (1941). J. Am. Ceram. Soc. 24, 189.

Keenan, Mooney and Wood (1951). J. Phys. Chem. 55, 1462.

Kelley (1948). Contributions to the Data on Theoretical Metallurgy p. 50. U.S. Bureau of Mines Bull. 477.

Kington and Aston (1951). J.A.C.S. 73, 1929 and 1934.

Kistemaker (1945). Physica 11, 277.

Lonel (1933). Z. Phys. Chem. B23, 379.

Macey (1942). Trans. Brit. Ceram. Soc. 41, 73.

Marshall (1949). The Colloid Chemistry of the Silicate Minerals, p.96. Academic Press Inc.

Mayer and Mayer (1940). Statistical Mechanics, p. 441. John Wiley and Sons, Inc.

Miller (1949). The adsorption of Gases on Solids, p. 121. Camb. Univ. Press.

Moelwyn-Hughes (1957a). Physical Chemistry, p. 300. Pergamon Press.

Moelwyn-Hughes (1957b). Physical Chemistry, p. 455. Pergamon Press.

Morrison and Drain (1951). J. Chem. Phys. 19, 1063.

Orchiston (1954). Soil Sci. 78, 463.

Orr (1939a). Proc. Roy. Soc. A173, 349.

Orr (1939b). Trans. Far. Soc. 35, 1247.

Pauling (1930). Proc. Nat. Acad. Sci. U.S. 16, 578.

Rhodin (1950). J.A.C.S. 72, 5691.

Roberts (1939). Some Problems in Adsorption p. 105. Cambridge Physical Tracts.

Spiel (1940). J. Am. Ceram. Soc. 23, 33.

Terzaghi (1928). Tech. Eng. News M.I.T. 9, 10 and 36.

Walker (1949). Nature 163, 726.

Williamson (1951). Trans. Brit. Ceram. Soc. 50, 10.